ISSN 2617-7609; eISSN 2617-7595

ӘЛ-ФАРАБИ атындағы ҚАЗАҚ ҰЛТТЫҚ УНИВЕРСИТЕТІ

Ашық жүйелер эволюциясының мәселелері

ЖУРНАЛЫ

КАЗАХСКИЙ НАЦИОНАЛЬНЫЙ УНИВЕРСИТЕТ имени АЛЬ-ФАРАБИ

ЖУРНАЛ

проблем эволюции открытых систем

AL-FARABI KAZAKH NATIONAL UNIVERSITY

JOURNAL

of open systems evolution problems

№3-4(25)

Алматы
«Қазақ университеті»
2023

ISSN 2617-7609; eISSN 2617-7595

KazNU Science · ҚазҰУ Ғылымы · Наука КазНУ

АШЫҚ ЖҮЙЕЛЕР ЭВОЛЮЦИЯСЫНЫҢ МӘСЕЛЕЛЕРІ

ЖУРНАЛЫ

№ 3-4 (25)

12.09.2003 ж. Қазақстан Республикасының Ақпарат және коммуникация министрлігінде тіркелген

Куәлік № 4213-Ж

Журнал жылына 4 рет жарыққа шығады
(наурыз, маусым, қыркүйек, желтоқсан)

ЖАУАПТЫ ХАТШЫ
Ережеп Дархан Есейұлы, т.ғ.к., PhD, аға оқытушы *(Қазақстан)*
E-mail: darhan_13@physics.kz

Ашық жүйелер эволюциясының мәселелері журналы – ашық теңдеспеген динамикалық табиғи жүйелердің пайда болуы мен эволюциясы мәселелері бойынша бірегей ғылыми және шолу мақалаларын жариялайтын ғылыми басылым.

ҚАЗАҚ УНИВЕРСИТЕТІ
БАСПА ҮЙІ

Жоба менеджері
Гульмира Шаккозова
Телефон: +7 701 724 2911
E-mail: Gulmira.Shakkozova@kaznu.kz

Пішімі 60x84/8. Көлемі 6,5 б.т. Тапсырыс № 122.
Әл-Фараби атындағы Қазақ ұлттық университетінің «Қазақ университеті» баспа үйі.
050040, Алматы қаласы, әл-Фараби даңғылы, 71.

IRSTI 29.01.11 https://doi.org/10.26577/JPEOS.2023.v25.i3-4.i1

S.H. Sohrab

Northwestern University, U.S.A., Illinois, Evanston
e-mail: s-sohrab@northwestern.edu

INVARIANT MODEL OF BOLTZMANN STATISTICAL MECHANICS AND ITS IMPLICATIONS TO HYDRODYNAMIC MODEL OF ELECTROMAGNETISM, PHYSICAL FOUNDATIONS OF QUANTUM MECHANICS, RELATIVITY, QUANTUM GRAVITY AND QUANTUM COSMOLOGY

Some implications of an invariant model of Boltzmann statistical mechanics to quantum nature of (space, time, mass), physical foundations of quantum mechanics, relativity, electromagnetism and Maxwell equations, quantum gravity and quantum cosmology will be discussed. In harmony with Huygens' analogy between propagation of sound in air and light in ether, propagation of light wave is shown to involve an exceedingly thin longitudinal component besides its Maxwellian transverse polarizations. Following Maxwell and Lorentz, an invariant hydrodynamic model of electromagnetism is presented. It is expected that time-dependence of the speed of light, identified as root-mean-square velocity of gravitons, could be determined by measurement of changes in period of geological events caused by periodic cosmic radiation bursts from sources such as pulsars. New interpretation of physical foundation of quantum mechanics, Dirac wave equation, pilot waves of de Broglie-Bohm model will be described.

Identifying physical space, Aristotle fifth element or Casimir vacuum, as a tachyonic compressible fluid, in harmony with Huygens and Planck compressible ether, Lorentz-FitzGerald contractions becomes causal (Pauli) leading to Poincaré-Lorentz dynamic as opposed to Einstein kinematic theory of relativity. Invariant forms of conservation equations lead to hydrodynamics of universe governed by quantum gravity as a dissipative deterministic dynamic system proposed by 't Hooft. The thermodynamics of universe suggests possible relevance of classical Nordström scalar, and Abraham vector theories of gravitation beside Einstein tensor theory. Also, some implications of the model to quantum cosmology, loop quantum gravity (LQG), and Everett multiverse are discussed.

Key words: electromagnetism, Maxwell equations, quantum mechanics, quantum cosmology, quantum gravity, relativity, T.O.E.

С.Х. Сохраб

Норствестерн университеті, АҚШ, Иллинойс штаты, Эванстон қ.
e-mail: s-sohrab@northwestern.edu

Больцманның статистикалық механикасының инвариантты моделі және оның электромагнетизмнің гидродинамикалық моделіне, кванттық механиканың физикалық негіздеріне, салыстырмалылық, кванттық гравитацияға және кванттық космологияға әсері

Мақалада Больцман статистикалық механикасының инвариантты моделінің кванттық табиғаты (кеңістік, уақыт, масса), кванттық механиканың физикалық негіздері, салыстырмалылық теориясы, электромагнетизм және Максвелл теңдеулері, кванттық гравитация және кванттық космологияның кейбір салдары талқыланады. Гюйгенстің ауадағы дыбыс пен жарықтың таралуы арасындағы ұқсастығына сәйкес, жарық толқынының таралуы көлденең поляризациядан басқа өте жұқа бойлық құрамдас бөлікті қамтиды. Максвелл мен Лоренцтен бөлек электромагнетизмнің инвариантты гидродинамикалық моделі ұсынылған. Гравитондардың орташа квадраттық жылдамдығы ретінде анықталған жарық жылдамдығының уақытқа тәуелділігін пульсарлар сияқты көздерден ғарыштық радиацияның жарқылынан туындаған геологиялық оқиғалар кезеңіндегі өзгерістерді өлшеу арқылы анықтауға болады деп күтілуде. Кванттық механиканың физикалық негіздерінің жаңа түсіндірмесі, Дирак толқын теңдеуі, де Бройль-Бом моделінің пилоттық толқындары сипатталады.

Физикалық кеңістікті, Аристотельдің бесінші элементін немесе Касимир вакуумын, Гюйгенс пен Планктың сығылатын эфирімен үйлесімде тахиондық сығылатын сұйықтық ретінде, Лоренц-Фиц-Джеральд жиырылулары Эйнштейннің кинематикалық реактивтілікке қарсы Пуанкаре-Лоренц динамикасына әкелетін себептік (Паули) болады. Сақтау теңдеулерінің инвариантты формалары Т Хоофт ұсынған диссипативті детерминирленген динамикалық жүйе ретінде кванттық гравитациямен басқарылатын ғаламның гидродинамикасына әкеледі. Әлемнің термодинамикасы Эйнштейннің тензорлық теориясымен қатар классикалық Нордстрем скалярының және Авраамның векторлық гравитация теорияларының ықтимал сәйкестігін болжайды. Сондай-ақ, модельдің кванттық космология, циклдік кванттық гравитация және Эвереттің көптік әлеміне қатысты кейбір салдар талқыланады.

Түйін сөздер: электромагнетизм, Максвелл теңдеулері, кванттық механика, кванттық космология, кванттық гравитация, салыстырмалылық, Т.О.Е.

С.Х. Сохраб

Университ Норсвестерн, штат Иллинойс, США, г. Еванстон
e-mail: s-sohrab@northwestern.edu

Инвариантная модель статистической механики Больцмана и ее последствия для гидродинамической модели электромагнетизма, физических основ квантовой механики, теории относительности, квантовой гравитации и квантовой космологии

В статье будут обсуждаться некоторые последствия инвариантной модели статистической механики Больцмана для квантовой природы (пространства, времени, массы), физических основ квантовой механики, теории относительности, электромагнетизма и уравнений Максвелла, квантовой гравитации и квантовой космологии. В соответствии с аналогией Гюйгенса между распространением звука в воздухе и света в эфире показано, что распространение световой волны включает в себя чрезвычайно тонкую продольную составляющую, помимо максвелловской поперечной поляризации. Вслед за Максвеллом и Лоренцем представлена инвариантная гидродинамическая модель электромагнетизма. Ожидается, что временная зависимость скорости света, определяемая как среднеквадратическая скорость гравитонов, может быть определена путем измерения изменений периода геологических событий, вызванных периодическими всплесками космического излучения от таких источников, как пульсары. Будет описана новая интерпретация физических основ квантовой механики, волнового уравнения Дирака, пилотных волн модели де Бройля-Бома.

Идентифицируя физическое пространство, пятый элемент Аристотеля или вакуум Казимира, как тахионную сжимаемую жидкость, в гармонии со сжимаемым эфиром Гюйгенса и Планка, сокращения Лоренца-Фитцджеральда становятся причинными (Паули), что приводит к динамике Пуанкаре-Лоренца, в отличие от кинематической теории относительности Эйнштейна. Инвариантные формы уравнений сохранения приводят к гидродинамике Вселенной, управляемой квантовой гравитацией как диссипативной детерминированной динамической системой, предложенной Т Хоофтом. Термодинамика Вселенной предполагает возможную значимость классической скалярной теории Нордстрема и векторной теории Абрагама гравитации рядом с тензорной теорией Эйнштейна. Также обсуждаются некоторые последствия модели для квантовой космологии, петлевой квантовой гравитации и мультивселенной Эверетта.

Ключевые слова: электромагнетизм, уравнения Максвелла, квантовая механика, квантовая космология, квантовая гравитация, относительность. Т.О.Е.

Introduction

What is common amongst the diverse fields of chromodynamics, electrodynamics, turbulent hydrodynamics, astrophysics, and cosmology is that they all involve statistical fields composed of very large number of "particles" and particle clusters under turbulent motion. Guided by similarities between small scale stochastic quantum fields [1-17] and large scale turbulent hydrodynamic fields [18-30], a scale invariant model of Boltzmann statistical mechanics was recently developed and applied to the investigation of fluid mechanics [31, 32], thermodynamics [33, 34], and quantum mechanics [35, 36, 37] at large, intermediate, and small scales.

The present study is focused on the application of invariant model of Boltzmann statistical mechanics to: (I) invariant model of quantization of space, time, and mass (II) physical foundation of quantum mechanics and theory of relativity (III) physical foundation of electromagnetism and invariant Maxwell equations (IV) physical foundations of quantum gravity and quantum cosmology. First, a very brief description of invariant model of Boltzmann statistical mechanics and conservation equations are discussed. Next, quantization of space, time, and mass and their invariant definitions are studied. Internal spacetime versus external space and time are described and the latter is identified as Rovelli *thermal time*. Next, a hydrodynamic model of Maxwell theory of electromagnetism is presented. Finally, some implications of invariant Schrödinger equation to cosmology, quantum gravity, quantum cosmology, and multiverse are discussed.

Scale–Invariant Model of Boltzmann Statistical Mechanics and Invariant Conservation Equations

The scale-invariant model of statistical mechanics for equilibrium galactic-, planetary-, hydro-system-, fluid-element-, eddy-, cluster-, molecular-, atomic-, subatomic-, kromo-, and tachyon-dynamics corresponding to the scale β = g, p, h, f, e, c, m, a, s, k, and t is schematically shown on the left hand side of Fig. 1.

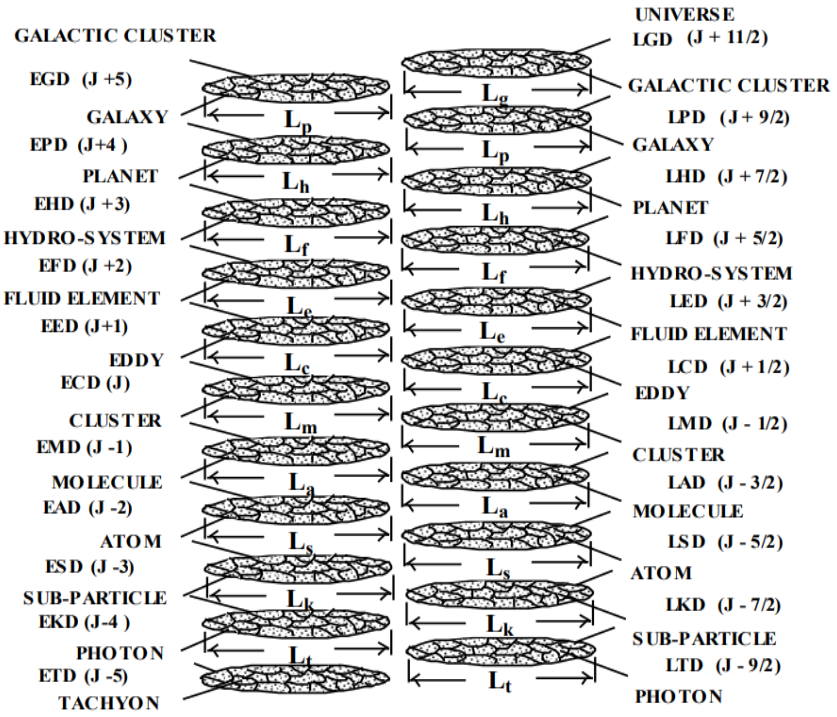

Figure 1 – A scale-invariant model of statistical mechanics. Equilibrium-β-Dynamics on the left-hand-side and non-equilibrium Laminar-β-Dynamics on the right-hand-side for scales β = g, p, h, f, e, c, m, a, s, k, and t as defined in [36]. Characteristic lengths of (system, element, "atom") are $(L_\beta, \lambda_\beta, \ell_\beta)$ and λ_β is the mean-free-path.

For each statistical field, one defines particles that form the background fluid and are viewed as point-mass or "*atom*" of the field. Next, the *elements* of the field are defined as finite-sized composite entities composed of an ensemble of "*atoms*". Finally, ensemble of a large number of "*elements*" is defined as the statistical "*system*" at that particular scale. The most-probable element of scale β defines the "atom" (system) of the next higher β+1 (lower β–1) scale.

Following the classical methods [19, 38-42], the invariant definitions of the density ρ_β, and the velocity of *atom* $\mathbf{u}_\beta$, *element* $\mathbf{v}_\beta$, and *system* $\mathbf{w}_\beta$ at the scale β are given as [31,36]

$$\rho_\beta = n_\beta m_\beta = m_\beta \int f_\beta du_\beta, \quad \mathbf{u}_\beta = \mathbf{v}_{w\beta-1} \tag{1}$$

$$\mathbf{v}_\beta = \rho_\beta^{-1} m_\beta \int \mathbf{u}_\beta f_\beta du_\beta, \quad \mathbf{w}_\beta = \mathbf{v}_{w\beta+1} \tag{2}$$

Similarly, the invariant definitions of the peculiar and diffusion velocities are introduced as

$$\mathbf{V}'_\beta = \mathbf{u}_\beta - \mathbf{v}_\beta, \quad \mathbf{V}_\beta = \mathbf{v}_\beta - \mathbf{w}_\beta, \quad \mathbf{V}_\beta = \mathbf{V}'_{\beta+1} \tag{2}$$

Following the classical methods [19, 38-42], the scale-invariant forms of mass, thermal energy, linear and angular momentum conservation equations at scale β are given as [31, 36]

$$\frac{\partial \rho_{i\beta}}{\partial t_\beta} + \nabla.(\rho_{i\beta}\mathbf{v}_\beta) = \Re_{i\beta} \tag{4}$$

$$\frac{\partial \varepsilon_{i\beta}}{\partial t_\beta} + \nabla.(\varepsilon_{i\beta}\mathbf{v}_\beta) = 0 \tag{5}$$

$$\frac{\partial \mathbf{p}_{i\beta}}{\partial t_\beta} + \nabla.(\mathbf{p}_{i\beta}\mathbf{v}_\beta) = -\nabla.\mathbf{P}_{ij\beta} \tag{6}$$

$$\frac{\partial \boldsymbol{\pi}_{i\beta}}{\partial t_\beta} + \nabla.(\boldsymbol{\pi}_{i\beta}\mathbf{v}_\beta) = \rho_{i\beta}\boldsymbol{\omega}_\beta.\nabla\mathbf{v}_\beta \tag{7}$$

involving the *volumetric density* of thermal energy $\varepsilon_{i\beta} = \rho_{i\beta}\tilde{h}_{i\beta}$, linear momentum $\mathbf{p}_{i\beta} = \rho_{i\beta}\mathbf{v}_{i\beta}$, and angular momentum $\boldsymbol{\pi}_{i\beta} = \rho_{i\beta}\boldsymbol{\omega}_{i\beta}$ (since $r_{a\beta-1} = 1$). Also, $\Re_{i\beta}$ is the chemical reaction rate and $\tilde{h}_{i\beta} = \hat{h}_{i\beta} / m_\beta$ is the absolute enthalpy [36]. It is noted that the time coordinates in equations (4-7) also have a scale subscript β.

As discussed in an earlier study on classical thermodynamics [34], and in harmony with perceptions of Clausius [43, 44], atoms of the field are assumed to have three *simultaneously independent* degrees of freedom associated with their translational, rotational, and vibrational (pulsation) motions. Thus, in axisymmetric cylindrical coordinates (z, θ, r), particles are assumed to undergo internal harmonic translation, rotation, and pulsation in two axial (z+, z–), angular (θ+, θ–), and radial (r+, r-) directions. The classical definition of vorticity involves the curl of linear velocity $\nabla \times \mathbf{v}_\beta = \boldsymbol{\omega}_\beta$ thus giving rotational velocity a secondary status since it depends on particle translational velocity $\mathbf{v}_\beta$. However, it is known that particle's rotation about its center of mass is independent of the translational motion of its center of mass. In other words, translational, rotational, and vibrational (pulsation) motions of particle are independent degrees of freedom that should not be necessarily coupled. To resolve this paradox, iso-spin of particle at scale β is defined as the curl of the velocity at the next lower scale of β – 1 [36]

$$\boldsymbol{\varpi}_\beta = \nabla \times \mathbf{u}_\beta = \nabla \times \mathbf{v}_{\beta-1} = \boldsymbol{\omega}_{\beta-1} \tag{8}$$

such that rotational velocity, while having a connection to some type of translational motion at internal scale β – 1 retains its independent degree of freedom at the external scale β as desired. A schematic description of iso-spin and vorticity fields is shown in Fig. 2.

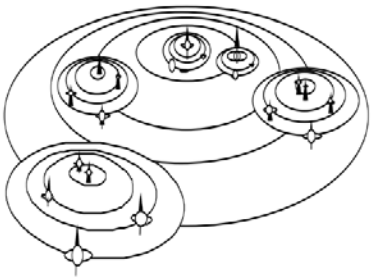

Figure 2 – Description of internal (iso-spin) versus external vorticity fields in cosmology [36].

The nature of galactic vortices in cosmology and the associated dissipation have been discussed [26, 45].

The invariant continuity equation (4) involves invariant form of classical formula for "chemical reaction rate" defined as [40]

$$\Re_{i\beta} = m_{i\beta}\int(\delta f_{i\beta}/\delta t)du_{i\beta} \tag{9}$$

To reveal the scale invariant form of the reaction rate $\Re_g$, it is noted that

$$\sum_i \Re_{i\beta} = \sum_i m_{i\beta}\int(\delta f_{i\beta}/\delta t)du_{i\beta} =$$

$$= \frac{\delta}{\delta t}\sum_i m_{i\beta}\int f_{i\beta}du_{i\beta} = \frac{\delta}{\delta t}\sum_i m_{i\beta}n_{i\beta} =$$

$$= \frac{\delta}{\delta t}\sum_i \rho_{i\beta} = \frac{\delta\rho_{\beta+1}}{\delta t} = \frac{\delta}{\delta t}(m_{\beta+1}n_{\beta+1}) =$$

$$= m_{\beta+1}\int(\delta f_{\beta+1}/\delta t)du_{\beta+1} = \Re_{\beta+1} \tag{10}$$

The local velocity $\mathbf{v}_\beta$ in (4)-(7) is expressed in terms of convective $\mathbf{w}_\beta$ and diffusive $\mathbf{V}_\beta$ velocities [36]

$$\mathbf{w}_\beta = \mathbf{v}_\beta - \mathbf{V}_{\beta g},\ \mathbf{V}_{\beta g} = -D_\beta\nabla\ln\rho_\beta \tag{11}$$

$$\mathbf{w}_\beta = \mathbf{v}_\beta - \mathbf{V}_{\beta tg}.\ \mathbf{V}_{\beta tg} = -\alpha_\beta\nabla\ln\varepsilon_\beta \tag{12}$$

$$\mathbf{w}_\beta = \mathbf{v}_\beta - \mathbf{V}_{\beta hg}.\ \mathbf{V}_{\beta hg} = -\tilde{\kappa}_\beta\nabla\ln\mathbf{p}_\beta \tag{13}$$

$$\mathbf{w}_\beta = \mathbf{v}_\beta - \mathbf{V}_{\beta rhg}.\ \mathbf{V}_{\beta rhg} = -\tilde{\kappa}_\beta\nabla\ln\boldsymbol{\pi}_\beta \tag{14}$$

where $(\mathbf{V}_{\beta g}, \mathbf{V}_{\beta tg}\mathbf{V}_{\beta hg}, \mathbf{V}_{\beta rhg})$ are respectively diffusive, thermo-diffusive, translational and rotational hydro-diffusive velocities and $\tilde{\kappa}_\beta = \eta_\beta/\rho_\beta$ is kinematic viscosity.

Because by definition fluids can only support compressive normal forces, following *Cauchy*, the total stress tensor for fluids is expressed as [46, 47]

$$P_{ij\beta} = p_\beta\delta_{ij} + (\lambda_\beta + \frac{1}{3}\eta_\beta)\nabla.\mathbf{v}_\beta\delta_{ij} \tag{15}$$

Also, the classical Stokes assumption of zero bulk viscosity relates the two *Lame* constants of ideal fluid by [47]

$$b_\beta = \lambda_\beta + \frac{2}{3}\eta_\beta = 0 \tag{16}$$

Hence, the total stress tensor (15) becomes [36]

$$P_{ij\beta} = p_\beta\delta_{ij} - \frac{1}{3}\eta_\beta\nabla.\mathbf{v}_\beta\delta_{ij} = (p_{t\beta} + p_{h\beta})\delta_{ij} \tag{17}$$

where the hydrodynamic pressure is

$$p_{h\beta} = (\tau_{xx\beta} + \tau_{yy\beta} + \tau_{zz\beta})/3 = -\frac{1}{3}\eta_\beta\nabla.\mathbf{v}_\beta \tag{18}$$

The occurrence of a single rather than two Lame constants is in accordance with the perceptions of Cauchy and Poisson who both assumed the limit of zero for the expression [48]

$$\lambda'_\beta + \eta_\beta = \lim_{R\to 0} R^4 f(R) \tag{19}$$

Therefore, in *Cauchy-Poisson* limit (19), as intermolecular spacing vanishes $R \to 0$, all tangential stresses will vanish as was emphasized by *Darrigol* [48]

"Poisson and Cauchy both assumed the limit to be zero. Then the medium loses its rigidity since the transverse pressures disappear"

leaving only normal stresses in (17).

Following the classical methods [19, 38-42], by substituting from (11)-(16) into (4)-(7), neglecting cross-diffusion terms, and applying Onsager [49] reciprocity relations, the invariant forms of conservation equations are written as [36]

$$\frac{\partial\rho_{i\beta}}{\partial t_\beta} + \mathbf{w}_\beta.\nabla\rho_{i\beta} = D_{i\beta}\nabla^2\rho_{i\beta} + \Re_{i\beta} \tag{20}$$

$$\frac{\partial T_{i\beta}}{\partial t_\beta} + \mathbf{w}_\beta.\nabla T_{i\beta} = \alpha_{i\beta}\nabla^2 T_{i\beta} + \tilde{h}_{i\beta}\Re_{i\beta}/\rho_{i\beta}c_{p\beta} \tag{21}$$

$$\frac{\partial \mathbf{v}_\beta}{\partial t_\beta} + \mathbf{w}_\beta.\nabla\mathbf{v}_\beta = \tilde{\kappa}_\beta\nabla^2\mathbf{v}_\beta - \frac{\nabla p_\beta}{\rho_\beta} + \frac{1}{3}\tilde{\kappa}_\beta\nabla(\nabla.\mathbf{v}_\beta) - \frac{\mathbf{v}_\beta\Re_\beta}{\rho_\beta} \quad (22)$$

$$\frac{\partial \boldsymbol{\omega}_{i\beta}}{\partial t_\beta} + \mathbf{w}_\beta.\nabla\boldsymbol{\omega}_{i\beta} = \tilde{\kappa}_\beta\nabla^2\boldsymbol{\omega}_{i\beta} + \boldsymbol{\omega}_{i\beta}\nabla.\mathbf{v}_{i\beta} - \frac{\boldsymbol{\omega}_{i\beta}\Re_{i\beta}}{\rho_{i\beta}} \quad (23)$$

Modified form of the viscous equation of motion (22) is to be compared with the classical Navier-Stokes equation

$$\frac{\partial \mathbf{v}}{\partial t} + \mathbf{v}.\nabla\mathbf{v} = \tilde{\kappa}\nabla^2\mathbf{v} - \frac{\nabla p}{\rho} + \frac{1}{3}\tilde{\kappa}\nabla(\nabla.\mathbf{v}) \quad (24)$$

The history of derivation of (24) has been studied in an excellent investigation by Darrigol [46]. The main difference between equations (22) and (24) is the occurrence of the global (not differentiable) convective velocity $\mathbf{w}_\beta$ as opposed to local (differentiable) velocity $\mathbf{v}_\beta$ in the second term. Thus, the former equation is more in harmony with the pioneering studies by Oseen [50] and Carrier [51]. As a result, in the absence of convection, (22) reduces to nonhomogeneous diffusion equation similar to (20) and (21). However, the absence of local velocity results in vanishing of almost the entire classical equation of motion (24). In Section 6, solution of the modified form of equation of motion (22) for the classical problem of Stokes viscous flow across a rigid cylinder and resolution of Stokes paradox will be discussed.

Similarly, modified form of Helmholtz [52] vorticity equation (23) is to be compared with the classical equation in absence of chemical reaction

$$\frac{\partial \boldsymbol{\omega}}{\partial t} + \mathbf{v}.\nabla\boldsymbol{\omega} = \tilde{\kappa}\nabla^2\boldsymbol{\omega} + \boldsymbol{\omega}\nabla.\mathbf{v} \quad (25)$$

An important difference between the modified (23) and the classical (25) forms of *Helmholtz* vorticity equation is the occurrence of convective velocity $\mathbf{w}_\beta$ as opposed to local velocity $\mathbf{v}_\beta$ in the second term. Because local vorticity $\boldsymbol{\omega}_\beta$ in (25) is itself related to the curl of local velocity it cannot be advected by this same velocity. On the other hand, advection of local vorticity by convective velocity $\mathbf{w}_\beta$ in (23) is possible. Moreover, in absence of convection (23) reduces to the diffusion equation similar to that in (20), (21), and (22) for mass, heat, and linear momentum transport. However, the absence of local velocity in (25) leads to vanishing of the entire equation.

Hierarchies of Quantum Fields with Atomic Mass Unit, Internal Spacetime, and External Space and Time

Like all statistical fields in the hierarchy shown in Fig. 1, the field of stochastic chromodynamics that is the physical space is also real. It is well known that in late 1800's, most scientists believed that space was filled with a fluid called luminiferous ether that was the seat of electromagnetic waves. In recent investigations [35-37], the ether was identified as the physical space itself rather than a substance filling the space. To use a glass of water as an example, physical space is identified as water itself rather than the glass. Hence, physical space is identified as a compressible tachyon fluid in harmony with perceptions of Aristotle [53], Huygens [54], Newton [55], Euler [56], Maxwell [57], Lorentz [58], Poincaré [59-62], de Broglie [3], Casimir [63], and Dirac [64] amongst many others. The history of classical ether theories is discussed in an excellent book by Whittaker [65].

As discussed in [36], physical space or Casimir vacuum [63] is identified as a compressible tachyonic fluid schematically shown in Fig. 3, from infinite rarefaction (*white hole* WH) to infinite compression (*black hole* BH).

Hence, four significant characteristics of ether are (a) ether is the physical space or Casimir [63] vacuum itself and not its occupier (b) in accordance with perceptions of Huygens [54], ether is a compressible fluid (c) ether is *stochastically stationary* because, as emphasized by Dirac [64], static ether cannot satisfy both relativity theory and quantum mechanics (d) ether is an atomic thus quantum fluid (Fig. 1).

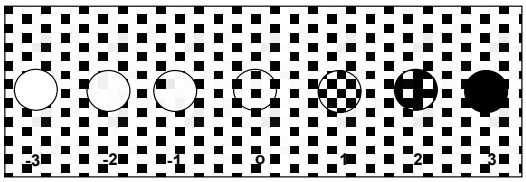

Figure 3 – Different degrees of rarefaction and compression of Casimir vacuum identified as a compressible fluid. **(-3)** White hole $\rho_{WH} = 0$ **(-2, -1)** Anti-matter $\rho_{AM} < \rho_v$ **(0)** Casimir vacuum $\rho = \rho_v$ **(1, 2)** Matter $\rho_{MA} > \rho_v$ **(3)** Black hole $\rho_{BH} = \infty$ [37].

Among various properties of physical space, its compressibility plays the most central role in physical foundations of theory of relativity discussed in next Section, and propagation of light in hydrodynamic model of Maxwell [57] theory of electromagnetism discussed in Section 5. Therefore, we begin the discussion of space and time with an important quotation from Huygens' treatise on light concerning analogy between propagation of sound in air and that of light in ether [54]

"As regards the different modes in which I have said the movement of Sound and of Light are communicated, one may sufficiently comprehend how this occurs in the case of Sound if one considers that the air is of such nature that it can be compressed and reduced to a much smaller space than that which it ordinarily occupies,"

"Now in applying this kind of movement to that which produces Light there is nothing to hinder us from estimating the particles of the ether to be of a substance as nearly approaching to perfect hardness and processing a springiness as prompt as we choose. It is not necessary to examine here the causes of this hardness, or of that springiness, the consideration of which would lead us too far from our subject. I will say, however, in passing that we may conceive that the particles of the ether, notwithstanding their smallness, are in turn composed of the other parts and that their springiness consists in the very rapid movement of a subtle matter which penetrates them from every side and constrains their structure to assume such disposition as to give to this fluid matter the most overt and easy passage possible. This accords with the explanation which Mr. Des Cartes gives for the spring, though I do not, like him, suppose the pores to be in the form of round hollow canals. And it must not be thought that in this there is anything absurd or impossible, it being on the contrary quite credible that it is this infinite series of different sizes of corpuscles, having different degrees of velocity, of which Nature makes use to produce so many marvelous effects,"

Therefore, Huygens considered atoms of ether to be further divisible and have different velocities in harmony with infinite hierarchies of statistical fields shown in Fig. 1. This is also in harmony with perceptions of Lorentz [66] who believed that ether fluid penetrates electrons as atoms of electrodynamics field

"Now, if within an electron there is ether, there can also be an electromagnetic field, and all we have got to do is to establish a system of equations that may be applied as well to the parts of the ether where there is an electric charge, i.e. to the electrons, as to those where there is none."

Also, the significance and central role of ether as carrier of electromagnetic waves in theory of electron was emphasized by Lorentz [58]

"I cannot but regard the ether, which is the seat of an electromagnetic field with its energy and its vibrations, as endowed with certain degree of substantiality, however different it may be from all ordinary matter"

Finally, even though he believed in relational concepts of space and time, the importance of reality of absolute space was emphasized by Leibniz [67]

"If space is an absolute reality, far from being a property or accident opposed to substance, it will have a greater reality than substances themselves,"

When physical space is identified as a compressible fluid described by Boltzmann statistical mechanics at thermodynamic equilibrium, the two *universal constants* of nature namely Planck and Boltzmann constants (h, k) are related to stochastic *spatial* and *temporal* aspects of Casimir [63] vacuum fluctuations as [34]

$$h = h_k = m_k c < \lambda_k^2 >^{1/2} = 6.626 \times 10^{-34} \text{ J-s} \quad (26)$$

$$k = k_k = m_k c < \nu_k^2 >^{1/2} = 1.381 \times 10^{-23} \ \text{J/m} \quad (27)$$

Stochastically stationary Planck and Boltzmann constants in (26-27) lead to four invariant *universal* thermodynamic properties namely gravitational mass of photon, atomic-mass-unit *amu*, Avogadro-Loschmidt number, and universal gas constant [34]

$$m_k = (hk / c^3)^{1/2} \approx 1.84278 \times 10^{-41} \ \text{kg} \quad (28)$$

$$amu = m_k c^2 = (hkc)^{1/2} \approx 1.6563 \times 10^{-27} \ \text{kg} \quad (29)$$

$$N^o = 1/(m_k c^2) = 1/(hkc)^{1/2} \approx 6.0376 \times 10^{26} \ \text{kmol}^{-1} \quad (30)$$

$$R^o = N^o k = (k / hc)^{1/2} \approx 8.338 \ \text{kJ/kmol-m} \quad (31)$$

According to (29), all atoms are composed of photons such that at the most fundamental level, the entire universe is constructed from physical space i.e., Casinir [63] vacuum in harmony with perceptions of Leibniz described in quotation above. Possible electromagnetic nature of all matter was anticipated by Newton [55], Lorentz [58], and Poincaré [59].

It was emphasized by Pauli [68] that

"No quantity with the dimension of time occurs in thermodynamics; at the most, time enters as the concept of "before" and "after". Therefore, in the case of rapidly occurring processes, only initial and final states are discussed."

More recently, Rovelli [69] in an excellent book about nature of time, compares Aristotle's concept of time as a measure of change with Newton concept of absolute time. Also, time was suggested to have a thermodynamic origin by Rovelli [70,71]

"The theory seems to indicate that there is no explanation for the peculiar properties of the time variable at the mechanical level. We suggest that such an explanation should be searched at the thermodynamical level. We propose the idea that the very concept of time is meaningful only in the thermodynamic context"

The nature of thermodynamic, psychological, as well as cosmological arrows of time were discussed by Hawking **[**72],

"Both Aristotle and Newton believed in absolute time. That is, they believed that one could unambiguously measure the interval of time between two events, and this time would be the same whoever measured it, provided they used a good clock. Time was completely separate from and independent of space. This is what most people would take to be the commonsense view. However, we have had to change our ideas about space and time. Although our apparently commonsense notions work well when dealing with apples, or planets that travel comparatively slowly, they don't work at all for things moving at or near the speed of light."

Concerning Aristotle's notion of time, we quote from Vladimirov et. al., [73]

"In the same manner that he denied the existence of the vacuum, Aristotle refused to accept the notion that time is independent of events. His argument was that time cannot exist without change, that is if the present were not different in each situation but remained the same, there would be no time,"

Therefore, perhaps from a different perspective, it may be said that Aristotle did not believe in the notion of *absolute time* contrary to assertion in the above quotation from Hawking [72]. In other words, if time is to be defined in terms of the state of *change* which is itself known to be easily altered, the notion of absoluteness may no longer be attributed to such a time. It is most natural to maintain that in the absence of all motions there is no time at all, since the concept of time in the *absence of all motions* (changes) is an empty and meaningless concept as emphasized by Aristotle [53].

Although the dimension of time does not explicitly occur in thermodynamics according to above quotation from Pauli [68], both space and time do occur in the definition of thermodynamic temperature as it relates to the kinetic energy of oscillators [74]

$$m_\beta u_\beta^2 = m_{\beta-1} v_{w\beta-1}^2 = kT_{\beta-1} = k\lambda_{w\beta-1} \quad (32)$$

resulting in introduction of the concepts of *internal spacetime* versus *external space and time* [74]. Hence, by definition of most-probable or Wien speed $v_{w\beta} = \lambda_{w\beta} \nu_{w\beta} = \lambda_{w\beta} / \tau_{w\beta}$, one associates

constant internal measures of (extension, duration) [74]

$$\begin{cases} \lambda_{ws} & \text{Internal measure of extension} \\ \tau_{ws} & \text{Internal measure of duration} \end{cases} \tag{33}$$

with every "point" or "atom" of space at constant temperature $T_\beta = T_{\beta-1}$.

According to Fig.1, the statistical field $\mathbb{F}_\beta$ at scale β resides within a background "space" $\mathbb{S}_\beta$ that is the statistical field $\mathbb{S}_\beta \Leftrightarrow \mathbb{F}_{\beta-1}$ at the adjacent lower scale $\beta-1$. For example, considering astrophysics $\beta = s$ at thermodynamic equilibrium, Wien wavelength of thermal oscillations of particles (stars) defines absolute thermodynamic temperature $T_s = \lambda_{ws}$ that leads to internal measures of spacetime $(\lambda_{ws}, \tau_{ws})$ associated with every "point" or "atom" of cosmological space $\mathbb{S}_g \Leftrightarrow \mathbb{F}_s$ at scale $\beta+1 = g$. Hence, for the study of dynamics of galaxies and their clusters in cosmology, *external* independent space and time coordinates (x_g, t_g) are defined in terms of the internal spacetime as [74]

$$(x_g, y_g, z_g) = (N_{xg}, N_{yg}, N_{zg})\lambda_{ws}, \quad t_g = N_{tg}\tau_{ws} \tag{34}$$

where $(N_{x\beta}, N_{y\beta}, N_{z\beta}, N_{t\beta})$ are independent numbers. The external time t_β in (34) is called Rovelli [69-71] *thermal time*.

According to (33)-(34), both internal and external space and time are quantized. The thermodynamic internal spacetime $(\lambda_{w\beta-1}, \tau_{w\beta-1})$ are *local sub-atomic dependent units* of space and time. On the contrary, the external space and time in (34) relate to *global* dynamics and are both *independent* and *irreversible*. Irreversibility of time or Eddington *arrow of time* is related to dissipations hence entropy according to second law of thermodynamics [74]. Irreversibility of space coordinates arises from its quantum nature through Heisenberg [75] *matrix mechanic* thus leading to noncommutative spectral geometry described by Connes [76]. The four dimensions $(x_\beta, y_\beta, z_\beta, t_\beta)$ constitute Poincaré [61] and Minkowski [77] pseudo-Riemannian space with three real space and one imaginary time dimensions.

Because time no longer explicitly appears in the field equations of general theory of relativity (GTR), some authors have claimed that time may be an illusion. However, as evident from their definitions in (34), external space and time retain their intuitive reality as measurable physically real entities. Also, and most importantly, external time and space in (34) are *totally different and independent coordinates that are not symmetric*. As noted by Verhulst [78], asymmetry of space and time was emphasized by Lorentz in his 1915 lecture at the Royal Academy of Sciences in Amsterdam:

"Why can we not speak of the ether instead of vacuum? Space and time are not symmetric; a material point can at different times be at different spots, but not in different places at the same time"

External space and time in (34) are only defined up to the critical atomic units $(N_{x\beta} = N_{t\beta} = 1)$. Below this atomic scale, one must move to statistical field at the next lower scale $\beta-1$ and employ (34) to obtain new space and time based on ruler and clock (spacetime) of scale $\beta-2$. At thermodynamic equilibrium between particle and radiation i.e., background "space" of Casimir [63] vacuum, following de Broglie's wavelength of matter waves, the definition of Boltzmann constant (27) naturally leads to the concept of *frequency of matter waves* [34]

$$\lambda_\beta = h / \overline{p}_\beta \quad \text{WAVELENGTH OF MATTER WAVE} \tag{35}$$

$$\nu_\beta = k / \overline{p}_\beta \quad \text{FREQUENCY OF MATTER WAVE} \tag{36}$$

where $\overline{p}_\beta = m_\beta v_{r\beta}$ is root-mean-square momentum of particle.

In usual quantum mechanics, unlike Heisenberg [79] uncertainty principle involving space and momentum, there is no uncertainty relation involving time and momentum as discussed by Schommers [80]

"Within usual quantum theory, space-coordinate and time are not symmetrical to each other, which is in contrast to the basic results of the special theory of relativity. In usual quantum

theory coordinates are operators and play the role of statistical quantities; time however does not behave statistically and remains a simple parameter when we go from classical to quantum mechanics. for this reason, there is no uncertainty relation for the time and energy within the quantum theory which would agree in its physical content with the coordinate and momenta."

However, because of the definition of Boltzmann constant (27), parallel to Heisenberg [79] *spatial uncertainty principle*, one can introduce *temporal uncertainty principle* [35,36]

$$\Delta\lambda_\beta \Delta\overline{p}_\beta \geq h \quad \text{SPATIAL UNCERTAINTY PRINCIPLE} \tag{37}$$

$$\Delta\nu_\beta \Delta\overline{p}_\beta \geq k \quad \text{TEMPORAL UNCERTAINTY PRINCIPLE} \tag{38}$$

Temporal uncertainty principle (38) places a limit on maximum resolution of time measurements.

Having defined space and time, the concept of atomic mass is examined next. Early literature concerning gravitational, electromagnetic, relativistic, aspects of concept of mass have been reviewed in an excellent book by Jammer [81]. The ambiguity associated with the meaning of mass was emphasized by Poincaré [82]

"There is no escape from the following definition, which is only a confession of failure: Masses are coefficients which it is found convenient to introduce into calculations".

Also, according to Einstein [83]

"Neither Newtonian nor the relativistic theory of gravitation has so far led to any advance in the theory of the constitution of matter".

Regarding another quotation from Einstein [84]

"Mass and energy are essentially alike; they are only different expressions for the same thing"

the fact that mass [kg] and energy [J] have *different dimensions* makes the understanding of such equivalence less intuitive.

By invariant definition (1) in the hierarchy of statistical fields shown in Fig. 1, one defines the "atomic" mass unit $\hat{m}_\beta$ at the scale β as the most-probable or Wien mass $m_{w\beta-1}$ of the lower scale $\beta-1$, that is the internal energy of the next lower scale $\beta-\tilde{2}$ For example, the classical atonic mass-unit *amu* at EAD scale in (29) is the most probable mass of ESD field

$$\hat{m}_a = amu_a = m_{ws} \tag{39}$$

that in turn is atomic internal energy of EKD field that is photon [33,34]

$$amu\ [\text{kg}] = \sqrt{hkc} = m_k c^2\ [\text{J}] = \hat{u}_k = 3kT_k \tag{40}$$

In (40), the origin of equivalence of *dimensions* of mass [kilogram] and energy [Joule] is fully revealed. Total internal energy or *electromagnetic mass* [34] of ideal photon gas becomes

$$M_{EM} = N(amu) = N\hat{u}_k = U_k = 3NkT_k \tag{41}$$

In his pioneering 1847 paper, Helmholtz [85] decomposed the total thermal energy of an ideal gas at thermodynamic equilibrium into two parts namely kinetic energy or *free heat* and potential energy or *latent heat* that were recently identified as *internal energy U* and *potential energy* pV [33,34]. Therefore, besides the internal energy (40), stability of particles requires an *external pressure* hence potential energy called Poincaré stress [34]. At thermodynamic equilibrium, due to equality of external and internal pressures, atomic potential energy of photon is

$$p_k \hat{v} = \hat{u}_k / 3 = kT_k \tag{42}$$

resulting in total potential energy, dark matter, or *gravitational mass* of photon [33,34]

$$M_{GR} = M_{DM} = p_k N\hat{v} = p_k V = NkT_k \tag{43}$$

Therefore, just like monatomic ideal gas, the total energy of photon gas at thermodynamic equilibrium is the sum of its electromagnetic and gravitational energy that is what Sommerfeld [86] called "total heat" or enthalpy

$$M_{\rm tot} = M_{\rm DE} + M_{\rm DM} = U_{\rm k} + {\rm p}V_{\rm k} = H_{\rm k} \qquad (44)$$

The ideal gas law (43) helps to reveal Joule-Mayer mechanical equivalent of heat and *mass-energy equivalence* discussed in an interesting but unfortunately little known 1904 study by Olinto de Pretto [87] who wrote:

"The vis viva $\mathrm{m}v^2$ *and the formula* $mv^2/8338$ *gives us, expressed in calories, such energy. Given that m = 1 and v equals three hundred thousand kilometers per second, that is 300 million meters, which would be the speed of light, also allowed for the ether, everyone will see that you get an amount of calories represented by 10794 followed by 9 zeros and that is over ten million million."*

containing de Pretto formula

$$\mathrm{mc}^2\,[\mathrm{kcal}] = \mathrm{mc}^2/8338 \;\; [\mathrm{Joule}] \qquad (45)$$

De Pretto number 8338 in (45) is numerically identical to the universal gas constant in (31) expressed in MKS units $\mathrm{R}^{\circ} = 8338$ [J/(kmol-m] [34]. This is because the factor of 2 in definition of temperature $T' = 2T$ [34] leads to modified value of Joule-Mayer mechanical equivalent of heat $J = 2J_{\rm c} = 2\times 4.169 = 8338$ [Joule/kcal] where the classical value $J_{\rm c} = 4.169 \approx 4.17$ kJ/kcal is the average of the two values $J_{\rm c} = (4.15, 4.19)$ reported by Pauli [68]. Hence, the ideal gas law in (43) gives

$$\mathrm{p_k}V = \textit{Work [J]} = (N^{\circ}\mathrm{k})(N/N^{\circ})T = \tilde{N}R^{\circ}T$$

$$= R^{\circ}\,[J/(kmol-m)](\tilde{N}T)[kmol-m] \qquad (46)$$

By definition, thermal energy unit kcal corresponds to the amount of energy required to raise the temperature of one kg of water by unity hence $T = 1$ m

$$R^{\circ}\,[J/(kmol-m)] = R^{\circ}\,[J/kcal] = \\ = J \approx 8338\,[J/kcal] \qquad (47)$$

and (47) assumes the classical form of mechanical equivalent of heat [34,68,86]

$$W = JQ \qquad (48)$$

Regarding mass energy equivalence, Okun [88] has argued that amongst the formulas

$$E = \mathrm{mc}^2 \quad \text{Poincaré} \qquad (49)$$

$$E_{\rm o} = \mathrm{mc}^2 \quad \text{Einstein} \qquad (50)$$

$$E_{\rm o} = \mathrm{mc}^2 \qquad (51)$$

$$E_{\rm o} = \mathrm{m_o c}^2 \qquad (52)$$

rather than the correct formula (49) introduced by Poincaré [59] in 1900, the formula (50) introduced later by Einstein [83] in 1905 is correct. Therefore, Okun [88] has in effect challenged the validity of the concept of relativistic mass of Lorentz [89]

$$\mathrm{m} = \mathrm{m_r} = \mathrm{m_o}/\sqrt{1-\mathrm{v}^2/\mathrm{c}^2} \qquad (53)$$

However, validity of (53) is evident from the fact that its multiplication with square of the speed of light results in the well-known relativistic energy transformation formula [59-62, 83-84]

$$E = E_{\rm o}/\sqrt{1-\mathrm{v}^2/\mathrm{c}^2} \qquad (54)$$

In formula (54), E refers to total or relativistic energy and hence involves total or relativistic mass of Lorentz (53), that upon expansion in powers of $\varepsilon = (\mathrm{v}/\mathrm{c})^2 << 1$ gives

$$E = \mathrm{m_r c}^2 \approx \mathrm{m_o c}^2 + \mathrm{m_o v}^2/2 + \\ +(3/8)\mathrm{m_o v}^4/\mathrm{c}^2 + \ldots \qquad (55)$$

However, expansion of the formula of Okun [88]

$$E = E_{\rm o} + E_{\rm kin} = \sqrt{\mathbf{p}^2\mathrm{c}^2 + \mathrm{m}^2\mathrm{c}^4} = \\ = \mathrm{mc}^2 + \frac{\mathbf{p}^2}{2\mathrm{m}} + \ldots \qquad (56)$$

to the next higher order of approximation gives

$$E = \mathrm{mc}^2 + \mathrm{mv}^2/2 - (1/8)\mathrm{mv}^4/\mathrm{c}^2 + \ldots \quad (57)$$

that is different from (55). The discrepancy is because (56) is equivalent to $E = E_o\sqrt{1+\mathrm{v}^2/\mathrm{c}^2}$ that does not agree with (54). Ironically, the quotation in Okun [88] paper contains the following statement by Einstein [84],

"The mass of a body is not a constant; it varies with changes in its energy"

The misunderstanding could in part be due to the fact that instead of Lorentz [89] relativistic mass transformation (53), Einstein [84] wrote

$$E = m/\sqrt{1-\mathrm{v}^2/\mathrm{c}^2} \quad (58)$$

Because both electromagnetic and gravitational mass in (41) and (43) are kinetic energy, the terminology "rest energy" used by Okun [88] could be modified to "stochastically stationary energy". This is because according to the present model, and in harmony with quantum mechanics, the state of rest or absolutely "static" state corresponds to $T_\beta = \lambda_{w\beta} = 0$ that is a singularity of the field inside black hole [90] as discussed in the last Section on cosmology.

In a related matter, it was stated by Einstein [84] and often repeated by others, that matter cannot be accelerated to the speed of light because by Poincaré-Einstein formula (54), this requires infinite amount of energy and hence is impossible. However, this is contrary to the fact that conversion of matter into light is very common occurrence in nature as anticipated by Newton [55] and in fact happens whenever we strike a match or light a candle!

In addition to (50) corresponding to *electromagnetic mass*, one must also account for potential energy or *gravitational mass* associated with *Poincaré stress* that is responsible for particle stability [34,37,90]. The infinite energy just mentioned is avoided because as matter is accelerated by heating, before reaching the speed of light $\mathrm{c} = \sqrt{3}\mathrm{v}_{wk+}$, it gets to the most probable or Wien speed [90]

$$\begin{aligned} \mathrm{v}_\beta^2 \to \mathrm{v}_{w\beta}^2 &= 2\mathrm{v}_{w\beta+}^2 = \\ &= 2\mathrm{v}_{r\beta+}^2/3 = 2\mathrm{c}_\beta^2/3 \end{aligned} \quad (59)$$

For example, for photon gas $\beta = \mathrm{k}$ in enclosures, substituting from (59) in (54) results in *finite* total energy given in 1905 by Hasenöhrl [91,92]

$$\begin{aligned} E &= E_o/\sqrt{1-\mathrm{v}^2/\mathrm{c}^2} \approx \\ &\approx m_o\mathrm{c}^2\left(1+\frac{\mathrm{v}^2}{2\mathrm{c}^2}\right) = \frac{4}{3}m_o\mathrm{c}^2 \end{aligned} \quad (60)$$

Total atomic energy of photon in (60) is the same as photon atomic enthalpy [36] obtained from (44)

$$\begin{aligned} \hat{\mathrm{h}}_k &= \mathrm{m}_k\mathrm{u}_k^2 = \hat{\mathrm{u}}_k + \mathrm{p}_k\hat{\mathrm{v}} = 4\mathrm{kT} = \\ &= 4\mathrm{m}_k\mathrm{v}_{wk+}^2 = (4/3)\mathrm{m}_k\mathrm{c}^2 \end{aligned} \quad (61)$$

By (61), the superluminal longitudinal root-mean square speed of *atomic* photon becomes

$$\mathrm{u}_k = 2\mathrm{v}_{wk} = 2\mathrm{c}/\sqrt{3} \quad (62)$$

The result (62) is in agreement with the ratio of *longitudinal* to *transverse* wave propagation speeds in elastic media given by Achenbach [93] as

$$\begin{aligned} \mathrm{C}_L/\mathrm{C}_T = \kappa &= \left[(\lambda+2\eta)/\eta\right]^{1/2} = \\ &= \left[\left(2(1-\nu)/(1-2\nu)\right)\right]^{1/2} = 2/\sqrt{3} \end{aligned} \quad (63)$$

with Lame constant $\lambda = -2\eta/3$, Poisson ratio $\nu = -1$ that marginally satisfies stability criteria $-1 < \nu < 1/2$ [47], $\mathrm{C}_{L\beta}^2 = 2\mathrm{v}_{w\beta}^2 = 4\mathrm{v}_{w\beta+}^2$ by (3) since $< \mathrm{v}_{w\beta}^2 > = < \mathrm{v}_{w\beta}'^2 >$ due to Boltzmann principle of equipartition of energy, and $\mathrm{C}_{T\beta}^2 = \mathrm{C}_\beta^2 = 3\mathrm{v}_{w\beta+}^2$. The Lame constant $\lambda = -2\eta/3$ satisfies Stokes assumption of vanishing *bulk modulus* or bulk viscosity (16). Also, as sum of two *stochastic velocities* according to (3), $\mathrm{C}_L = 2\mathrm{C}/\sqrt{3}$ is superluminal [94,95].

To conclude this Section, it is instructive to note that definition of (space, time, mass) of each statistical field within hierarchies of scales (Fig. 1)

$$(x_\beta, y_\beta, z_\beta, t_\beta, m_\beta) =$$
$$= [(N_{x\beta}, N_{y\beta}, N_{z\beta})\lambda_{w\beta-1}, N_{t\beta}\tau_{w\beta-1}, N_{m\beta}m_{w\beta-1}] \quad (64)$$

are relegated to the corresponding entities at the next lower scale by *independent* numbers $(N_{x\beta}, N_{y\beta}, N_{z\beta}, N_{t\beta}, N_{m\beta})$. Matter is considered to be infinitely divisible [90,96] because space, time, and mass must follow the philosophy of Anaxagoras [97]

"Neither is there a smallest part of what is small, but there is always a smaller, for it is impossible that what is should ever cease to be"

By infinite regression in (64), the reality of space, time, and matter hence epistemology of all existence (Fig. 1) reduces to *pure numbers*. This is in harmony with the perceptions of Pythagoras and Plato who ascribed all physical reality to *pure numbers* as eloquently described by Sommerfeld [98]

"Our spectral series, dominated as they are by integral quantum numbers, correspond, in a sense, to the ancient triad of the lyre, from which the Pythagoreans 2500 years ago inferred the harmony of the natural phenomena; and our quanta remind us of the role which the Pythagorean doctrine seems to have ascribed to the integers, not merely as attributes, but as the real essence of physical phenomena"

Physical Foundations of Quantum Mechanics and Theory of Relativity

Our discussion of physical foundation of quantum mechanics starts with an important quotation from Boltzmann, who anticipated quantum mechanics by about three decades, taken from his pioneering and unfortunately often neglected 1872 paper [99]

"We wish to replace the continuous variable x by a series of discrete values ε, 2ε, 3ε ... pε. Hence, we must assume that our molecules are not able to take up a continuous series of kinetic energy values, but rather only values that are multiples of a certain quantity ε. Otherwise, we shall treat exactly the same problem as before. We have many gas molecules in a space R. They are able to have only the following kinetic energies:

ε, 2ε, 3ε, 4ε, . . . pε

No molecule may have an intermediate or greater energy. When two molecules collide, they can change their kinetic energies in many different ways. However, after the collision the kinetic energy of each molecule must always be a multiple of ε. I certainly do not need to remark that for the moment we are not concerned with a real physical problem. It would be difficult to imagine an apparatus that could regulate the collisions of two bodies in such a way that their kinetic energies after a collision are always multiples of ε. That is not a question here."

Boltzmann significant contributions to the foundation of quantum mechanics include statistical definition of entropy and combinatoric methods that played central roles in Planck's [100] introduction of quantum of action and his theory of equilibrium thermal radiation.

In view of Fig. 1, following Boltzmann statistical mechanics [99], one considers a hierarchy of statistical quantum fields composed of (… gravitons, neutrinos, photons, electrons, atoms, …., planets, stars, galaxies, galactic clusters, …) particles. If one considers a universe initially composed of extremely large numbers of gravitons (tachyons) as ideal superluminal gas with estimated most probable graviton wave speed of $c_t = 7.7 \times 10^{13} c$ [37], the entire cosmos will be *causally connected*. As one lowers the temperature by expansion, the number of oscillators hence entropy S = 4NK [34] decreases until a critical temperature at which Cooper pairs of gravitons become stable. As temperature is further decreased, more and more clusters are formed until the state of equilibrium between ETD and END (equilibrium neutrino-dynamics) at $T_g = T_n$. Continued cooling of the field results in further condensations and formation of EKD, ESD, EAD, … statistical fields.

The hierarchy of statistical fields in the above thought experiment will have a corresponding hierarchy of Maxwell-Boltzmann distributions shown in Fig. 4

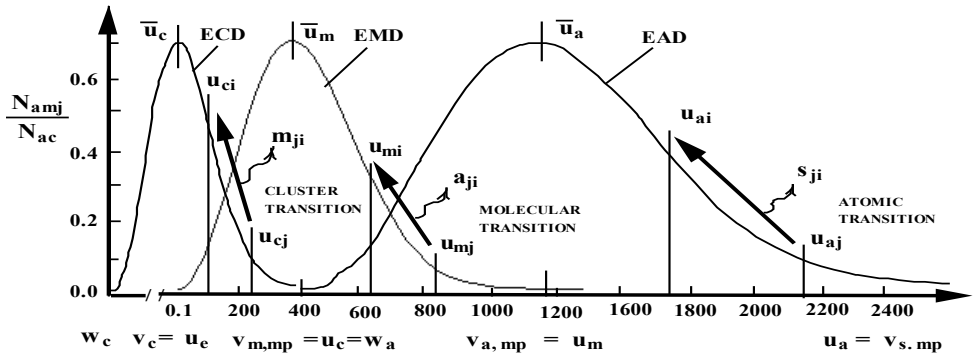

Figure 4 – Maxwell-Boltzmann speed distribution viewed as stationary spectra of cluster sizes for ECD, EMD, and EAD scales at T = 300 m [34].

In Fig. 4, the atomic mass and mass of most probable element of adjacent field are related as $\hat{m}_\beta = m_{w\beta-1}$ in accordance with (40). The smallest element or "atom" of each statistical field is a *composite boson* formed by "Cooper pair" of *most probable element* of the lower scale [36]. The atom is smallest element and is therefore the most stable element of the field. Internal energy of all elements will be the same due to Boltzmann principle of equipartition of energy [36]. Therefore, at *thermodynamic equilibrium*, each statistical field shown in Fig. 4 is composed of a spectrum of cluster sizes, also called energy levels, containing a corresponding spectrum of atoms that are under constant random transitions between different energy levels. Transitions of "atoms" between different clusters, energy levels, result in emission (absorption) of "sub-particle" in accordance with Bohr frequency relation $\Delta\varepsilon_{ji\beta} = h(\nu_{j\beta} - \nu_{i\beta})$ [101]. Atomic transitions between different clusters is in harmony with recent *cellular automaton* model of quantum mechanics [102].

Schematic diagrams of atomic transitions between two different clusters, de Broglie [2] wave packets, are shown in Fig. 5.

For example, at cosmic scales $\beta = g$, transition of a galaxy from a small rapidly oscillating cluster (high-energy-level j) to a large slowly oscillating cluster (low-energy-level i) results in emission of a star s_{ij} as a sub particle of cosmic field [37]. Hence, according to the new physical foundation of quantum mechanics [37], Bohr *stationary states* [101] correspond to *stochastically stationary* sizes of atomic clusters, *energy levels*, shown in Fig. 5. Clusters or de Broglie [3] wave packets are stabilized by an external pressure called Poincaré stress [36]. In Fig. 5, it is noted that transition energies $\Delta\varepsilon_{ji\beta} = h(\nu_{j\beta} - \nu_{i\beta})$ are double-indexed in accordance with Heisenberg [75] *matrix mechanics* that naturally lead to *noncommutative spectral geometry* of Connes [76].

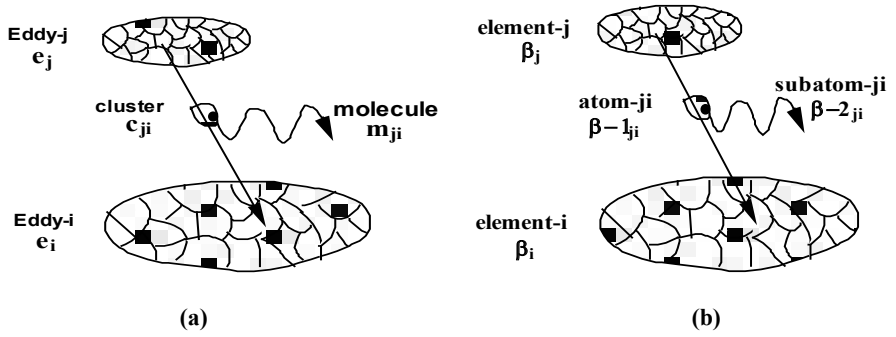

Figure 5 – (a) Transition of cluster c_{ij} from eddy-j to eddy-i leading to emission of molecule m_{ij}. **(b)** Generalized transition [36].

Under the assumption of potential incompressible flow, invariant Cauchy equation of motion (6) results in invariant Bernoulli equation that through Hamilton-Jacobi equation of classical mechanics leads to invariant Schrödinger equations [37,103]

$$\frac{\hbar^2}{2m_\beta}\nabla_\xi^2\psi_\beta + (\tilde{H}_\beta - \tilde{V}_\beta)\psi_\beta = 0 \qquad (65)$$

$$i\hbar\frac{\partial\Psi_\beta}{\partial t_\beta} + \frac{\hbar^2}{2m_\beta}\nabla_\xi^2\Psi_\beta - \tilde{V}_\beta\Psi_\beta = 0 \qquad (66)$$

with wave function defined as [37]

$$\Psi_\beta(\xi,t) = \rho^{1/2}\Phi'_\beta(\xi,t) = \rho^{1/2}\, e^{ik_r\xi}\, e^{-i\tilde{H}t_\beta/\hbar} \qquad (67)$$

such that $\Psi_\beta\Psi_\beta^* = \rho_\beta$ accounts for *particle localization* in accordance with classical results [104]. Therefore, for incompressible potential flows, invariant Schrödinger (65-67) governs the dynamics of Heisenberg-Kramers virtual oscillators [105] in all statistical fields shown in Fig. 1. Also, in harmony with perceptions of de Broglie [2,3], hierarchies of statistical fields in Fig.1 are embedded *wave-packets* that guide motion of "particles" as schematically shown in Fig. 6 at EUD, EGD, …, EMD, and EAD scales.

The direction of peculiar velocity of particle is that of the gradient of its velocity potential $V'_\beta = -\nabla\Phi'_\beta$. However, since the direction of atomic, mean, and peculiar translational velocities in (3) are the same, quantum mechanics wave function (43) *guides* the motion of particle in accordance with de Broglie-Bohm interpretation of quantum mechanics [3,37,106].

As one moves to smaller scales, most probable element is composed of an entire statistical field (see Fig. l), one can define a new velocity potential $\Phi'_{\beta-1}$, thereby a new wave function $\Psi_{\beta-1} = \rho^{1/2}\Phi'_{\beta-1}$. The cascade of particles as singularities embedded in *guidance waves* shown in Fig. 6 is in exact agreement with the perceptions of *de Broglie* concerning interactions between the particle and the *"hidden thermostat"* [3]

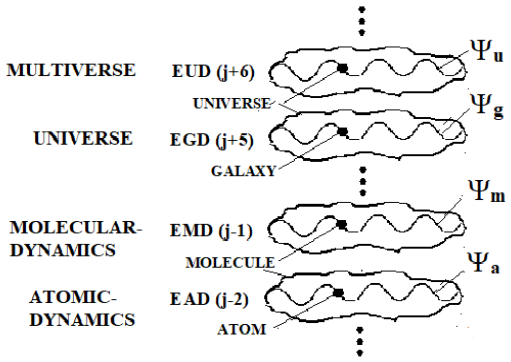

Figure 6 – Hierarchy of quantum mechanics wave functions m_{ij} or de Broglie guidance waves from multiverse (EUD) to atomic (EAD) scales [90].

"Here is another important point. I have shown in my previous publications that, in order to justify the well-established fact that the expression $|\Psi(x,y,z,t)|^2\, d\tau$ *gives, at least with Schrodinger' equation, the probability for the presence of the particle in the element of volume d□ at the instant t, it is necessary that the particle jump continually from one guidance trajectory to another, as a result of continual perturbation coming from subquantal milieu. The guidance trajectories would really be followed only if the particle were not undergoing continual perturbations due to its random heat exchanges with the hidden thermostat. In other words, a Brownian motion is superposed on the guidance movement. A simple comparison will make this clearer. A granule placed on the surface of a liquid is caught by the general movement of the latter If the granule is heavy enough not to feel the action of individual shocks received from the invisible molecules of the fluid, it will follow one of the hydrodynamic streamlines. If the granule is a particle, the assembly of the molecules of the fluid is comparable with the hidden thermostat of our theory, and the streamline described by the particle is its guiding trajectory. But if the granule is sufficiently light, its movement will be continually perturbed by the individual random impacts of the molecules of the fluid. Thus, the granule will have, besides its regular movement along one of the streamlines of the global flow of the fluid, a Brownian movement which will make it pass from one streamline to another. One can represent Brownian movement approximately by diffusion equation of the form* $\partial\rho/\partial t = D\Delta\rho$, *and it is interesting to seek, as various authors have done recently, the value of the coefficient D in the case*

of the Schrodinger eq nation corresponding to the Brownian movement.

I have recently studied [14] the same question starting from the idea that, even during the period of random perturbations, the internal phase of the particle remains equal to that of the wave. I have found the value $D = \hbar/3m$*, which differs only by a numerical coefficient from the one found by other authors.*

This concludes the account of my present ideas on the reinterpretation of wave mechanics with the help of images which guided me in my early work. My collaborators and I are working actively to develop these ideas in various directions. Today, I am convinced that the conceptions developed in the present article, when suitably developed and corrected at certain points, may in the future provide a real physical interpretation of present quantum mechanics."

When particles act as composite bosons [107] by forming Cooper-pairs, following classical methods [108, 109], quantum mechanics wave function may be expressed as products of translational, rotational, vibrational, and potential wave functions [110]

$$\Psi_\beta = \Psi_{t\beta}\Psi_{r\beta}\Psi_{v\beta}\Psi_{p\beta} = \Psi_{t\beta}\Psi_{r\beta}\Psi_{v\beta}\Psi_{\beta-1} = \ldots \quad (68)$$

At cosmological scale Ψ_g, the wave-particle duality of galaxies is evidenced by their observed quantized red-shifts [111]. Therefore, scale-invariance of the model (Fig. 1) and (68) leads to hierarchy of embedded statistical fields with translational TKE, rotational RKE, vibrational VKE kinetic energy and potential energy PE resulting in energy cascade shown in Fig. 7

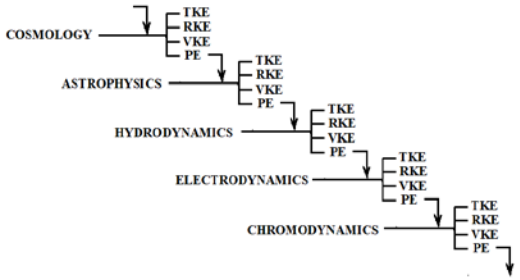

Figure 7 – Cascades of kinetic energy TKE, RKE, VKE (dark energy), and potential energy PE (dark matter) from cosmic to photonic scales [90].

Besides its complex nature that allows for normalization thus satisfying Born [112] probabilistic interpretation, the quantum mechanics wave function (67) resolves the problem of *empty waves* or what Einstein referred to as *Gespensterfelder* (Ghost fields) discussed by Selleri [113]. This problem arises from the fact that in usual quantum mechanics, the wave function is considered to carry neither energy nor momentum hence the name "empty wave" by Selleri [113].

"Whatever the approach, the question is always: How can one hope to reveal the presence of a wave which does not carry observable amounts of energy and momentum?"

According to the definition in (67), the complex wave function acts as "hidden variable" since it is related to an objectively real wave associated with particle *peculiar velocity.* Peculiar velocity of particles, although appreciated in cosmology, have been neglected in classical fluid mechanics. By (67), gradient of wave function through particle peculiar velocity hence Poincaré stress [35. 36] "guides" the motion of particle in harmony with de Broglie-Bohm "*pilot wave"* interpretation [3, 106] of quantum mechanics.

Although the validity of quantum mechanics is fully established, there are many interpretation problems confronting physical foundation of quantum mechanics seven of which were discussed in a recent investigation [37]

1. The nature of wave function and its probabilistic interpretation.
2. Wave-particle-duality.
3. Particle-particle entanglement.
4. Double-slit experiment.
5. EPR and problem of action-at-a-distance.
6. Quantum-jumps and trajectory problems.
7. Schrödinger cat.

In the following, the new paradigm of physical foundation of quantum mechanics [37] is applied to present very brief response to the interpretation problems identified in the list (1-7) above.

1. Schrödinger cat paradox is much more complex since it involves 1. By definition of wave function (67), both real or objective part namely density hence particle localization as well as its statistical complex or subjective part hence Born [112] probabilistic interpretation become self-evident.

2. In (1), "atom" or particle of scale β is by definition the most probable cluster or de Broglie "wave packet" $\mathbf{u}_\beta = \mathbf{v}_{w\beta-1}$ of the lower scale $\beta-1$ (see Fig. 6), thus resolving wave-particle duality problem [114].

3. By definition (1), particles or wave-packets are local "condensation" of the participating background field i.e., physical space in harmony with modern QFT. Therefore, separation of two entangled "particles" could be viewed as separation of two droplets, Wheeler-Bohr model of particle, schematically shown in Fig. 8.

Clearly, initially entangled droplets will retain correlation due to the external participating field surrounding them regardless of their separation distance. Thus, separated particles communicate through *"ontological"* [102] sub-atomic background field accounting for what appears as action-at-a- distance or Bell non-locality.

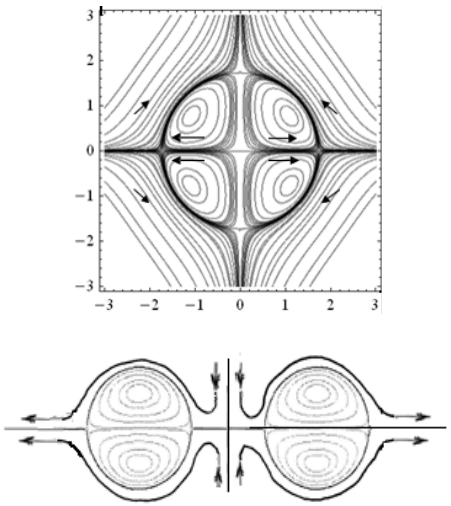

Figure 8 – Hydrodynamic model of fission of two hemispherical vortices into two Hill spherical vortices [37].

4. Since physical space or Casimir vacuum is identified as a compressible fluid, particle motion results in sub-photonic waves in the fabric of space or ether leading to interference patterns schematically shown in Fig. 9.

5. The EPR paradox is resolved due to particle entanglement in item-3 above as well as super-luminal tachyonic signals by *gravitational radiation* with estimated speed of $c_t = 7.7\times10^{13}c$ [37] making the entire universe causally connected. Possible superluminal velocities in ether to resolve Bell non-locality problem has been emphasized by Eberhard [94].

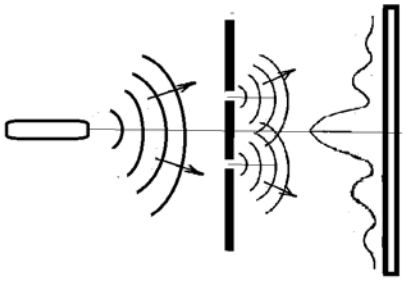

Figure 9 – Double-slit experiment and interference patterns due to formation of de Broglie guidance waves in Casimir vacuum.

6. Each statistical field is composed of a spectrum of clusters containing *integral numbers* of *identical* atoms that are nonetheless distinguishable because of their different energy. Hence, any atom of cluster j can make transition *through any arbitrary trajectory* to cluster i and emit a sub particle with energy ε_{ji} with exactly the same final results (see Fig. 5). Because probability of any intermediate energy level between level-j and level-i is zero, transitions can only occur through *quantum jumps* (see Fig. 4). At higher energies, higher frequencies, the spacing between energy levels decreases and the spectrum approaches a continuum corresponding to "bremsstrahlung" radiation for photon gas.

7. Schrödinger cat paradox is much more complex since it involves phenomena of life and death that are not understood. In a recent study [89], it was noted that because of the well know decoupling of radiation and matter fields in cosmology, one cannot rule out possible decoupling at sub-photonic scales within hierarchies of wave functions in (68)

$$\cdots\Psi_{\beta=d+2}\Psi_{\beta=d+1} \Leftarrow \quad \Rightarrow \Psi_{\beta=d}\Psi_{d-1}\Psi_{d-2}\cdots$$

at the moment of death $t = t_f$ or what Hegel called *the moment when the spirit transcends temporality* [115]. It is most fascinating that similar perception about possible relationship between material and non-material world was discussed by Lorentz in his letter of 1915 to the theologian H. Y. Groenewegen qouted in a recent wonderful book about Lorentz' life by Kox and Schatz [116]

"The single observation that the spirit of different people can understand each other, that the emotions and opinions of one are not indifferent to another, must lead us to the assumption of a connection between them, which many of us would like best to imagine in such a form that all these individual spirits are part of one great whole, a world spirit or deity. […] But if the spirit is part of a great whole, just like the body is part of the entire material world, then naturally one arrives at the generalization that, as a rule, every event in the psychic realm responds to a change in the material realm. […] The concept one arrives at in this way is that the spiritual and the material are inextricably connected, that they are the two sides of the same thing, that the material world is a representation of the world spirit"

Next, the impact of the model on theory of relativity will be briefly discussed. Since *physical space* or ether is identified as compressible ideal gas in harmony with perceptions of Huygens [54] and Planck [58], its density when isentropically brought to rest will be given by [117]

$$\rho = \frac{\mathrm{M}}{V} = \rho_{\mathrm{o}}\left[1+\frac{\gamma-1}{2}\frac{\mathrm{v}^2}{\mathrm{c}^2}\right]^{\frac{1}{\gamma-1}} = \\ = \frac{\mathrm{M}}{V_{\mathrm{o}}}\left[1+\frac{\gamma-1}{2}Mi^2\right]^{\frac{1}{\gamma-1}} \tag{69}$$

where $\gamma = \mathrm{c}_{\mathrm{p}} / \mathrm{c}_{\mathrm{v}}$ is Poisson adiabatic index. For Casimir [63] vacuum or photon gas $\gamma = 4/3$ and assuming that *transverse coordinates* do not change [118] for one dimensional compressible flow, (69) leads to Lorentz-FitzGerlad contraction [33, 36, 117]

$$V = V_{\mathrm{o}}\sqrt{1-\mathrm{v}^2/\mathrm{c}^2}, \quad \ell = \ell_{\mathrm{o}}\sqrt{1-\mathrm{v}^2/\mathrm{c}^2}, \\ \rho = \frac{\rho_{\mathrm{o}}}{1-\mathrm{v}^2/\mathrm{c}^2} \tag{70}$$

According to (70), compressibility of physical space accounts for Lorentz-FitzGerald contractions and provides a *causal* explanation of such relativistic effects as noted by Pauli [118]. When Michelson number *Mi* = v/c approaches unity, relativistic effects due to compressibility of ether i.e., physical space, become appreciable. Therefore, two different and experimentally distinguishable paradigms of special theory relativity (STR) in harmony with ideas of Darrigol [119] and Galison [120] were recently presented [117]

(A) Poincaré-Lorentz
Dynamic Theory of Relativity
Space and time (x, t) are altered due to causal effects of motion on the ether.

(B) Einstein
Kinematic Theory of Relativity
Space and time (x, t) are altered due to the two postulates of relativity:

1- Velocity of light is a universal constant independent of the motion of its source.
2- The laws of physics do not change form for all inertial frames of reference.

Although above postulates 1 and 2 are extremely accurate, strictly speaking they are not valid. This is because the speed of light is not constant but a function of temperature of Casimir [63] vacuum and hence decreases extremely slowly at cosmic time scales (eons) with expansion of universe. The second postulate is not valid because all inertial frames are *distinguishable* through measurements with respect to *stochastically stationary* isotropic cosmic microwave background radiation temperature of Penzias-Wilson [121, 122, 123] as emphasized by Prokhovnik [124].

Poincaré [59, 60] and Lorentz [89] introduced their *dynamic theory of relativity* in order to explain the relativistic Lorentz-FitzGerald contractions *causally* as emphasized by Pauli [118] and described in more details in an excellent study by Hirosige [125]

"In contrast to Einstein, Lorentz, Poincaré, and most other contemporary physicists saw the Michelson-Morley experiment as one of the most urgent problems requiring their theoretical efforts."

And similarly [125]

"Poincaré anticipated the principle of relativity as an empirical law, looking forward to a theory which could explain or prove the principle."

Also, Helmholtz is known to have developed very complicated equations to describe motion of atoms of ether according to Lorentz [126]. It is therefore natural to search for a *causal* relativistic theory of gravitation based on solution of conservation equations (4)-(7) for Huygens' [54] compressible ether as discussed in Section 6 on cosmology. Accordingly, one expects the problem to primarily involve *scalar* and *vector* fields and shock waves in unsteady gas dynamics. For example, the analogy between fluid mechanics of air and ether suggests that supersonic $Ma > 1$ (superluminal $Mi > 1$) flow of air (ether) leads to the formation of *Mach* (*Poincaré-Minkowski*) cone that separates the zone of sound (light) from the zone of silence (darkness) [37, 117] as schematically shown in Fig. 10.

Einstein [127] on the other hand, introduced his *kinematic theory of relativity* based on two *postulates* in order to account for asymmetries in Maxwell [57] theory of electromagnetism when applied to moving bodies. The fundamental limitation of such scientific theory based on *postulates* is that it cannot reveal the true underlying causes of the observed relativistic effects such as space and time interactions. In other words, the kinematic theory based on postulates (1)-(2) in paradigm B above cannot address the exact reasons and the dynamic mechanisms that are responsible for relativistic interdependence of space and time.

It is also important to emphasize that dynamic versus kinematic theories of relativity in paradigms (A) versus (B) above are *experimentally distinguishable*. This is because higher /lower local densities will be measured in front/rear by an observer moving with respect to *stochastically-stationary* compressible ether as schematically shown in Fig. 11.

Since Lorentz-FitzGerald contractions are *physically real*, they only agree with predictions of kinematic theory of relativity locally in one-dimensional experiments. For the same reasons, Einstein principle of equivalence is only locally true. It is expected that future multi-dimensional experiments will detect *transverse* topological change of space curvature due to *three-dimensional* nature of compressibility effects (Fig. 11) in accordance with predictions of paradigm (A) above. Furthermore, in dynamic theory of relativity, spacetime is governed by thermodynamic temperature as discussed in Section 3. For example, in the classical problem of *twin paradox*, different times experienced by the twins are real and attributed to the different *biological reaction rates* in their bodies induced by the compressibility of physical space [128] governed by dynamic theory of relativity of Poincaré [59,61] and Lorentz [89].

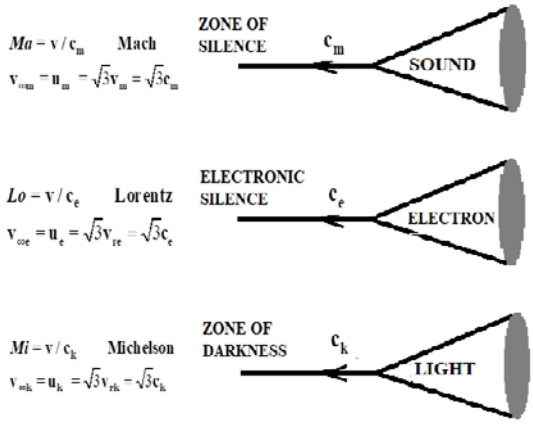

Figure 10 – "Supersonic" flows at molecular-, electro-, and chromo-dynamics scales leading to the formation of Mach, Lorentz, and PoincaréMinkowski cones [37].

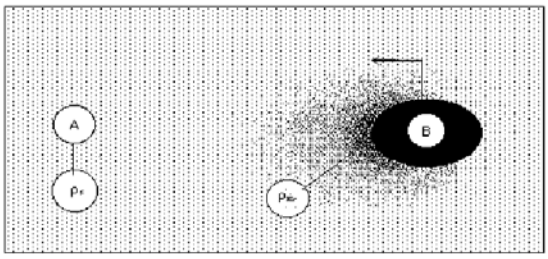

Figure 11 – Density of a medium as measured by an observer that is (A) stationary (B) moving with respect to the medium.

It is instructive to compare the singular behavior of relativistic transformations of mass (53) by Lorentz and energy (54) by Poincare-Einstein in Section 3 with the singularity in shock density formula (70) of gas-dynamics. It is well known that when Mach number $Ma = v / c_m$ exceeds unity, a shock wave occurs leading to transition from supersonic flow $v > c_m$ at equilibrium cluster-dynamics ECD to subsonic flow $v < c_m$ at equilibrium molecular dynamics EMD across the shock wave [37]. Naturally, one anticipates similar shock waves to occur at much higher velocities, when Lorentz

number $Lo = \mathrm{v}/\mathrm{c}_\mathrm{e}$ (Michelson number $Mi = \mathrm{v}/\mathrm{c}$) exceeds unity, leading to transition $\mathrm{v} > \mathrm{c}_\mathrm{e} \rightarrow \mathrm{v} < \mathrm{c}_\mathrm{e}\,(\mathrm{v} > \mathrm{c}_\mathrm{k} \rightarrow \mathrm{v} < \mathrm{c}_\mathrm{k})$ associated with ESD and EKD scales as shown in Fig. 10 [37]. Therefore, superluminal flow of tachyons [129] (gravitons) becomes understandable since critical root-mean-square wave velocities $(\mathrm{c}_\mathrm{m}, \mathrm{c}_\mathrm{e}, \mathrm{c}_\mathrm{k})$ in (Ma, Lo, Mi) are average speeds of much smaller "subatomic" particles at the next lower scale. By (62) in Section 3, the maximum "atomic" photon speed shown in Fig. 10 becomes $\mathrm{u}_{\infty\mathrm{k}} = \sqrt{3}\mathrm{u}_\mathrm{k} = 2\mathrm{c}$.

In regards to Lorentz perceptions concerning reality of ether and Lorentz-FitzGerald contractions it is important to quote directly from the treatise of Lorentz [126]

"I cannot speak here of the many highly interesting applications which Einstein has made of this principle, His results concerning electromagnetic and optical phenomena (*leading to the same contradiction with Kaufmann's results that was pointed out in* §179[1]) *agree in the main with those which we have obtained in the preceding pages, the chief difference being that Einstein simply postulates what we have deduced, with some difficulty and not altogether satisfactorily, from the fundamental equations of the electromagnetic field. By doing so, he may certainly take credit for making us see in the negative results of experiments like those of Michelson, Rayleigh and Brace, not a fortuitous compensation of opposing effects but the manifestation of a general and fundamental principle.*

Yet, I think, something may also be claimed in favor of the form which I have presented the theory. I cannot but regard the ether, which can be the seat of electromagnetic field with its energy and its vibrations, as endowed with a certain degree of substantiality, however different it may be from all ordinary matter. In this line of thought, it seems natural mot to assume at starting that it can never make any difference whether a body moves through the ether or not, and to measure distances and lengths of time by means of rods and clocks having fixed position relative to the ether.

It is important to examine the reasons for the dismissal of the prior ether theories [65]. As stated in [36], classically, ether was considered as a medium that occupied space in harmony with perceptions of Aristotle [53], Huygens [54], Newton [55], Euler [56], Maxwell [57], Lorentz [58], Poincaré [59-62], de Broglie [3], Casimir [63], and Dirac [64] amongst many others. However, in his kinematic theory of relativity Einstein [127] found ether to be "*superfluous*" since it is undetectable and could be replaced by abstract concept of *spacetime* instead of classical Newtonian absolute space and time. Therefore, many physicists were convinced that Einstein kinematic theory of relativity proved non-existence of ether and the null result of Michelson-Morely [130] experiments. Other physicists were convinced because of mathematical beauty of Poincaré-Minkowski four dimensional spacetime. As a result, Lorentz-FitzGerald contraction as a causal explanation of null result of Michelson-Morely [130] experiment was dismissed as ad hoc assumption. The author agrees with Dirac [131] that mathematical beauty and symmetry in the expression of the laws of Nature are extremely important. However, perhaps it is also important to emphasize that even when mathematically beautiful theories have been established, in the absence of a clear *physical and intuitive* explanations to compliment such theories, the search for alternative theories as well as different interpretation of the existing theory should continue with open mind. Further details about significant role of ether in research programs of Lorentz and Poincaré are discussed in the excellent study of Hirosige [125].

It appears that distinction between dynamic (A) versus kinematic (B) paradigms identified above was known to Poincaré based on fundamental principles as suggested by the lecture he delivered in London in 1912 shortly before he died [132]

"Today some physicists want to adopt a new convention. It is not that they are constrained to do so; they consider this new convention more convenient; that is all. And those who are not of this opinion can legitimately retain the old one in order not to disturb their old habits. I believe, just between us, that this is what they shall do for a long time to come,"

The perceptions of Poincaré concerning relativity theory are known to be also shared by Lorentz who stated in a 1915 lecture at the Royal Academy of Sciences in Amsterdam [78]

I could point out to you [if I had more time] how Poincaré in his study of dynamics of electron, about the same time as Einstein, formulated many ideas that are characteristic for his theory, and also formulated what he calls "le postulat de relativité"

It is clear that because of introduction of privileged frame of ether, Galilean transformation will be always violated because of the fact that all inertial frames are in reality not precisely equivalent. Therefore, the problem of relativity reduces to the problem of simple allowance for the compressibility of the manifold within which dynamic processes occur**.** From the perspective of the present field theory, the notion of STR then states that if one desired to arrive at a constant and *finite propagation velocity* within a *compressible medium*, but erroneously assumes that the medium within which the dynamics occur is *incompressible***,** then the application of STR will modify the local space and time such as to compensate for this erroneous assumption. The apparent artificiality of such a procedure is because physical space for relativistic events is obviously a compressible medium since the propagation velocity of light is finite.

In closing this Section, it is instructive to note that derivation of invariant Schrödinger equation from invariant Bernoulli equation was based on two important assumptions, namely (a) incompressible flow (b) potential flow [37]. Relaxation of assumption (a) hence inclusion of compressibility effects means including relativistic effects (70) as discussed above. Relaxation of assumption (b) implies presence of viscous effects i.e., vorticity hence iso-spin (8) thus requiring consideration of modified Navier-Stokes (19) rather than Cauchy equation of motion (6). Interestingly, it was precisely the viscous equation of motion (19) that was employed in a recent investigation [35] to derive Dirac [133] relativistic wave equation of quantum field theory (QFT)

$$i\hbar\left(\frac{1}{c}\frac{\partial \Psi_{D\beta}}{\partial t_{\beta}}+\alpha_{j\beta}\frac{\partial \Psi_{D\beta}}{\partial x_{j\beta}}\right)+(\alpha_{m\beta}m_{\beta}c)\Psi_{D\beta}=0 \quad (71)$$

Dirac [133] arrived at his relativistic wave equation (71) through shear genius being guided by his superb mathematical intuition. Therefore, the physical basis of his relativistic wave equation (71) and hence QFT remains abstract and mysterious. The simple derivation of Dirac equation in [35] may help the understanding of physical foundation of this important equation. It is also important to note that as long as $\nabla\times\mathbf{v}_{\beta}=\nabla\times\mathbf{u}_{\beta}$ is true such that $\nabla\times\mathbf{V}'_{\beta}=0$ by (3), Dirac wave function $\Psi_{D\beta}$ remains well defined insuring validity of (71) for particles with spin such as election as is to be expected. Finally, Dirac [133] anticipated that the 4×4 tensors (α_j,α_m) in (71) may be related to *internal coordinates*. Hence, in harmony with Dirac's mathematical intuition, it is reasonable to suspect that tensors (α_j,α_m) are somehow connected to the four-coordinates $(z_{\beta},\theta_{\beta},r_{\beta},z'_{\beta})$ and the corresponding four-velocities $(\mathbf{v}_{z\beta},\mathbf{v}_{\theta\beta},\mathbf{v}_{r\beta},\boldsymbol{V}'_{z\beta})$ discussed after Fig. 15 of the following Section.

Physical Foundation of Electromagnetism and Invariant Maxwell Equations

It is well known that, following Faraday's intuitive concept of line of force, Maxwell developed equations of electrodynamics guided by analogy with hydrodynamics of a "fictitious fluid" called ether. In particular, the important connection between magnetic field and fluid rotation was emphasized by Maxwell as described in his 1891 treatises on electrodynamics [57]:

"Whatever light is, at each point of space there is something going on, whether displacement, or rotation, or something not yet imagined, but which is certainly of the nature of a vector or directed quantity, the direction of which is normal to the direction of the ray. This is completely proved by the phenomena of interference."

"The only resemblance which we can trace between a medium through which circularly polarized light is propagated, and a medium through which lines of magnetic force pass, is that in both there is a motion of rotation about an axis. But here the resemblance stops, for the rotation in the optical phenomena is that of the vector which represents the disturbance. This vector is always perpendicular to the direction of the ray, and rotates about it a known number of times in a second. In a magnetic phenomenon, that which rotates has no properties to which its sides can be distinguished, so that we cannot determine how many times it rotates in a second."

According to Maxwell [57], Faraday conceived such lines of force as individually rotating lines in accordance with the Rankine hypothesis of molecular vortices. We quote another statement by Maxwell [57]

"If we adopt Ampere's theory, we consider a magnet not as a continuous substance, the magnetization of which varies from point to point according to some easily conceived law, but as a multitude of molecules, within each of which circulates a system of electric currents, giving rise to a distribution of magnetic force of extreme complexity, the direction of the force in the interior of the molecule being generally the reverse of that of the average force in its neighborhood, and the magnetic potential, where it exists at all, being a function of as many degrees of multiplicity as there are molecules in the magnet."

Following Dirac [131], a hydrodynamic model of Faraday line of force was recently introduced [90] on the basis of flow field surrounding spinning spherical particles in an otherwise stationary background fluid as schematically shown in Fig. 12

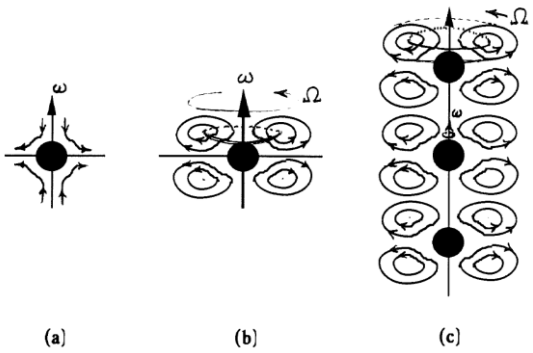

Figure 12 – Schematic model (a) flow near a spinning particle (b) locally conserved flow streamlines (c) formation of Faraday line of force from a row of co-spinning particles and the associated vortex field within the subquantum background fluid [90].

In general, interactive forces between spinning particles within participating background fluid is very complex and depends on the orientation of iso-spins of particles as schematically shown in Fig. 13

As discussed in [90], due to such hydrodynamic forces, spinning particles such as electrons form a chain composed of alternative particle/anti-particle or electron/positron called *hydrodynamic model of Faraday lines of force* schematically shown in Fig. 14

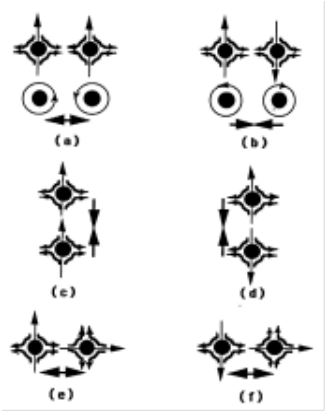

Figure 13 – Some possible interactions between spinning spherical particles within a participating background fluid. (a) parallel up-up (b) parallel up-down (c) co-axial up-up (d) co-axial up-down (e) anti-parallel up-right (f) anti-parallel down-right.

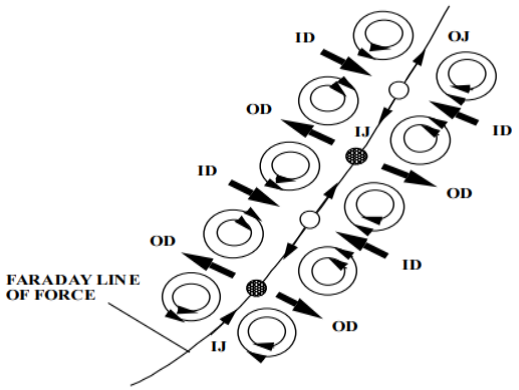

Figure 14 – Faraday line of force as electron (black) and positron (white) string with inflow jet (IJ) of one matching the outflow jet (OJ) of its neighbor. Also shown are alternating outflow (OD) and inflow discs (ID) [90].

The breakage of a line of force corresponds to creation of an electron and positron pair as described by Dirac [131]. It is reasonable to anticipate that what is known as "charge" is related the magnetic field and hence to iso-spin of particles with positive and negative charges associated with the sense of rotation of matter and anti-matter particles. At much smaller scales, such a hydrodynamic model of Faraday lines of force is in harmony with chains of quark-antiquark in stochastic chromodynamics "*like beads on a necklace*" to borrow the description by 't Hooft [134].

Therefore, in harmony with hydrodynamic model of Faraday line of force [89] and following Maxwell [57] and Lorentz [126], generalized model of electrodynamics is expressed by invariant Maxwell equations

$$\nabla.\mathbf{D}_\beta = \rho_\beta \tag{72}$$

$$\nabla \times \mathbf{E}_\beta = -\frac{\partial \mathbf{B}_\beta}{\partial t_\beta} \tag{73}$$

$$\nabla.\mathbf{B}_\beta = 0 \tag{74}$$

$$\nabla \times \mathbf{H}_\beta = \mathbf{J}_\beta + \frac{\partial \mathbf{D}_\beta}{\partial t_\beta} \tag{75}$$

Also, following Maxwell, at any scale one introduces a displacement vector $\mathbf{D}_\beta$ defined by (72) such that the continuity equation (4) in the absence of reactions leads to

$$\nabla.(\rho_{i\beta}\mathbf{v}_\beta) + \frac{\partial \rho_{i\beta}}{\partial t_\beta} = \nabla.(\mathbf{J}_\beta + \frac{\partial \mathbf{D}_\beta}{\partial t_\beta}) = 0 \tag{76}$$

Therefore, the quantity within parathesis must be curl of a vector called $\mathbf{H}_\beta$ leading to (75).

According to classical theory of electromagnetism [57, 126, 135-137], electromagnetic waves are *transverse waves*. However, following Huygens' [54] analogy between propagation of sound in air and light in ether, it is suggested that light waves also possess a longitudinal polarization associated with periodic *compression* and *rarefaction* of physical space. The neglect of longitudinal component could be due to exceedingly small thickness of chromodynamic shock. For example, assuming shock thickness to be of the order of size of nucleus $\delta \approx 10^{-15} m$, time scales of fluctuations in speed of light will be of order $\delta / c \approx 10^{-23} s$ and hence difficult to detect. Longitudinal wave could account for finite gravitational mass of photon (28) in harmony with Higgs mechanism [138]. With vector potential $\mathbf{A}_\beta$ herein identified as velocity field, magnetic field strength $\mathbf{B}_\beta$ is related to vorticity $\boldsymbol{\omega}_\beta$ by

$$\mathbf{B}_\beta = -\nabla \times \mathbf{A}_{z\beta} = -\nabla \times \mathbf{v}_{z\beta} \tag{77}$$

that results in Maxwell equation (74). The reason for the choice of negative sign in (77) is to have positive sign for the time derivative of electric field strength defined as longitudinal acceleration

$$\mathbf{E}_{z\beta} = \frac{\partial \mathbf{A}_{z\beta}}{\partial t_\beta} = \frac{\partial \mathbf{v}_{z\beta}}{\partial t_\beta} = \mathbf{a}_{z\beta} \tag{78}$$

Hence, by (76) and (78), the curl of $\mathbf{E}_{z\beta}$ gives

$$\nabla \times \mathbf{E}_{z\beta} = \frac{\partial}{\partial t_\beta}(\nabla_\beta \times \mathbf{A}_{z\beta}) = -\frac{\partial \mathbf{B}_\beta}{\partial t_\beta} \tag{79}$$

that is Maxwell second equation (73).

The sign convention in (77) leading to (79) ensures that a charge in electric field $\mathbf{E}_{z\beta}$ experiences a force $\mathbf{F}_{z\beta}$ in the same direction as the momentum since

$$\mathbf{F}_{z\beta} = \frac{\partial \mathbf{J}_{z\beta}}{\partial t_\beta} = \frac{\partial (\rho_\beta \mathbf{v}_{z\beta})}{\partial t_\beta} = \rho_\beta \frac{\partial \mathbf{v}_{z\beta}}{\partial t_\beta} = \rho_\beta \mathbf{E}_{z\beta} \tag{80}$$

in accordance with classical results.

For the important case of propagation of electromagnetic waves in Casimir vacuum, equations (73) and (75) result in wave equations

$$\frac{\partial^2 \mathbf{E}_{z\beta}}{\partial t_\beta^2} = c_\beta^2 \nabla^2 \mathbf{E}_{z\beta} \tag{81}$$

$$\frac{\partial^2 \mathbf{H}_\beta}{\partial t_\beta^2} = c_\beta^2 \nabla^2 \mathbf{H}_\beta \tag{82}$$

Next, a third wave equation [37] will be associated with radial electric field intensity $\mathbf{E}_{r\beta}$ given by (78). Hence, for propagation of electromagnetic waves in Casimir vacuum one obtains wave equations

$$\partial^2 \boldsymbol{\phi}_\beta / \partial t_\beta^2 = c_\beta^2 \nabla^2 \boldsymbol{\phi}_\beta, \ \boldsymbol{\phi}_\beta = (\mathbf{E}_{z\beta}, \mathbf{H}_\beta, \mathbf{E}_{r\beta}) \tag{83}$$

and corresponding momentum waves as discussed in [37]

$$\partial^2 \boldsymbol{\zeta}_\beta / \partial t_\beta^2 = c_\beta^2 \nabla^2 \boldsymbol{\zeta}_\beta, \ \boldsymbol{\zeta}_\beta = (\mathbf{v}_{z\beta}, \boldsymbol{\omega}_\beta, \mathbf{v}_{r\beta}) \tag{84}$$

The three velocity waves (84) result in atomic energies due to translational, rotational, and radial harmonic motions given by

$$\varepsilon_{z\beta} = \int \mathbf{F}_{z\beta}.\mathrm{d}\mathbf{z}_\beta = \int \frac{\mathrm{d}\mathbf{p}_{z\beta}}{\mathrm{dt}_\beta}.\,\mathrm{d}\mathbf{z}_\beta = \\ = \mathrm{m}_\beta \mathbf{v}_{z\beta}^2/2 = \mathrm{m}_\beta \mathbf{v}_{+z\beta}^2 = \mathrm{k}T_\beta \tag{85}$$

$$\varepsilon_{\theta\beta} = \int \mathbf{F}_{\theta\beta}.\mathbf{d}\sigma = \int \frac{\mathbf{dp}_{\theta\beta}}{\mathrm{dt}_\beta}.\,\mathrm{rd}\boldsymbol{\theta}_\beta = \\ = \mathrm{m}_\beta \mathrm{r}^2 \boldsymbol{\omega}_{\theta\beta}^2/2 = \mathrm{I}_\beta \boldsymbol{\omega}_{+\theta\beta}^2 = \mathrm{k}T_\beta \tag{86}$$

$$\varepsilon_{r\beta} = \int \mathbf{F}_{r\beta}.\mathrm{d}\mathbf{r} = \int \chi_{r\beta}\mathbf{r}_\beta.\,\mathrm{d}\mathbf{r}_\beta = \\ = m_\beta \boldsymbol{\omega}_{r\beta}^2 \mathrm{r}_\beta^2/2 = \mathrm{m}_\beta \mathrm{v}_{+r\beta}^2 = \mathrm{k}T_\beta \tag{87}$$

For radial potential energy in (87) substitution from definition of spring constant $\chi_{r\beta} = \mathrm{m}_\beta \omega_{r\beta}^2$ has been made. Hence, the three energies (85)-(87) correspond to three fields $(\mathbf{E}_{z\beta}, \mathbf{H}_{\theta\beta}, \mathbf{E}_{r\beta})$.

At thermodynamic equilibrium, the energies due to harmonic oscillations in axial, angular, and radial coordinate directions give *atomic internal energy* or photon *electromagnetic mass* [34]

$$\hat{\mathrm{u}}_\beta = \hat{\varepsilon}_{EM} = \varepsilon_{z\beta} + \varepsilon_{\theta\beta} + \varepsilon_{r\beta} = 3\mathrm{k}T_\beta \tag{88}$$

The correction factor of 3/2 discussed by Bass and Schrödinger [139] is no longer encountered because the factor of ½ is taken care of by 2 coordinate directions mentioned above, and the factor 3 is accounted for by axial, radial, and angular degrees of freedoms.

Finally, photon peculiar velocity (3) results in *Poincaré stress* or pressure wave [37] giving photon *potential energy* or *gravitational mass* [36,37]

$$\varepsilon_{p\beta} = \hat{\varepsilon}_{GR} = \varepsilon_o \mathrm{E}_{+\mathrm{p}\beta}^2 = p_\beta \hat{\mathrm{v}} = \\ = m_\beta < V_{+\beta}'^2 > /3 = m_\beta < V_{+z\beta}'^2 > = \mathrm{k}T_\beta \tag{89}$$

At thermodynamic equilibrium, Boltzmann principle of equipartition of energy requires equality of energy of all four degrees of freedom [34]

$$\varepsilon_{z\beta} = \varepsilon_{\theta\beta} = \varepsilon_{r\beta} = \varepsilon_{p\beta} = \mathrm{k}T_\beta \tag{90}$$

Hence, total photon atomic energy or atomic enthalpy is

$$\hat{\varepsilon}_{\mathrm{total}} = \hat{\varepsilon}_{EM} + \hat{\varepsilon}_{GR} = \varepsilon_o \mathrm{E}_{+z\beta}^2 + \mu_o \mathrm{H}_{+\theta\beta}^2 + \\ + \varepsilon_o \mathrm{E}_{+r\beta}^2 + \varepsilon_o \mathrm{E}_{+p\beta}^2 = 4\mathrm{k}T_\beta \tag{91}$$

The result (91) is in agreement with the classical [57,126,135-137] total electromagnetic energy

$$\hat{\varepsilon}_{\mathrm{total}} = \varepsilon_o \mathrm{E}'^2/2 + \mu_o \mathrm{H}'^2/2 = \\ = \varepsilon_o \mathrm{E}_+'^2 + \mu_o \mathrm{H}_+'^2 = 2\mathrm{k}T_\beta' = 4\mathrm{k}T_\beta \tag{92}$$

since $T' = 2T$ as discussed in [34].

In summary, photons are assumed to have harmonic oscillations in axial (z_+, z_-), angular (θ_+, θ_-), and radial $(\mathrm{r}_+, \mathrm{r}_-)$ *coordinate directions* as schematically shown in Fig. 3,

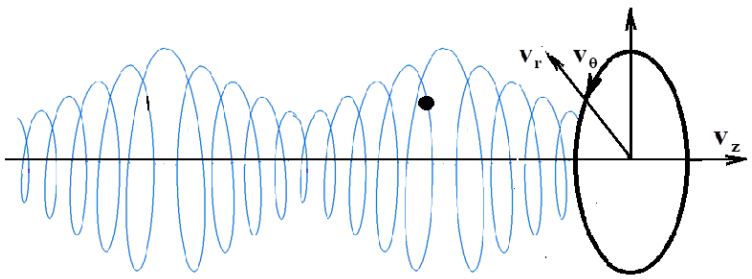

Figure 15 – Trajectory of photon "torpedo" with axial, angular, and radial harmonic velocities. The influence of random peculiar velocity is not shown.

Thus, we have four-coordinates $(z_\beta, \theta_\beta, r_\beta, z'_\beta)$ and corresponding four-velocity $(\mathbf{v}_{z\beta}, \mathbf{v}_{\theta\beta}, \mathbf{v}_{r\beta}, V'_{z\beta})$ and four-energy $(\varepsilon_{z\beta}, \varepsilon_{r\beta}, \varepsilon_{v\beta}, \varepsilon_{p\beta})$. The new hydrodynamic model has four fields $(\mathbf{E}_{z\beta}, \mathbf{H}_{\theta\beta}, \mathbf{E}_{r\beta}, \mathbf{E}_{p\beta})$ as opposed to the two classical electromagnetic fields $(\mathbf{E}', \mathbf{H}')$. The first field is new electric field and is called Lorentz *longitudinal electric field* $\mathbf{E}_{z\beta} = \mathbf{L}_{z\beta}$ associated with periodic compression and rarefaction of light wave. The last electric field $\mathbf{E}_{p\beta}$ is also new and corresponds to the wave function $\Psi_{z\beta}$ defined in (67) hence associated with the velocity potential of peculiar velocity $V'_{z\beta} = -\nabla\Phi'$ that is the hidden *pilot wave* of de Broglie-Bohm [3, 90, 106]. The four-waves associated with translational, rotational, vibrational, and "internal" degrees of freedom are schematically shown in Fig 16.

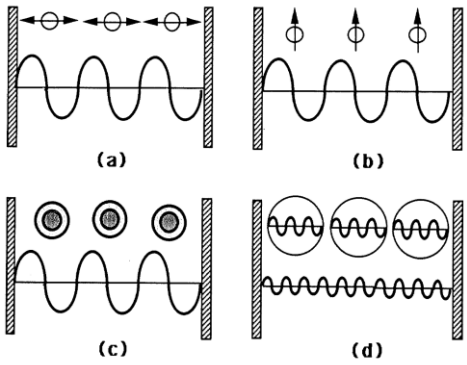

Figure 16 – Quantization of (a) translational (b) rotational (c) vibrational (d) internal waves of particles.

In Section 4, it was shown that particle peculiar velocity leads to *external pressure* that was identified as *Poincaré stress* responsible for particle stability [35-37]. The velocity potential of peculiar velocity is the imaginary part of quantum mechanics wave function (67). Since for stable particle, external pressure must be equal to internal pressure that accounts for the potential energy part (71) of Helmholtz decomposition of total thermal energy (84) identified as dark energy [33, 34]. Also, as discussed in [33], potential energy or dark matter of scale β is identified as the total energy (enthalpy) of the adjacent lower scale β–1. Finally, in the hierarchies of wave functions shown in (68), *internal wave function* of scale β decompactifies into four-wave functions of the next lower scale β–1 (see Fig. 7). Therefore, the internal wave function plays a more complex and significant role in the hierarchical model (Fig. 1) and hence cannot be explicitly revealed in Fig. 16.

The invariant hydrodynamic model described above is harmonious with Maxwell [57] and Lorentz [126] classical electrodynamics (72)-(75). Of course closer equivalence requires addition of a Coulomb scalar potential to account for electrostatic forces parallel to Newton gravitational potential. Also, in the hydrodynamic model, Lorentz [126] force on charged particles assumes the form

$$\mathbf{F}_\beta = \rho_\beta(\mathbf{E}_\beta + \mathbf{v}_\beta \times \mathbf{B}_\beta) = \rho_\beta(\mathbf{a}_\beta - 2\mathbf{v}_\beta \times \boldsymbol{\omega}_\beta) \quad (93)$$

with the two terms respectively representing linear and Coriolis accelerations, thus providing a reasonable hydrodynamic interpretation of Lorentz force. Therefore, the results presented in this Section suggest that future development of exact hydrodynamic model of Maxwell classical theory of electromagnetism is conceivable and in need of further investigations.

The primary obstacle in bridging the gap between hydrodynamics and electrodynamics concerns uncertainty about the exact nature of concept of electric *charge*. In view of the well-known similarity between Newton law of gravity and Coulomb law in electrostatics, it is natural to expect that the concept of charge is somehow related to mass. This is also supported by occurrence of charge in the expression of electric force when electric field strength $\mathbf{E}_\beta$ is identified as acceleration (78). It is most interesting that the numerical magnitude of the elementary charge of electron is almost exactly given by

$$e = \frac{1843 \times m_e \times c}{\pi} \approx$$
$$\approx \frac{1843 \times 9.10956 \times 10^{-31} \times 2.998 \times 10^{8}}{\pi} = \quad (94)$$
$$= 1.60215 \text{ C}$$

where the proton to electron mass ratio is based on photon mass in (28)

$$\frac{m_p}{m_e} \approx 1843 \quad (95)$$

If instead of (95), the classical ratio $m_{\rm p}/m_{\rm e} \approx 1836.2$ is employed in (94), one gets a smaller value $e \approx 1.59624\times10^{-19}$ C for elementary electron charge.

A second major difficulty to resolve is that as opposed to gravitation forces that are always attractive, electromagnetic forces could also be repulsive. Amongst many possibilities, the observed attractive and repulsive forces between "charged" particles could be related to the sense of their rotation in view of Biot-Savart law [137]

$$\mathbf{H} = \mathrm{I}d\boldsymbol{\ell}\times\hat{\mathbf{r}}/\mathrm{r}^2 \tag{96}$$

Also, because of the definition of magnetic field and its connection to vorticity by (77), the concept of charge is expected to be related to electron iso-spin defined in (8) as

$$\varpi_\beta = \nabla\times\mathbf{u}_\beta = \boldsymbol{\omega}_{\beta-1} \tag{97}$$

Indeed, spring constant that involves both mass and angular frequency

$$\chi_\beta = \boldsymbol{\omega}_\beta^2 \mathrm{m}_\beta \tag{98}$$

has been connected to electron charge by Jackson [136] and hence may also help in future understanding of exact physical nature of charge in physics.

In closing this section, it is instructive to note that the universality of transition between turbulent (highly dissipative) and laminar (weakly dissipative) flows across many scales (Fig. 1) discussed in a recent study [140], is in complete harmony with the hydrodynamic model of electrodynamics described above. Therefore, starting with the pioneering discovery of superconductivity by Onnes [141] at electrodynamic scale, one identifies super-luminosity (laser action) at much smaller scale of optics or dry hydrodynamics [17], super-fluidity at larger molecular dynamics scale, and laminar flow at much larger hydrodynamic scale. At the exceedingly large cosmic scales, besides the well-known cosmic lasers due to amplification of light waves, one anticipates much more powerful rays associated with stimulated amplification of tachyon waves. Hence, generalization of all such phenomena could be referred to as *matter-wave amplification due to stimulated emission of de Broglie matter wave packets*.

Implications to Quantum Cosmology, Everett Multiverse, and Quantum Gravity

An important advantage of the invariant model of Boltzmann statistical mechanics and the associated generalized thermodynamics (Fig. 1) is in helping to extrapolate knowledge from intermediate scales to much larger and much smaller scales that are less accessible to our ordinary physical intuition. As described in recent studies [90, 140], a factor of approximately 10^{17} separates the scales of five major statistical fields in our universe starting with tachyon (graviton)-dynamics at exceedingly small Planck scale 10^{-35} m, followed by electrodynamics 10^{-18} m, hydrodynamics 10^{0} m, astrophysics 10^{18} m, and finally galactic-dynamics (cosmology) 10^{35} m. Each statistical field has its "atomic" particle namely, graviton, electron, fluid-element, star, and galaxy. In the previous Section, the intuitively accessible hydrodynamics at intermediate scale was employed to model extremely small scale of electrodynamics. In the same spirit, in the present section, physical concepts from intermediate scale of classical hydrodynamics will be employed to model the exceedingly large scale of cosmology.

In view of the extremely large number of galaxies and large distances between them, flow of galaxies in cosmology [142-145] may be assumed as ideal gas thus follow invariant Boltzmann statistical mechanics and the associated generalized thermodynamics [140,146]. Hence, conservation equations (4)-(7) describe dynamics of spectrum of galactic clusters containing a corresponding spectrum of galaxies as "atoms" of *turbulent statistical field* $\mathbb{F}_\beta = \mathbb{F}_{\rm g}$ that resides within a *background space* $\mathbb{S}_{\rm g}$ defined as the field of astrophysics $\mathbb{S}_{\rm g} = \mathbb{F}_{\rm s}$ at the next lower scale of $\beta - 1 = {\rm s}$.

Ironically, turbulent hydrodynamic model of cosmology following conservation equations (4)-(7) is precisely the quantum theory of gravity as a *dissipative deterministic dynamic system* recommended by 't Hooft [147]. At cosmic scales, Navier-Stokes equation motion (19) and Helmholtz vorticity equation (20) account for dissipation of

ordered motions across hierarchy of scales into random thermal motions. Dissipations of ordered translational, rotational, and pulsational velocities into random thermal velocities are schematically shown in Fig. 17.

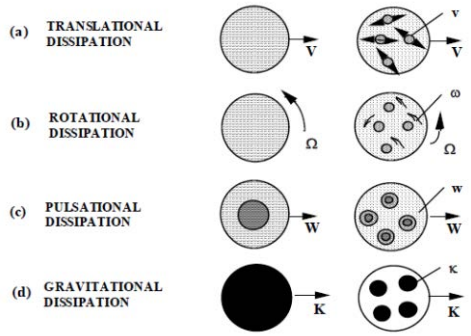

Figure 17 – Dissipation of momentum from global $(\mathbf{V}_z, \Omega_\theta, \mathbf{W}_r, \mathbf{K})$ to local $(\mathbf{v}_z, \omega_\theta, \mathbf{w}_r, \kappa)$: (a) translational (b) rotational (c) vibrational (d) gravitational degrees of freedom [33].

The last type of dissipation in Fig. 17 called *gravitational dissipation* [33, 147] corresponds to dissipation of large-scale curvature to random small-scale curvature such as a large droplet breaking up into many small droplets in sprays.

In equilibrium galactic-dynamics EGD field at scale $\beta = \mathbf{g}$, every "point" of cosmic space will be occupied by either "atom", i.e., a galaxy or vacuum [73]

$$\mathbb{S}_g = \begin{cases} \hat{\mathbf{m}}_g \equiv \text{vacuum} = \mathbf{V}_g \\ \varnothing \equiv (\text{vacuum} - \text{vacuum}) = \mathbf{V}\mathbf{V}_g = \mathbf{V}_s \end{cases} \tag{99}$$

Therefore, cosmic vacuum like Casimir vacuum shown in Fig. 3 is not empty and the model (Fig. 1) suggests a hierarchy of vacua defined as [33]

$$\begin{aligned} (\text{vacuum} - \text{vacuum})_\beta &= \mathbf{V}\mathbf{V}_\beta = \\ &= (\text{vacuum})_{\beta-1} = \mathbf{V}_{\beta-1} \end{aligned} \tag{100}$$

To emphasize the importance of such hierarchies of vacua to cosmology we make the following quotation from 't Hooft [148]

This means that there is one very special state where all energies are zero: the vacuum state. Identifying the vacuum state is particularly difficult in our theory, but it seems that the vacuum also poses problems in other approaches. In loop quantum gravity, it is notoriously difficult to say exactly what the vacuum state is in terms of the fundamental loop states that were introduced there. In superstring theory, there are many candidates for the vacuum, all being distinctly characterized by the boundary conditions and the fluxes present in the compactified par of space-time. String theory ends up leaving an entire 'landscape' of vacuum states with no further indication as to which of these to pick. It is of crucial importance in any theory of Planck length physics to identify and describe in detail the vacuum state.

It is emphasized that according to the present model of physical space (Fig. 3), the only true and absolute vacuum-vacuum is the *white hole* that is a singularity of the field with exact density $\rho_{WH} = \mathbf{0}$.

To describe hydrodynamics of the universe, following Section 3, the atomic (length, time, mass) of cosmic field are defined as the *most probable* (length, time, mass) of astrophysical statistical field

$$(\hat{\lambda}_g, \hat{\tau}_g, \hat{\mathbf{m}}_g) = (\lambda_{w,s}, \tau_{w,s}, \mathbf{m}_{w,s}) \tag{101}$$

At thermodynamic equilibrium, the equality of temperature of cosmic and astrophysical fields $T_g = T_s = \lambda_{w,s}$ gives the atomic mass unit of cosmic field $\hat{\mathbf{m}}_g = \mathbf{m}_{w,s}$. Also, from the definition of temperature $\mathbf{k}\mathbf{T}_s = \mathbf{m}_{w,s}\mathbf{v}_{w,s}^2$ and most probable speed $\mathbf{v}_{w,m} = \lambda_{w,m} / \tau_{w,m}$, one obtains the atomic time $\hat{\mathbf{t}}_g = \tau_{w,m}$ of equilibrium galactic dynamics (EGD) field.

Having defined the atomic units of space, time, and mass, one asks the question that was asked by both Boltzmann and Planck namely: given the total number of atoms (galaxies) N and the total energy $H = 4N\mathrm{k}T$ of the universe, what is the distribution of sizes of galactic clusters N_j that results in *stochastically stationary* cosmic field. The probability of cluster of size N_j is identified as the *inverse* of what Boltzmann called *number of complexions* W_j that is given by Boltzmann-Planck formula [34]

$$P_j = \frac{N_j!\,(g_j - 1)!}{(N_j + g_j - 1)!} = \frac{1}{W_j}, \quad P = \prod_j P_j = \frac{1}{W} \tag{102}$$

Following Planck [100], equation (102) leads to invariant distribution for energy spectra of galaxies.

$$\frac{\varepsilon_g dN_g}{V} = \frac{8\pi h}{u_g^3}\frac{\nu_g^3}{e^{h\nu_g/kT}-1}d\nu_g \qquad (103)$$

At thermodynamic equilibrium between matter and radiation, equation (103) corresponds to Planck [100] spectral energy distribution of equilibrium radiation with ¾ and ¼ fractions of total energy on $\nu_j > \nu_w$ and $\nu_j < \nu_w$ sides of Wien frequency ν_w as shown in Fig. 18.

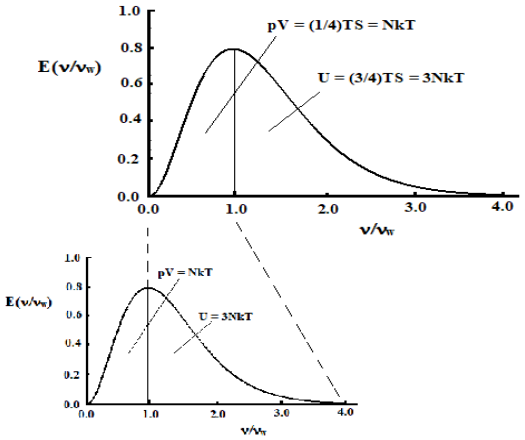

Figure 18 – Re-normalized Planck energy distributions as a function of ν / ν_w [36].

Comparison of astrophysical measurements [149] with Planck equilibrium energy spectrum at approximate temperature 2.73 m is shown in Fig. 19.

The fluctuations of the observed temperature perturbations in Fig. 19 corresponding to Penzias-Wilson [121,122,123] cosmic microwave background temperature $T_{CMB} \approx 2.73\ \mathrm{m}$ is known to be about $\nabla T \approx 1/10{,}000\ \tilde{\mathrm{m}}$ Normalizing data in Fig. 19 with Wien frequency $\nu / \nu_w = \nu / 225$, leads to $\nu_\infty / \nu_w \approx 900/225 = 4$ as the limit beyond which the spectral energy vanishes in close agreement with normalized Planck distribution in Fig. 18.

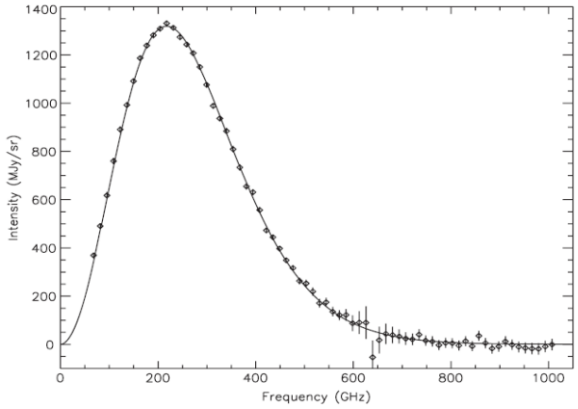

Figure 19 – Mean spectrums associated with the velocity of the solar system with respect to the CMB. The line is the a priori prediction based on the *WMAP* velocity and the previous FIRAS calibration. The uncertainties are the noise from the FIRAS measurements. The error bars are slightly misleading, because they do not show the correlations, but the correlated errors are properly treated in the fit. [149].

Close agreement of cosmic microwave background temperature with Planck distribution (Fig. 19) is strong evidence for near equilibrium state of universe. Therefore, it is natural to expect that distribution of speed of galaxies should follow invariant normalized Maxwell-Boltzmann distribution [36]

$$\frac{dN_{u\beta}}{N} = 4\pi \left(\frac{m_\beta}{2\pi k T_\beta}\right)^{3/2} u_\beta^2 \, e^{-m_\beta u_\beta^2/2kT_\beta} du_\beta \quad (104)$$

Calculated Normalized Maxwell-Boltzmann (NMB) distribution as a function of speed re-normalized with respect to the most-probable or Wien speed $v / v_w = \lambda_w / \lambda$ at two adjacent scales are shown in Fig. 20.

NMB distribution in Fig. 20 closely agrees with typical observed distribution of fractions of galaxy clusters containing *N* galaxies reported by Saslaw and Crane [150], Lahav and Saslaw [151], and Saslaw [152] shown in Figs. 21 and 22.

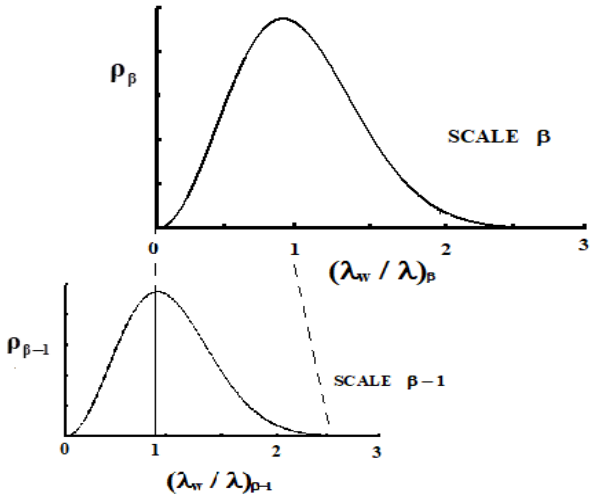

Figure 20 – Re-normalized Maxwell-Boltzmann distribution as a function of dimensionless speed $v / v_w = \lambda_w / \lambda$ [36].

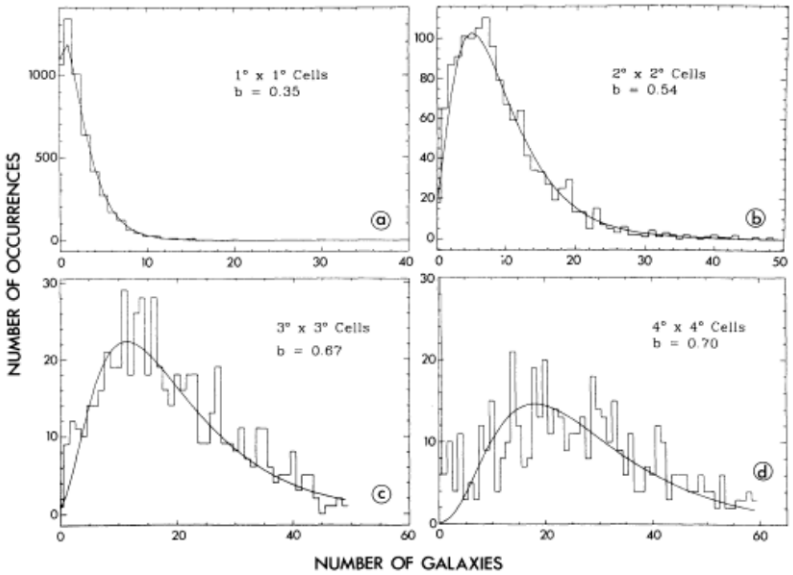

Figure 21 – Observed distribution fraction of galaxy clusters containing N galaxies [150].

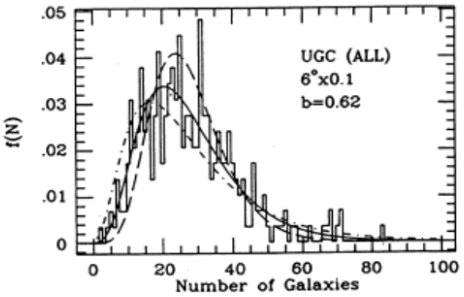

Figure 22 – Observed distribution fraction of galaxy clusters containing N galaxies [151].

Normalizing the data in Figs. 21d or 22 with Wien number $N_w = 20$, leads to maximum $N_\infty / N_w \approx 60/20 = 3$ in agreement with NMB distribution in Fig. 20.

Planck distribution of cosmic microwave background radiation energy in Figs. 18 and 19, Maxwell-Boltzmann distribution of galactic sizes hence speeds in Figs. 20-22, derivation of invariant Schrödinger equation from invariant Bernoulli equation [37], and finally the observed *quantum jumps* in red shifts of galaxies [153] are all in harmony with the hypothesis of quantum cosmology. Assuming incompressible potential flow, dynamics of universe will be governed by invariant Schrödinger equation with peculiar velocity of galaxies defining its wave function. However, a more realistic model will be the *dissipative deterministic dynamic system* theory of quantum gravity proposed by 't Hooft [147], involving solutions of conservation equations (4)-(7) under relativistic (compressible) and viscous hydrodynamics. In view of invariant Schrödinger (65)-(67) and Dirac relativistic wave equation (71), the present invariant hydrodynamic model may help in closure of the gap between quantum theory of gravitation and quantum mechanics. The connection of quantum mechanics with Einstein [154] GTR is less intuitive due to the complex mathematical structure of tensors and differential geometry of Riemann.

Interestingly, in a recent excellent investigation by Nugayev [155], concerning the historical development of GTR, research programs of Nordström *scalar theory*, Abraham *vector theory*, and Einstein *tensor theory* of gravitation were described. Clearly, the hydrodynamic model of cosmology involving (4)-(7) contain primarily scalar and vector terms, and only one tensor namely total stress tensor P_{ij} in (6). Therefore, it is expected that scalar and vector theories of Nordström and Abraham discussed in [155] will play important roles in future development of quantum theories of gravitation. This is in part because scientific developments also follow Hamiltonian principle of least energy, and following more familiar classical hydrodynamics with scalar and vector theories are much simpler and intuitively accessible than complex tensor theories of Riemannian geometry!

When physical space is identified as a fluid, it is natural to attribute gravitational forces to gradients of ether density hence pressure as schematically shown in Fig. 23.

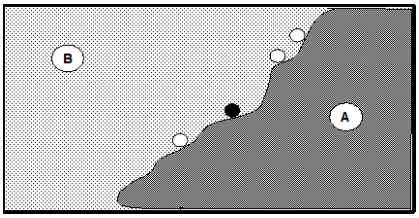

Figure 23 – Schematic diagram of motion in a "curved space". The particle moves along the trajectory defined as the interface between higher density medium A and lower density medium B.

Hence, in a recent investigation [140], gravitational force was related to normal stress expressed as diffusional flux of momentum applying (11)

$$\tau_{iig} = \frac{\boldsymbol{F}_g}{\mathrm{A}} = \rho_e \mathbf{v}_{ie} \boldsymbol{V}_{iie} = \rho_e \mathbf{v}_{ie} (-D_e \nabla \rho_e / \rho_e) \quad (105)$$

leading to Newton law of gravitation as pressure gradient of ether or Casimir [63] vacuum [140, 156]

$$\boldsymbol{F}_g = -m_e \nabla p_e / \rho_e = m_e \mathbf{g} \quad (106)$$

with gravitational acceleration defined as

$$\mathbf{g} = -\nabla p_e / \rho_e \quad (107)$$

According to (105)-(107), solution of conservation equations (4)-(7) under appropriate boundary conditions provide (ρ, T, p) scalar fields hence gravitational forces at each location. Following Poincaré [82] description of hyperbolic

geometry and Gauss classical definition of intrinsic surface curvature, a one-dimensional line curvature was recently defined as atomic line density [140] in accordance with (64)

$$\kappa_x \equiv \frac{N_x}{L_x} = \frac{N_x}{N_x \lambda_w} = \frac{1}{\lambda_w} = \frac{1}{T} \qquad (108)$$

Also, since for ideal gas $p_\beta = \rho_\beta R_\beta T_\beta$, density and temperature are inversely related, by (109) local scaler curvature is defined as deviation of density from that of equilibrium Casimir vacuum [37,140]

$$\kappa = \rho - \rho_v \qquad (109)$$

Hence, cosmic field involves three geometries

$$\begin{aligned} &\kappa > 0 \text{ Matter (Riemannian space)} \\ &\kappa = 0 \text{ Casimir Vacuum (Euclidean space)} \\ &\kappa < 0 \text{ Anti-matter (Lobachevskian space)} \end{aligned} \qquad (110)$$

In his description of hyperbolic geometry, Poincaré [82] introduced what is known as *Poincaré disk* schematically shown in Fig. 24.

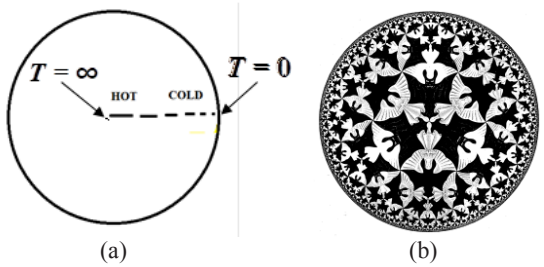

(a) (b)

Figure 24 – (a) Poincare disk with white hole at origin $T \to \infty$ and black hole on circumference $T \to 0$ **(b)** Circle Limit IV (Heaven and hell) by M.C. Escher [74].

Also shown in Fig, 24, is the wonderful woodcut print by Escher [157] called Circle Limit IV (heaven and hell) graphically showing hyperbolic geometry. The one-dimensional line density as curvature (108) hence (109) may be viewed as *generalized non-Euclidean geometry* that is in harmony with perceptions of Poincaré [82] as well as non-standard analysis discussed in [158].

The temperature limits $(T \to \infty, T \to 0)$ correspond to (white hole, black hole) at the (origin, circumference) of Poincaré disk. Concerning the temperature limits in Fig. 24, it is interesting to examine Maxwell-Boltzmann distribution in Fig. 5 for ether or Casimir vacuum (Fig. 3) at three different thermodynamic temperatures as schematically shown in Fig. 25. One notes that as temperature is increased, eventually all photons as Bose-Einstein liquid evaporate into gravitons and the entire distribution function collapses on the horizontal axis that is identified as *white hole* in accordance with Figs. 3 and 24. On the other hand, as the temperature is steadily decreased, eventually all space, i.e., superfluid Bose-Einstein condensate solidify and all distribution curves shown in Fig. 25 "freeze" by collapsing on the vertical axis corresponding to *solid light* or "black hole" [37,90] singularity in accordance with Figs. 3 and 24.

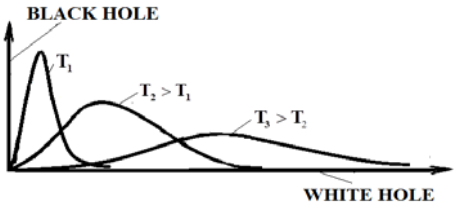

Figure 25 – Black-hole and White-hole limits on maxwell-Boltzmann speed distribution as temperature of ether or Casimir vacuum approaches zero and infinity.

Because of the change of units $(\mathrm{cm/m} \to 1/100)$ required by Wien displacement law $\lambda_w T = 0.29\ \mathrm{cm.K} = 0.0029\ \mathrm{m^2}$ due to modified dimension of absolute thermodynamic temperature [34], the classical formula for transformation to Kelvin absolute temperature becomes

$$T(\mathrm{m}) = {}^\circ C(\mathrm{m}) + 2.731(\mathrm{m}) \qquad (111)$$

The constant 2.731 in (111) is close to Penzias-Wilson [121-123] cosmic microwave background temperature $T_{CMB} \approx 2.73\ \mathrm{m}$ suggesting that the entire universe is at ice temperature. The fact that our universe is very close to the state of thermodynamic equilibrium is evidenced by the observed thermal nature of Penzias-Wilson [121-123] cosmic background temperature $T_{CMB} \approx 2.73\ \mathrm{m}$ (Fig. 19), as well as equilibrium distribution of speed of galaxies shown in Figs. 21 and 22.

As discussed in [140], the magnitude of Planck temperature

$$T_{\rm p} = (\hbar c^5 / Gk^2)^{1/2} \approx 3.55\times 10^{32}\ {\rm m} \qquad (112)$$

introduces a paradox since it corresponds to most probable wavelength of photon thermal oscillation that is larger than the reported size of our universe 10^{26}. In view of Fig. 1, this suggests that our universe with (atom, element, system) lengths

$$\text{EGD} \quad (\ell_{\rm g},\ \lambda_{\rm g},\ {\rm L_g}) = (10^{18},\ 10^{26},\ 10^{35})\ {\rm m} \qquad (113)$$

is Lemaître [159] "*primordial atom*" of a much larger Everett [160] *multiverse* with (atom, element, system) lengths [140]

$$\text{EUD} \quad (\ell_{\rm u},\ \lambda_{\rm u},\ {\rm L_u}) = (10^{35},\ 10^{43},\ 10^{52})\ {\rm m} \qquad (114)$$

This is in harmony with hierarchy shown in Fig. 1 as well as inflationary theories of cosmology [161-164].

Interestingly, recent cosmological observations have revealed a small asymmetry in the power spectrum from the right versus the left side of our universe [165] schematically shown in Fig. 26.

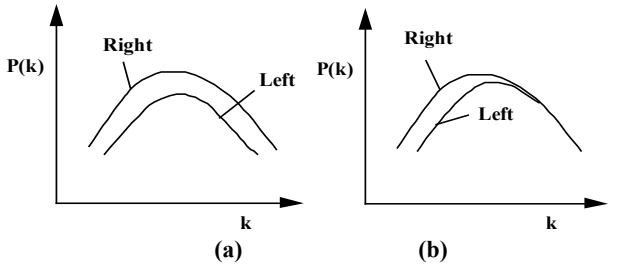

Figure 26 – Asymmetry in measured cosmic power spectrum (a) calculated (b) measured [165].

It is reasonable to attribute the asymmetry in Fig. 26 to the fact that our universe is rotating [35]. When our universe is identified as Lemaître [159] "*primordial atom*" of a much larger Everett [160] *multiverse*, finite "iso-spin" of our universe within multiverse becomes understandable and harmonious with the observed rotation of almost all galaxies. Moreover, this is also in harmony with Gödel [166] wonderful 1949 study introducing *closed time-like solutions* of Einstein field equations in rotating universe with non-vanishing cosmological constant. Furthermore, Gödel [166] rotating universe is in harmony with Kerr [167] solution for rotating black hole.

In view of the scale-invariant nature of quantum mechanics (65)-(67), it is interesting to view the spectral sizes of ether or space "quanta" at thermodynamic equilibrium in "empty" de Sitter [168] universe given by Maxwell-Boltzmann distribution [140]. At any temperature, Poincaré *thermal measure* $T_\beta = \lambda_{w\beta}$ [90] could be applied to define respectively microscopic (intensive) *most probable atomic* volume $\hat{\rm v}_{w\beta}$ and macroscopic (extensive) *system* volume V_β as

$$\hat{\rm v}_{w\beta} = \lambda_{w\beta}^3 = T_\beta^3\ ,\ \ V_\beta = \sum \hat{\rm v}_{w\beta} = N_\beta \hat{\rm v}_{w\beta} \qquad (115)$$

Similarly, one defines a *spectrum* of *atomic* and *cluster* or "element" volumes

$$\hat{\rm v}_{j\beta} = \lambda_{j\beta}^3\ ,\ \ V_{j\beta} = \sum_{\rm i} \hat{\rm v}_{ij\beta} = N_{i\beta} \hat{\rm v}_{ij\beta} \qquad (116)$$

such that the total system volume in (115) can also be expressed as

$$V_\beta = \sum_{\rm j} V_{j\beta} \qquad (117)$$

Therefore, according to the model (Fig. 1), physical space is composed of a spectrum of *element volumes* that contain corresponding spectrum of *atomic volumes* at thermodynamic equilibrium in harmony with modern concepts of loop quantum gravity [147,169-175]. Clearly, transformation of Wheeler-DeWitt equation [169-171] into Schrödinger equation (65)-(67) through resurrection of *internal* thermodynamic time [140], will help the closure of the gap between quantum gravity and quantum mechanics. A most fundamental aspects of quantum gravity is the critical role of probability due to stochastic nature of Casimir vacuum hence universality of chance [112,176-178] as an indispensable feature of quantum mechanics in harmony with perceptions of Heisenberg [75,79].

An outstanding problem of cosmology [142-145] is the origin of initial perturbations responsible for galaxy formation. Since universe is a chemically reactive system [179], in view of the scale invariance of the model (4)-(7), it is reasonable to expect that, similar to combustion

science at molecular-dynamic scale [40], thermos-diffusive instabilities govern hydrodynamics of the universe after explosion of Lemaître [159] "primordial atom" or Big Bang. Two examples of thermos-diffusive instability leading to cellular flames in rich premixed butane-air are shown in Fig. 27.

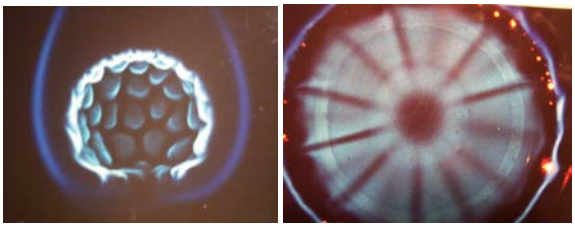

(a) (b)

Figure 27 – Formation of cellular thermo-diffusive instability in rich butane-air premixed flame with Lewis number based of deficient species Le < 1 stabilized on (a) A porous sphere (b) Stagnation-point flow against planer quartz plate.

The geometry of cellular flame depends on boundary conditions as seen in Fig. 27. For example, in 2-dimensional stagnation point flow as opposed axi-symmetric one shown in Fig. 27b, cellular flame instability leads to a row of parallel flame stripes. Relative scale-invariant diffusivities [36] of mass D_β, heat $\alpha_\beta = \sigma_\beta / \rho c_p$, and momentum $\tilde{\kappa}_\beta = \eta_\beta / \rho_\beta$ in (4)-(7) govern "flame" instabilities and their interactions according to hydro-thermo-diffusive theory of laminar flames [180].

In closing this Section, it is instructive to briefly consider another interesting and outstanding problem of cosmology namely the lack of knowledge of the boundary conditions of universe. Of course, without knowing such boundary conditions, the global hydrodynamics of universe cannot be determined from solution of (4)-(7). According to quantum mechanics (65-67), stability of particle is due to an external pressure known as Poincaré stress [36,37]. It is therefore reasonable to attribute stability of galactic clusters to a surrounding halo due to chaotic random motion of galaxies. Similarly, halos due to chaotic random motion of stars could be responsible for stability of galaxies.

Although the present thermodynamic model of cosmology cannot resolve the boundary condition problem, perhaps the following analogy will help in visualization of the problem. A classical problem of boundary conditions in fluid mechanics is known as *Stokes paradox* and concerns solution of equation of motion for creeping uniform laminar flow of viscous fluid across a rigid cylinder. No solutions that simultaneously satisfy vanishing velocity on the rigid cylinder and uniform velocity far away from cylinder could be found. However, recently Stokes paradox was resolved by finding the solution of modified form of equation of motion (19) for viscous flow across a rigid cylinder given by stream function [32]

$$\Psi_{RC} = -\xi(1 - 2/\xi + 1/\xi^2)\sin\theta \qquad (118)$$

where $\Psi_{RC} = \Psi'_{RC} / R'_i U$, $\xi = r'/R'_i$, and R'_i is radius of rigid cylinder. Some streamlines calculated from (118) are shown in Fig. 28.

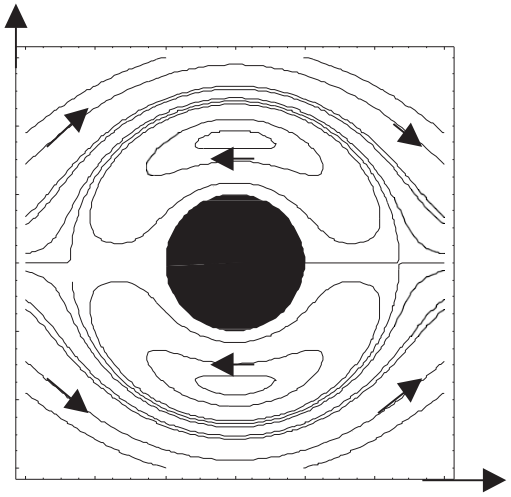

Figure 28 – Streamlines for Stokes uniform viscous flow across a rigid cylinder [32].

The radial and angular velocities obtained from (118) are

$$v_r = -(1 - 2/\xi + 1/\xi^2)\cos\theta\,, \qquad v_\theta = (1 - 1/\xi^2)\sin\theta \qquad (119)$$

As seen in Fig. 28, the problem of matching of solution to have vanishing velocities at the wall and uniform flow in far field is resolved through formation of two cylindrical line-vortices forming a closed viscous *boundary layer* with flow recirculation that in effect isolates the rigid cylinder from the outer potential flow. Thus, Stokes paradox helps to illustrate that nature in its infinite possibilities can accommodate diverse boundary

conditions through creation of intermediary transition layers such as the recirculation zone in Fig. 28. Although the boundary conditions of our universe remain to be determined by future investigations, it is reasonable to anticipate that like galaxies and cluster of galaxies, the boundary condition of our universe within much larger Everett [160] multiverse is also chaotic in nature [78,181].

Concluding Remarks

The study was focused on some implications of a scale-invariant model of Boltzmann statistical mechanic to four different areas pertaining to fundamental problems of theoretical physics. First part concerned quantization of space, time, and mass leading to clarification of concept of internal time, Rovelli [70] thermal time, invariant definition of atomic mass, mass-energy equivalence, and Joule-Mayer mechanical equivalent of heat. In the second part the model was applied to physical foundations of invariant Schrödinger equation of quantum mechanics as well as special theory of relativity. In particular, new perspectives concerning resolution of seven important problems regarding physical interpretation of quantum mechanics were presented.

In the third part of study the implication of the model to Maxwell theory of electromagnetism was studied. A hydrodynamic model of electromagnetism was introduced leading to new perspectives concerning the nature of electric and magnetic fields as well as that of electric charge. Finally, in part four of the study, some of the implications of the model to the fields of cosmology, quantum gravity, and quantum cosmology were addressed. The predicted equilibrium speed distribution of galaxies was found to be in good agreement with existing cosmological data. Physical space or Casimir vacuum was found to be composed of a spectrum of quantized space volume elements each composed of corresponding spectrum of atomic space volume quanta in harmony with modern theories of loop quantum gravity. The results were found to be in accordance with quantum gravity as a dissipative deterministic dynamic system proposed by ‘t Hooft [147].

Acknowledgments

This research was in part supported by NASA grant No. NAG3-1863.

References

1. L. de Broglie, Interference and corpuscular light, Nature 118, 441-442 (1926); Sur la possibilité de relier les phénomènes d'Interférence et de diffraction à la théorie des quanta de lumière, C. R. Acad. Sci. Paris, 183, 447-448 (1927); La structure atomique de la matière et du rayonnement et la mécanique ondulatoire, 184, 273-274 (1927); Sur le rôle des ondes continues en mécanique ondulatoire, 185, 380-382 (1927).
2. L. de Broglie, *Non-Linear Wave Mechanics: A Causal Interpretation*, Elsevier, New York, 1960.
3. L. de Broglie, The reinterpretation of wave mechanics, Found. Phys. 1(5), 5-15 (1970).
4. E. Madelung, Quantentheorie in hydrodynamischer form, Z. Physik. 40, 332-326 (1926).
5. E. Schrödinger, Über die Umkehrung der Naturgesetze, Sitzber Preuss Akad Wiss Phys-Math Kl 193, 144-153 (1931).
6. R. Fürth, Über Einige Beziehungen zwischen klassischer Staristik und Quantenmechanik, *Z.* Phys. 81, 143-162 (1933).
7. D. Bohm, A suggested interpretation of the quantum theory in terms of “Hidden Variables" I, Phys. Rev. 85(2), 166-179 (1952).
8. T. Takabayasi, On the foundation of quantum mechanics associated with classical pictures, Prog. Theor. Phys. 8(2), 143-182 (1952).
9. D. Bohm, and J. P. Vigier, Model of the causal interpretation of quantum theory in terms of a fluid with irregular fluctuations, Phys. Rev. 96 (1), 208-217 (1954).
10. E. Nelson, Derivation of the Schrödinger equation from Newtonian mechanics, Phys. Rev. 150 (4), 1079-1085 (1966).
11. E. Nelson, *Quantum Fluctuations*, Princeton University Press, Princeton, NJ,1 985.
12. L. de la Peña, New Foundation of Stochastic Theory of Quantum Mechanics, J. Math. Phys. 10(9), 1620-1630 (1969).
13. L. de la Peña, and A. M. Cetto, Does quantum mechanics accept a stochastic support? Found. Phys. 12(10), 1017-1037 (1982).
14. A. O. Barut, Schrödinger’s interpretation of □ as a continuous charge distribution, Ann. der Phys. 7(4-5), 31-36 (1988).
15. A. O. Barut, and A. J. Bracken, Zitterbewegung and the internal geometry of the electron, Phys. Rev. D 23 (10), 2454-2463 (1981).
16. J. P. Vigier, De Broglie waves on Dirac aether: A testable experimental assumption, *Lett. Nuvo Cim*. 29(14), 467-475 (1980); C. Cufaro Petroni, and J. P. Vigier, Dirac’s aether in relativistic quantum mechanics, Found. Phys. 13(2), 253-286 (1983);

J. P. Vigier, Derivation of inertia forces from the Einstein-de Broglie-Bohm (E.d.B.B) causal stochastic interpretation of quantum mechanics, Found. Phys. 25(10), 1461-1494 (1995).

17. F. T. Arecchi, and R. G. Harrison, *Instabilities and Chaos in Quantum Optics*, Springer-Verlag, Berlin, 1987.

18. O. Reynolds, On the dynamical theory of incompressible viscous fluid and the determination of the criterion, Phil. Trans. Roy. Soc. A 186(1), 123-164 (1895).

19. D. Enskog, Kinetische Theorie der Vorgange in Massig Verdunnten Gasen, Almqvist and Wiksells Boktryckeri-A.B., Uppsala, 1917. English translation: G. S. Brush, *Kinetic Theory*, 125-225, Pergamon press, New York, 1965.

20. G. I. Taylor, Statistical theory of turbulence-parts I-IV, Proc. Roy. Soc. A 151(873), 421-478 (1935).

21. T. Kármán, and L. Howarth, On the statistical theory of isotropic turbulence, Proc. Roy. Soc. A 164(917), 192-215 (1938).

22. H. P. Robertson, The Invariant theory of isotropic turbulence, Proc. Camb. Phil. Soc. 36, 209-223 (1940).

23. A. N. Kolmogorov, Local structure on turbulence in incompressible fluid, C. R. Acad. Sci. U. R. S. S. 30, 301-305 (1941); A refinement of previous hypothesis concerning the local structure of turbulence in a viscous incompressible fluid at high Reynolds number, J. Fluid Mech. 13, 82-85 (1962).

24. A. M. Obukhov, On the distribution of energy in the spectrum of turbulent flow, C. R. Acad. Sci. U. R. S. S. 32, 19-22 (1941); Some specific features of atmospheric turbulence, J. Fluid *Mech.* 13, 77-81 (1962).

25. S. Chandrasekhar, Stochastic problems in physics and astronomy, Rev. Mod. Phys. 15(1), 1-89 (1943).

26. S. Chandrasekhar, *Stochastic, Statistical, and Hydrodynamic Problems in Physics and Astronomy*, Selected Papers, vol.3, University of Chicago Press, Chicago, 199-206, 1989.

27. W. Heisenberg, On the theory of statistical and isotropic turbulence, Proc. Roy. Soc. A 195, 402-406 (1948); Zur Statistischen Theorie der Turbulenz, Z. Phys. 124(7-12), 628-657 (1948).

28. G. K. Batchelor, *The Theory of Homogeneous Turbulence*, Cambridge University Press, Cambridge, 1953.

29. L. D. Landau, and E. M. Lifshitz, *Fluid Dynamics*, Pergamon Press, New York, 1959.

30. H. Tennekes, and J. L. Lumley, *A First Course in Turbulence*, MIT Press, 1972.

31. S. H. Sohrab, Invariant forms of conservation equations and some examples of their exact solutions, J. Energy Resources Technol. 136, 1-9 (2014).

32. S. H. Sohrab, Solutions of modified equation of motion for laminar flow across (within) rigid (liquid) and sphere and cylinder and resolution of Stokes paradox, *AIP Conference Proceedings* 1896, 130004 (2017).

33. S. H. Sohrab, Some implications of a scale invariant model of statistical mechanics to classical and relativistic thermodynamics, Int. J. Thermo. 17(4), 233-248 (2014).

34. S. H. Sohrab, On a scale-invariant model of statistical mechanics and the laws of thermodynamics J. Energy Resources and Technol. 138(3), 1-12 (2016).

35. S. H. Sohrab, Quantum theory of fields from Planck to cosmic scales, WSEAS Trans. Math. 9, 734-756 (2010).

36. S. H. Sohrab, On a scale invariant model of statistical mechanics, kinetic theory of ideal gas, and Riemann hypothesis, Int. J. Mod. Communication Tech. & Research. 3(6), 7-37 (2015).

37. S. H. Sohrab, Connecting Bernoulli and Schrödinger Equations and its Impact on Quantum-Mechanic Wave Function and Entanglement Problems, C.H. Skiadas and Y. Dimotikalis (eds.), *13th Chaotic Modeling and Simulation international Conference,* Springer Proceedings in Complexity, 2021.

38. R. S. de Groot, and P. Mazur, *Nonequilibrium Thermodynamics*, North-Holland, 1962.

39. H. Schlichting, *Boundary-Layer Theory*, McGraw Hill, New York, 1968.

40. F. A. Williams, *Combustion Theory*, 2nd Ed., Addison Wesley, New York, 1985.

41. J. O. Hirschfelder, C. F. Curtiss, and R. B. Bird, *Molecular Theory of Gases and Liquids,* Wiley, New York, 1954.

42. S. Chapman, and T. G. Cowling, *The Mathematical Theory of Non-Uniform Gases*, Cambridge University Press, Cambridge, 1953.

43. R. Clausius, "Uber die Art der Bewegung, welche wir W€arme nennen," Ann. Phys., 176(3), pp. 353–380 (1857).

44. R. Clausius, Ueber einen auf die Warme anwendbaren mechanischen Satz, Sitzungsberichte der Niedderrheinischen Gesellschaft, Bonn, Germany, 114–119 (1870).

45. J. H. Lugt, *Vortex Flow in Nature and Technology*, Wiley, New York, 1983.

46. O. Darrigol, Between hydrodynamics and elasticity theory: The first five births of the Navier-Stokes equation, *Arch. Hist. Exact Sci.* 56, 95-150, 2002.

47. A. B. Bahatia, and R. N. Singh, *Mechanics of Deformable Media*, IOP publication, Boston, 153, 1986.

48. O. Darrigol, *World of Flow,* Oxford University Press, New York, 123, 2005.

49. H. B. G. Onsager, Reciprocal relations in irreversible processes, I., *Phys. Rev.* 37, 405-425 (1931).

50. C, W, Oseen, Stokes formula and a related theorem in hydrodynamics, Ark. Mat. Astr. Fys. 6, 20. (1910).

51. G. Carrier, On slow viscous flow, Nonr-653-00-1 (1953).

52. H. von Helmholtz, Uber Integrale der hydrodynamischen Gleichungen, welche der Wirbelbewegung entsprechen, J. f˙ur die reine und angewandte Math-ematik, 55, 25-55, (1858).

53. Aristotle, in: *Time,* Westphal J. and Levenson, C., (Eds.), Hackett Publishing Company, Indianapolis, Indiana, 1993.

54. C. Huygens, *Treatise on Light*, p.14, Dover, 1912.

55. I. Newton, *Optics;* Dover: New York, 1952.

56. L. Euler, Réflexions sur l'espace et le temps. *Histoire de l'Academie Royale des sciences et belles lettres* 4, 324–333 (1748).

57. J. C. Maxwell, *A Treatise on Electricity and Magnetism*, Volumes 1 & 2, Dover Publication, New York, 1891.

58. J. Knox, Hendrik Antoon Lorentz, the Ether, and the General Theory of Relativity. In: *Einstein and the History of General Relativity*, Howard, D., and Stachel, J. (Eds.), 201-212, Birkhauser, Boston, 1989.

59. H. Poincaré, La théorie de Lorentz et le principe de réaction. Arch. Neerland. 5, 252-278 (1900); http://www.physicsinsights.org/poincare-1900.pdf

60. H. Poincaré, Sur la dynamique de l'électron, C. R. Acad. Sci., Paris 140, (1905).

61. H. Poincaré, Sur la dynamique de l'electron, Rend. Circ. Mat. Palermo 21(12), 9-175 (1906).

62. A. A. Logunov, *On the Articles by Henri Poincaré: "On the Dynamics of the Electron"*, Dubna: JINR, 2001.

63. H. B. G. Casimir, On the attraction between two perfectly conducting plates, Proc. K. Ned. Akad. Wet. 51, 793-795 (1948).

64. P. A. M. Dirac, Is there an aether?; Nature 168, 906 (1951).

65. E.T. Whittaker, *A History of the Theories of Aether and Electricity*, Vols. 1 &2, Tomash Publishers, New York, 1987.

66. H. A. Lorentz, Aether Theories and Aether Models, in: *Selected Works of L.H. Lorentz,* vol.5, Nersessian, N. J., and Cohen, H. F., (Eds.), Palm Publications, Nieuwerkerk, 1987, pp. 7-12.

67. G. Leibniz, Time is a Relation, In: *Time*, I. Westphal and C. Levenson, (Eds.), Hackett Publishing Company, Indianapolis, Indiana, p. 45, 1993.

68. W. Pauli, *Pauli Lectures on Physics,* Vol. 3, MIT Press, New York, 1973.

69. C. Rovelli, *The Order of Time*, Riverhead Books, 2018.

70. C. Rovelli, Statistical mechanics of gravity and the thermodynamical origin of time, Class. Quantum Grav. 10, 1549 (1993).

71 C. Rovelli, General relativistic statistical mechanics. *General Relativity and Quantum Cosmology*, 10.1103, Phys. Rev. D 87.084055, arXiv:1209.0065v2 (2012).

72. S. Hawking, *A Brief History of Time*, Bantam Book, New York, 1988.

73. Y. Vladimirov, N. Mitskievich, and J. Horsky, *Space Time Gravitation*, Mir Publishers, Moscow, 1987.

74. S. H. Sohrab, An invariant model of Boltzmann statistical mechanics and some of its implications to thermodynamics and quantum nature of space and time, WSEAS Tran, Appl. Theo. Mech. 13, 199-212 (2018).

75. W. Heisenberg, *The Physical Principles of Quantum Theory,* Dover, New York,1949.

76. A. Connes, On the Fine Structure of Spacetime. In: *On Space and Time*, Shahn M., ed.; Cambridge University Press, 2008, pp. 196-237.

77. H. Minkowski, Space and Time, in *Theory of Relativity*, p. 75, Dover, New York, 1952.

78. F. Verhulst, *Henri Poincaré, Impatient Genius*, 64, Springer, 2012.

79. W. Heisenberg, Ueber den anschaulichen Inhalt der quantentheoretischen Kinematik and Mechanik, *Zeitschrift für Physik*, 43: 172–198 (1927). English translation in Wheeler and Zurek 1983: 62–84.

80. W. Schommers, Space-Time and Quantum Phenomena, in *Quantum Theory and Pictures of Reality*, W. Schommers (ed.), Springer, Berlin, 217-277, 1989.

81. M. Jammer, *The Concept of Mass in Classical and Modem Physics*, Harvard University Press, Cambridge, Massachusetts, 1961.

82. H. Poincaré, *Science and Hypothesis*, Dover, New York (1952).

83. A. Einstein, Does the Inertia of a Body Depend Upon its Energy Content, *The Principle of Relativity*. Dover Publications, New York, (1956).

84. A. Einstein, *The Meaning of Relativity*, Dover Publications, New York, (1956).

85. H. Helmholtz, (Leipzig), Uber der Ehaltung der Kraft, Eine Physikalische Abhandlung 18(13), pp. 639–641, 1847.

86. A. Sommerfeld, *Thermodynamics and Statistical Mechanics*, Academic Press, New York, 1956.

87. O. De Pretto, Ipotesi dell'Etere nella Vita dell'Universo, *Reale, Inst. Veneto di Scienze*, *Lettere en Arti* 63(2) 439-500 (1904).

88. L. B. Okun, The concept of mass, Physics Today, April, 31-36 (1989).

89. A. Lorentz, Electromagnetic phenomena in a system moving with any velocity less than that of light, Proc. Acad. Sci. Amst. 6, 809-831 (1904)

90. S. H. Sohrab, Universality of Boltzmann Statistical Mechanics, Thermodynamics, Quantum Mechanics, and Shannon Information Theory, C.H. Skiadas and Y. Dimotikalis (eds.), *14th Chaotic Modeling and Simulation International Conference,* Springer Proceedings in Complexity, 2022.

91. F. Hasenöhrl, Zur Theorie der Strahlung in bewegten Körpern. *Ann. der Phys*. 16, 589-592, 1905.

92. S. H. Sohrab, Invariant laws of thermodynamics and validity of Hasenöhrl mass- energy equivalence formula m = (4/3) E/c^2 at photonic, electrodynamic, and cosmic scales, Bull. Amer. Phys. Soc. 62(1) 124 (2017).

93. J. D. Achenbach, *Wave Propagation in Elastic Solids*, p.124, North-Holland, 1973.

94. P. H. Eberhard, Restoring Locality with Faster-than-light Velocities, in *Waves and Particles in Light and Matter,* Alwyn van der Merwe and Augusto Garuccio (Eds.). Plenum Press, New York,19 (1994).

95. I. Recami, Classical tachyons and possible applications (A review of "Extended Special Relativity", *Nuovo Cim.* 9, No.6, (1986); *Tachyons. Monopoles and Related Topics.* North-Holland, Amsterdam, 1978.

96. V.M. Somsikov, The method of the description of dynamics nonequilibrium systems within the frames of classical mechanics, arxiv: 0710.0078v1 [physics.gen-ph] 29 September, 2007.

97. J. L. Bell, *The Continuous and the Infinitesimal in Mathematics and Philosophy*, Polimetrica, Milano, Italy, 2006.

98. H. Sommerfeld, *Die Bedeutung der Röntgenstrahlen für die heutige Physik*, Munich, 1925, p. 11. Cited in H. Weyl, *Philosophy of Mathematics and Natural Science*, Princeton, 1949.

99. L. Boltzmann, Weitere Studien uber das Warmegleichgewicht unter Gasmoleculen, *Sitzungsberichte Akad.Wiss.,* Vienna, Part II, 66, 1872, pp. 275-370. English translation: G. S. Brush, *Kinetic Theory*, 88-175, Pergamon press, New York, 1965.

100. M. Planck, On the law of the energy distribution in the normal spectrum, Ann. der Phys. 4, 553-558 (1901).

101. B. L. van der Waerden, *Sources of Quantum Mechanics,* B. L. van der Waerden (ed.), Dover, New York, 1967. 95.

102. G. 't Hooft, *The Cellular Automaton Interpretation of Quantum Mechanics*, Springer, 2016.

103. E. Schrödinger, Quantization as a problem of proper values, Part I, Ann. der Phys. 79, (4), 361-376 (1926), Quantization as a problem of proper values, Part II, Ann. der Phys. 79 (4), 489-527 (1926); Part III, Ann. der Phys. 81, 109-139 (1926).

104. W. Schommers, Evolution of Quantum Mechanics, in *Quantum Theory and Pictures of Reality*, W. Schommers (ed.), Springer, Berlin, 1-48, 1989.

105. B. L. van der Waerden, Towards Quantum Mechanics, in: *Sources of Quantum Mechanics,* van der Waerden, B. L. (ed.), Dover: New York, 1967, pp. 1-59.

106. J. T. Cushing, *Quantum Mechanics*, the University of Chicago Press, Chicago, 1994.

107. F. Laloe, and J. H. Freed, The effects of spin in gases. Sci. American 258(4) 94-101 (1988).

108. R. E. Sonntag, and G. J. van Wylen, *Fundamentals of Statistical Thermodynamics; John* Wiley, New York, 1966.

109. M. Kardar, *Statistical Physics of Particles;* Cambridge University Press, New York, 2007.

110. S. H. Sohrab, The physical foundation of a grand unified statistical theory of fields and the invariant Schrödinger equation. *WSEAS* Transactions on Circuits and Systems 3(4), 1017-1025 (2004).

111. M. Dersarkissian, Does wave-particle duality apply to galaxies? Lett. Nuovo Cim. 40(2), 390-394 (1984).

112. M. Born, Zur Quantenmechanik der Stoßvorgänge, *Z. Physik* 37, 863*,* 1926.

113. F. Selleri, Wave-Particle Duality: Recent Proposals for the Detection of Empty Waves, in: *Quantum Theory and Pictures of Reality*, W. Schommers (ed.), Springer, Berlin, 279-332, 1989.

114. J.S. Bell, Six Possible Worlds of Quantum Mechanics, in: *On the Foundations of Quantum Mechanics,* M. Bell, K. Gottfried and M. Veltman (Eds.). World Scientific Publishing,193 (2001).

115. C. Rovelli, On the meaning of time, *Financial Times*, April 20, 2018.

116. A. J. Kox, and H. F. Schatz, "*A Living Work of Art" The Life and Science of Hendrik Antoon Lorentz,* Oxford University Press, 2021.

117. S. H. Sohrab, Scale invariant model of statistical mechanics and quantum nature of space, time, and dimension, Chaotic Modeling and Simulation (CMSIM) 3, 231-245 (2016).

118. W. Pauli, *Theory of Relativity*, p. 204, Dover, 1958.

119. O. Darrigol, The mystery of the Einstein Poincaré connection, Isis 95(4) 614-626 (2004).

120. P. Galison, *Einstein's Clocks, Poincaré's Maps,* W. W. Norton & Company, New York, 2003.

121. A. A. Penzias, and R. W. Wilson, A measurement of excess antenna temperature at 4080 Mc/s. Astrophysics J. 142, 419-421 (1965).

122. P. J. E. Peebles, Lyman A, Page, Jr., and R, B. Partridge, *Finding the Big Bang, Cambridge* University Press, 2009.

123. D. Lambert, *The Atom of the Universe, The Life and Work of George Lemaître,* Copernicus Center Press, Krakow, 2015.

124. S. J. Prokhovnik, The physical interpretation of special relativity, in *Waves and Particles in Light and Matter,* Alwyn van der Merwe and Augusto Garuccio *(Eds.),* Plenum Press, New York, 85 (1994); *Found. Phys.* 9, 883 (1979).

125. T. Hirosige, The ether problem, the mechanistic world view, and the origins of the theory of relativity, *Historical Studies in the Physical Sciences,* 7(3)-82 (1976).

126. H. A. Lorentz, Electromagnetic Phenomena in A System Moving with Any Velocity Less Than the That of Light, in: *The Theory of Electrons*, Dover, New York, 1952.

127. A. Einstein, On the Electrodynamics of Moving Bodies, in: *The Principle of Relativity*. Dover Publications, New York, (1956).

128. S. H. Sohrab, Some thermodynamic considerations on the physical and quantum nature of space and time, International Conference on Efficiency, Cost, Optimization, Simulation, and Environmental Aspects & Energy Process Systems, Enschede, The Netherlands, July 4-7, 2000. WSEAS Transactions on Mathematics 3(4) (2004).

128. I. Recami, Classical tachyons and possible applications (A review of "Extended Special Relativity", *Nuovo Cim.* 9, No.6, (1986); *Tachyons. Monopoles and Related Topics.* North-Holland, Amsterdam, 1978.

130. A. A. Michelson, and E. W. Morley, On the relative motion of the Earth and the luminiferous ether, Am. J. Sci. 34, p.333 (1887).

131. Dirac, P.A. M., The evolution of the physicist's picture of nature, Sci, Amer. 208(5) 45-53 (1963).

132. H. Poincaré, *Mathematics and Science Last Essay*, p.19, General Books, Memphis, Tennessee, 2010.

133. A. M. P. Dirac, *Directions in Physics*, Wiley, New York, 1978.

134. G. 't Hooft, *In Search of The Ultimate Building Blocks*, p. 161, Cambridge University press, 1998.

135. O. Darrigol, *Electrodynamics from Ampère to Einstein,* Oxford University Press, 2021.

136. J. D. Jackson, *Classical Electrodynamics,* Wiley*,* New York, 1975.

137. P. G. Huray. *Maxwell's Equations*, Wiley, 2010.

138. W. P. Higgs, Broken symmetry and the masses of gauge bosons, *Phys. Rev. Lett.*13(16), 508-509 (1964).

139. L. Bass, and E. Schrödinger, Must mass of photon be zero? *Proc. Roy. Soc.* A 232, 1-6 (1955).

140. S. H. Sohrab, Examples of Applications of an Invariant Statistical Theory of Field to Cosmology, Astrophysics, Hydrodynamics, Electrodynamics, and Photonics, C.H. Skiadas and Y. Dimotikalis (eds.), *15th Chaotic Modeling and Simulation international Conference,* Springer Proceedings in Complexity, 2023.

141. D. Van Delft, and P. Kes, The discovery of superconductivity, Physics Today 66, 9, 38 (2010).

142. M. Lachièze-Rey, *Cosmology, A First Course,* Cambridge University Press, 1995.

143. M. V. Berry, *Principles of Cosmology and Gravitation, IOP* Publishing, Ltd., 1989.

144. P. Collier, *A Most Incomprehensible Thing: Notes Towards a Very Gentle Introduction to the Mathematics of Relativity,* Published by Incomprehensible Books, 3rd Edition, 2001

145. P. J. E. Peebles, *Cosmology's Century, An Insider History of our Modern Understanding of Universe,* Princeton University Press*,* 2020*.*

146. S. H. Sohrab, Scale-invariant model of Boltzmann statistical mechanics and generalized thermodynamics, ISTE Open Science Ltd. London, (2021).

147. G. 't Hooft, Quantum gravity as a dissipative deterministic system, Class. Quantum. Grav. 16, 3263-3279 (1999).

148. G. 't Hooft, The fundamental nature of space and time, in: *Approaches to Quantum Gravity, Towards a New Understanding of Space and Time and Matter*, D. Oriti Ed., Cambridge Univ. Press 2009, ISBN 978-0-521-86045-1, pp.13-25.

149. D. J. Fixsen, The temperature of the cosmic microwave background, *Astro. Phys. J.* 707, 916-920 (2009).

150. W. C. Saslaw, P. Crane. The scale dependence of galaxy distribution functions, Astro. Phys. J. 180, 315-319, (1991).

151. W. C. Saslaw, *Distribution of Galaxies.*, Cambridge University Press, 2000.

152. O. Lahav, W. C. Saslaw, S. Biasing and distribution functions for different galaxy types in optical and IRAS catalogs, Astro. Phys. J. 396, 430-444, (1992).

153. M. Dersarkissian, Does wave-particle duality apply to galaxies? Lett*.* Nuovo Cim*.* 40(2), 390-394 (1984).

154. A. Einstein, The Foundation of the General Theory of Relativity, in: *The Principle of Relativity*. Dover Publications, New York, (1956).

155. M. R. Nugayev, The genesis of general relativity: Interaction between Einstein's, Abraham's and Nordström's research programs, *Kairos Journal of Philosophy & Science* 19, (2017).

156. M. Arminjon, Scalar theory of gravity as a pressure force, Rev. Roum. Sci. Tech.- Méc. Appl. 42(1-2), 27-57 (1997).

157. M. C. Escher, *The Graphic Work of M. C. Escher*, p. 23, Hawthorn Books, New York, 1960.

158. S. H. Sohrab, Implications of a scale invariant model of statistical mechanics to nonstandard analysis and the wave equation, WSEAS Trans. Math. 7, 3, 95-103, 2008.

159. G. H. J. É. Lemaître, A homogeneous universe of constant mass and growing radius accounting for the radial velocity of extragalactic nebulae, Monthly Notices of the Roy. Astr. Soc. 91(5) 483–490 (1931); PNAS 20(1) 12-17 (1934).

160. H. Everett, III, Relative state formulation of quantum mechanics. Rev. Mod. Phys. 29, 454 (1957).

161 A. H Guth, S. H. H. Tye, Phase transitions and magnetic monopole production in the very early universe. Phys. Rev. Lett*.* 44(10), 631-634 (1980).

162. A. H. Guth, Inflationary universe: A possible solution to the horizon and flatness problems. Phys*.* Rev. D 23(2), 347-356 (1981).

163. A. Albrecht, J. P. Steinhardt, Cosmology for grand unified theories with radiatively induced symmetry breaking. Phys*.* Rev. Lett*.*48(17), 1220-1223 (1982).

164. A. D. E. Linde, A new inflationary universe scenario: A possible solution of the horizon, flatness, homogeneity, isotropy and primordial monopole problems. Phys*.* Lett*.* B, 108, 6*94* (1982)*;* 389-393 (1988).

165. M. Kamionkowski, Is the universe (statistically) isotropic? Lecture delivered at physics department of Northwestern University*,* Evanston, Illinois*,* March, (2010).

166. K. Gödel, An Example of a New Type of Cosmological Solutions of Einstein's Field Equations of Gravitation, *Rev. Mod. Phys.* 21 (3), 447 (1949).

167. R. P. Kerr, Gravitational field of a spinning mass as an example of algebraically special metrics, *Phys. Rev. Let.* 11 (5), 237 (1963).

168. W. de Sitter, On Einstein's theory of gravitation and its astronomical consequences. Monthly Notices of the Royal Astronomical Society 78 (1) 3-28 (1917).

169. S. B. DeWitt, Quantum mechanics and reality, Physics Today 23(9), 30 (1970).

170. B. S. DeWitt, Quantum gravity, Scientific American 249(6)112 (1983).

171. J. A. Wheeler, Superspace and the Nature of Quantum Geometro-dynamics. *Battelle Rencontres*, C. M. DeWitt, and J. A. Wheeler (Eds)., Benjamin, New York 1968.

172. A. Ashtekar, The winding road to quantum gravity, Current Science 89(12), 2064 (2005).

173. C. Rovelli, and L. Smolin, Loop space representation of quantum general relativity. Nucl*.* Phys. B331, 80 (1990).

174. S. A. Major, and K. L. Setter, Gravitational statistical mechanics: A model, Class. Quantum Grav. 18(23), 5125–5142 (2001).

175. C. Rovelli, and F. Vidotto, *Covariant Loop Quantum Gravity*, Cambridge University Press, 2015.

176. G. 't Hooft, How does God play dice? (Pre-) determinism at the Planck scale, arXiv:hep-th/0104219v1 25, 2001, Netherlands.

177. S. H. Sohrab, Scale-invariant model of Boltzmann statistical mechanics and generalized thermodynamics, ISTE Open Science Ltd. London, (2021).

178. G. Cirier, A probabilistic approach at the Poincaré-Bendixon problem in R^d, Advances in Pure Mathematics 12, 724-741, (2022).

https://www.scirp.org/journal/apm

179. S. Arrhenius, *Worlds in The Making*, Harper & Brothers, New York. 1908.

180. S. H. Sohrab, Invariant forms of conservation equations for reactive fields and hydro-thermo-diffusive theory of laminar flames, J. Energy Resources Technol. 137, 1-10 (2015).

181. F. Verhulst, Henry Poincaré's Inventions in Dynamical Systems and Topology, in: *The Foundations of Chaos Revisited: From Poincaré to Recent Advancements*, edited by C. H. Skiadas, 1-25, Springer, Switzerland, 2016.

IRSTI 37.31.19 https://doi.org/10.26577/JPEOS.2023.v25.i3-4.i2

V.S. Lyutikova , I.N. Litovchenko*

Institute of Seismology of the Ministry of Emergency Situations
of the Republic of Kazakhstan, Kazakhstan, Almaty
*e-mail: litovira@rambler.ru

ON THE AFTERSHOCKS OF SOME STRONG EARTHQUAKES IN THE SOUTH-EAST OF KAZAKHSTAN

The proposed article presents the results of a comprehensive study of the aftershocks of some strong earthquakes in the south-east of Kazakhstan during the period 1960-2023.

Strong earthquakes in the studied region are accompanied by numerous aftershocks, therefore it is very important to consider the behavior of aftershock attenuation processes in more detail. The relevance of this topic determines the subject, the object, as well as the choice of the method of research. Special attention was paid to the spatial and temporal distribution of aftershocks relative to the epicenters of strong earthquakes during the period 2016-2023. For the research, an earthquake catalog was used for the territory of 39-47°N, 70-85°E with an energy class K≥7.

The results of the research are schematic maps of strong earthquakes and their aftershocks that occurred in the last few years in the selected study area. The statistics of the number of aftershocks after strong earthquakes have occurred are presented, the time dependence of strong earthquakes (main aftershocks) and their aftershocks in the time interval 2016-2023, which occurred on the territory of 39-46°N, 70-85°E is constructed. A qualitative analysis of the results obtained makes it possible to more clearly understand the physical and mechanical conditions of the occurrence of aftershocks after strong earthquakes and to understand in detail the law of attenuation of aftershocks.

Key words: seismicity, strong earthquakes, aftershocks, geological structures, the law of attenuation of aftershocks.

В.С. Лютикова, И.Н. Литовченко*

Қазақстан Республикасы Төтенше жағдайлар министрлігінің
Сейсмология институты, Қазақстан, Алматы қ.
*e-mail: litovira@rambler.ru

Қазақстанның оңтүстік-шығысындағы кейбір күшті жер сілкінісінің салдары туралы

Ұсынылған мақалада 1960-2023 жылдар кезеңінде Қазақстанның оңтүстік-шығысындағы кейбір күшті жер сілкіністерінің афтершоктарын кешенді зерттеу нәтижелері берілген.

Зерттелетін аймақтағы күшті жер сілкіністері көптеген жер сілкіністерімен бірге жүреді, сондықтан жер сілкінісінің әлсіреу процестерінің әрекетін толығырақ қарастырған жөн. Бұл тақырыптың өзектілігі тақырыпты, объектіні, сондай-ақ жүргізілетін зерттеу әдісін таңдауды анықтайды. 2016-2023 жылдар кезеңінде болған қатты жер сілкіністерінің эпицентрлеріне қатысты жер сілкіністерінің кеңістіктік және уақытша таралуына ерекше назар аударылды. зерттеу үшін K≥7 энергетикалық класы бар 39-46°СБ, 70-85°ШБ, аумақтары үшін жер сілкіністерінің каталогы қолданылды.

Зерттеу нәтижелері соңғы бірнеше жылда таңдалған зерттеу аумағында болған қатты жер сілкінісі мен олардың жер сілкіністерінің диаграммалары болып табылады. Күшті жер сілкіністерінен кейінгі жер сілкіністерінің саны туралы статистика ұсынылған, 39-46°СБ, 70-85°ШБ аумағында болған 2016-2023 жылдар аралығындағы күшті жер сілкіністерінің (негізгі дүмпулердің) және олардың жер сілкіністерінің уақытша тәуелділігі салынған. Алынған нәтижелерді сапалы талдау үлкен жер сілкіністерінен кейін жер сілкіністерінің пайда болуының физикалық-механикалық жағдайларын неғұрлым нақты түсінуге және жер сілкіністерінің әлсіреу Заңын егжей-тегжейлі түсінуге мүмкіндік береді.

Түйін сөздер: сейсмикалық, күшті жер сілкіністері, дүмпулер, геологиялық құрылымдар, дүмпулердің әлсіреу заңы.

В.С. Лютикова, И.Н. Литовченко*
Институт сейсмологии МЧС РК, Казахстан, г. Алматы
*e-mail: litovira@rambler.ru

О последствиях некоторых сильных землетрясений на юго-востоке Казахстана

Предлагаемая статья представляет собой результаты комплексного исследования афтершоков некоторых сильных землетрясений юго-востока Казахстана за период 1960-2023 гг.

Сильные землетрясения в исследуемом регионе сопровождаются многочисленными афтершоками, поэтому весьма актуально рассмотреть поведение процессов затухания афтершоков более подробно. Актуальность данной темы определяет предмет, объект, а также выбор метода проводимых исследований. Особое внимание было обращено на пространственное и временное распределение афтершоков относительно эпицентров произошедших сильных землетрясений за период 2016-2023 гг. Для исследований применялся каталог землетрясений для территории 39-46°СШ, 70-85°ВД, с энергетическим классом К≥7.

Результатами исследований являются карты-схемы сильных землетрясений и их афтершоков, произошедших в последние несколько лет на выбранной территории исследования. Представлена статистика количества афтершоков после произошедших сильных землетрясений, построена временная зависимость сильных землетрясений (основных толчков) и их афтершоков в интервале времени 2016-2023 гг., произошедших на территории 39-46°СШ, 70-85°ВД. Качественный анализ полученных результатов позволяет более четко понять физико-механические условия возникновения афтершоков после сильных землетрясений и детально понять закон затухания афтершоков.

Ключевые слова: сейсмичность, сильные землетрясения, афтершоки, геологические структуры, закон затухания афтершоков.

Introduction

The current stage of activation of the Earth's seismicity dictates the need to conduct research on the processes of occurrence and attenuation of aftershocks after strong earthquakes. Strong earthquakes (two strong earthquakes with a magnitude of more than 7.8) that occurred in Turkey on February 6, 2023, after which many aftershocks were recorded, can serve as a vivid confirmation and example. So [1,3]: "On February 6, 2023, with an interval of nine hours, two powerful earthquakes occurred in southeastern Turkey. The epicenter of the first with a magnitude of 7.8 (± 0.1) was located in the Shehitkamil area in Gaziantep (Turkey), the epicenter of the second with a magnitude of 7.5 (± 0.1) was located in the Ekinozu area in Kahramanmaras (Turkey)." Therefore, modern studies of aftershocks after strong earthquakes have occurred are becoming very relevant. On September 9, 2023, a strong earthquake with M=7 occurred for the first time in Morocco.2. Aftershocks with a magnitude of M = 4.5 occurred after it. According to the US Geological Survey, the earthquake occurred about 72 kilometers east of the Moroccan city of Marrakech. The second aftershock, magnitude 3.9, was recorded at a depth of 10 km also near the city of Marrakech [1,3].

Strong earthquakes are always accompanied by numerous aftershocks. Their number and intensity decrease over time, and the duration of manifestation can last for months. The probability of strong aftershocks is especially high in the first hours after the main shock. There are many cases when buildings damaged by the main impact were destroyed precisely by repeated, less violent tremors. Aftershocks pose a threat during rescue operations. An aftershock is a repeated seismic shock of lower intensity compared to the main seismic event.

Therefore, special attention in this study was paid to the aftershocks of strong earthquakes in the South-East of Kazakhstan, in order to comprehensively study the spatial and temporal distribution of aftershocks after strong earthquakes and the law of their attenuation.

Materials and methods

The materials of the research and analysis were scientific sources [1-12]. A catalog of earthquakes for the period 1960-2023 was used for the territory of 39-46°N, 70-85°E, [4]. Special attention was paid to the current stage of activation of the seismicity of the region for the period 2016-2023.

In order to understand the physico-mechanical meaning of the process and the nature of the occurrence of aftershocks, some strong earthquakes in the region and their aftershocks have been studied. The whole process can be described as follows. The

presence of aftershocks is associated not so much with residual stresses directly in the hearth, as with a rapid (during the main shock of the earthquake) increase in stresses in the vicinity of the hearth of the earthquake, due to the redistribution of stresses. When the main impact of an earthquake is plastic (and brittle) deformation of the earth's crust in the earthquake site, the hard surface of the earth's crust shifts in general from tens of centimeters to several meters. At the same time, the mechanical stresses in the hearth decrease from the maximum (from the level of ultimate strength) to the minimum residual ones. On the other hand, stresses in the vicinity of the hearth (source of rupture) increase significantly (as a result of displacement of the Earth's crust), sometimes bringing this stress closer to the ultimate strength. When the strength limit is exceeded (near the source of the main shock), aftershocks occur. With this displacement of the earth's surface, mechanical stresses increase at a great distance from the epicenter (source) (similar to how it happens near the epicenter). The essence of the concept of aftershocks is always associated with major aftershocks (strong earthquakes). After the main shock, not only residual stresses arise directly in the hearth, but also quickly (during the main earthquake) stresses increase in the vicinity of the hearth of the earthquake due to the redistribution of stresses. During the main shock (strong earthquake) – plastic (and brittle) deformation of the earth's crust in the earthquake site, the hard surface of the earth's crust shifts, from several tens of centimeters to several meters.

A comprehensive study of the processes of occurrence and attenuation of aftershocks, and the application of the law and the Omori method [2] revealed some statistical patterns. According to the law proposed by Swedish seismologist M. Bot, the magnitude of the strongest aftershock is less than the magnitude of the main shock by one. Aftershocks can occur over a long period of time (months and years). A statistical pattern is also found in the time sequence of their occurrence [3]. The mechanical stresses in the hearth decrease from the maximum (from the level of ultimate strength) to the minimum residual stresses. Stresses in the epicenter area increase significantly, sometimes approaching the ultimate strength. When the strength limit is exceeded (near the focus of the main shock), repeated aftershocks occur. Mechanical stresses also increase at a great distance from the epicenter. Stress increases at the plate boundaries may approach the limit of strength of the earth's crust along its perimeter, then after strong earthquakes – displacements along the plate boundary, a series of man-made earthquakes may occur. Thus, in [5], the time statistics of the strongest aftershocks were considered relative to the moments of the corresponding main shocks. It follows from the considered material that the occurrence of the strongest aftershocks in time obeys the power law of distribution. This is similar to Omori's law [2] for the sequence of all aftershocks (see Fig. 1). As the authors note [6]: "the hypothesis of the independence of times and magnitudes in aftershock sequences has been confirmed." After strong earthquakes, aftershocks usually occur, which can cause significant additional damage, sometimes even exceeding the damage from the main shock. Strong aftershocks are often accompanied by a temporary increase in the number of events per unit of time. Presumably, a strong aftershock is likely to occur at the beginning of a series of events. A more likely scheme is the occurrence of aftershocks due to stresses accumulated before the main shock [6]. Figure 1 shows the time dependence of aftershocks on the main shock, which occur in the time interval 2017-2023. Taking into account all the features of the occurrence of aftershocks after strong aftershocks, special attention was paid to their spatial distribution.

Results and discussion

According to the catalog of aftershocks, major aftershocks (SOMS) [4], it can be concluded that aftershocks do not occur instantly, but with some delay after the main (main) shock. It is obvious that small impacts similar in strength to direct impacts from seismic events, for example, tides or even surface waves from the main shock that rounded the Earth, can also act as triggers that increase the likelihood of aftershocks [6]. At the same time, a trigger is understood as a specific cause of events, conditions under which a prescribed action should occur-an event, an event that sets in motion, a provoking factor, a signal that causes predetermined conditions. Let's take a closer look at the analysis of the occurrence of a sequence of aftershocks. For this purpose, the temporal sequence of major aftershocks (strong earthquakes) and their aftershocks is considered (see Fig. 1) for the period 2017-2023. Figure 1 shows how the sequence of aftershocks is distributed over time after the main shock.

According to the accumulated data on the aftershocks of the earthquake catalog (SOME) [4] for 1960-2023, it can be assumed that the assessment of the probability of subsequent aftershocks is based

on the assumption that the magnitude of aftershocks does not depend on time; under this assumption, the maximum magnitudes depend only on the intensity of the aftershock flow (the number of events per unit of time) or do not depend directly on the time elapsed since the main shock [6]. Each aftershock can be characterized by a pair of quantities: time relative to the main shock and magnitude, which can be considered as a two-dimensional random variable. It can be assumed that if the magnitudes are independent of time, any of the aftershocks may be equally likely to be the strongest. There are 34 main aftershocks in the catalog of strong earthquakes, each of which may or may not have its own sequence of aftershocks (see Table 1). Provided reliable estimates of parameters based on data on the interval from the main (main) shock, it is possible to estimate such characteristics as the maximum magnitude, the waiting time for shocks of a given force, the occurrence of events of a given force in a given interval. The corresponding parameters were identified in the sequence of aftershocks of each of the 34 main aftershocks. In the earthquake catalog, the main (main) tremors are marked -3, the corresponding aftershocks are marked – 40-41 [4]. Table 1 shows the sequences of the main aftershocks and the number of their aftershocks for 1970-2023. Some strong earthquakes in the studied region, their coordinates, magnitude, depth and number of aftershocks are given. For the spatial representation of aftershocks, the main aftershocks with K>14.0 and the number of their aftershocks were taken from the indicated table. 1. K is the energy class. For example, some strong earthquakes (major aftershocks and their aftershocks) were considered starting from 2016-2023. The results of the spatial distribution of aftershocks of some strong earthquakes in the studied region are shown in Figures 2-5. In the sequence of aftershocks of each strong earthquake, there are sufficiently strong events of class K = 9.7, 9.2, they are timed to the main shock and obey the law of attenuation of aftershocks.

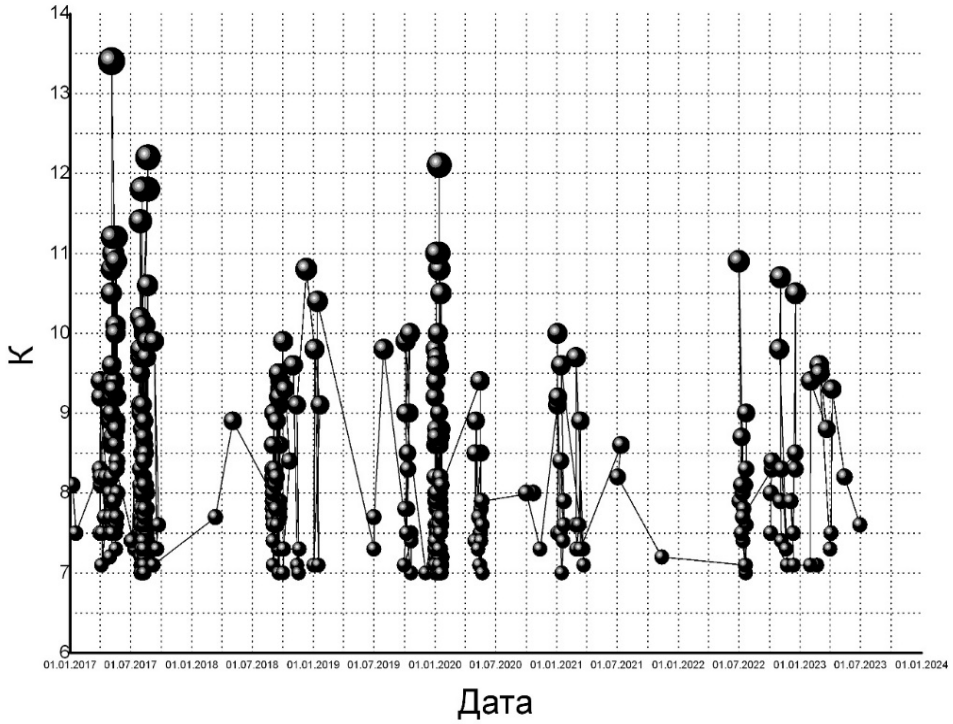

Figure 1 – Time dependence of the main aftershocks and their aftershocks in the time interval 2017-2023, which occurred on the territory of 39-46°N, 70-85°E

Table 1 – List of strong earthquakes (K≥14) and the number of their aftershocks in the south-east of Kazakhstan in 1970-2023. (compiled from materials [4])

№	Дата, время	Координаты		Энергетический класс, *K*	Магнитуда, *M*	Глубина гипоцентра, *H*, км	Количество афтершоков
		Широта	Долгота				
1	05.06.70 4:53	42.47	78.80	15.6	6.3	15	4
2	10.05.71 14:51	43.00	71.20	14.2	-	-	4
3	15.06.71 22:04	41.52	79.12	14.2	6	11.9	71
4	15.01.72 20:21	40.28	79.38	14.4	6.2	10.2	6
5	24.03.78 21:05	42.87	78.58	16.0	7.1	33	95
6	25.09.79 13:05	45.00	77.00	14.0	5.9	40	0
7	13.02.83 1:40	40.13	75.15	14.6	6.2	16.1	401
8	23.08.85 12:42	39.15	75.30	17.5	7	6.8	271
9	24.08.85 20:46	39.45	75.80	14.9	-	-	181
10	24.01.87 8:09	41.40	79.17	15.3	6.2	28.9	301
11	12.11.90 12:28	42.93	77.93	14.6	6.4	19.1	87
12	25.02.91 14:30	40.33	78.92	14.4	6	20.6	23
13	15.05.92 8:07	41.10	72.42	15.0	6.2	49.5	43
14	19.08.92 2:04	42.07	73.63	17.0	7.3	27.4	141
15	30.12.93 14:24	44.82	78.77	15.0	5.5	14.9	62
16	19.03.96 15:00	40.22	76.58	14.6	6.3	28.2	3
17	09.01.97 13:43	41.17	74.20	14.2	5.8	22.2	3
18	21.01.97 1:47	39.43	76.98	14.4	5.9	33	3
19	01.03.97 6:04	39.72	76.82	14.2	5.6	22.4	2
20	11.04.97 5:34	39.60	76.93	14.6	6.2	15	1
21	14.02.05 23:38	41.80	79.18	14.3	6.1	22	125
22	19.04.09 4:08	41.32	78.18	14.0	5.4	39	11
23	19.07.11 19:35	39.92	71.45	14.3	6.1	20	3
24	28.01.13 16:38	42.52	79.67	14.7	6.1	15	836
25	26.06.16 11:17	39.75	73.73	14.2	6.4	13	45
26	25.11.16 14:24	39.25	74.27	14.4	6.6	17	2
27	03.05.17 4:47	39.45	71.58	14.3	6	11	42
28	08.08.17 23:27	44.40	82.48	16.7	6.3	20	130

To analyze the number of strong aftershocks, a series of aftershocks that occurred in 2016-2023 was taken. Figures 2-5 show the spatial and temporal distributions of aftershocks after strong earthquakes. As you can see, in space, aftershocks are grouped in the epicentral region of the main shock. The number of aftershocks for each strong earthquake is different. There are single aftershocks after a strong earthquake, and there are numerous aftershocks, up to 100 and more.

Thus, the aftershocks of some strong earthquakes in the south-east of Kazakhstan that occurred during the observation period were considered.

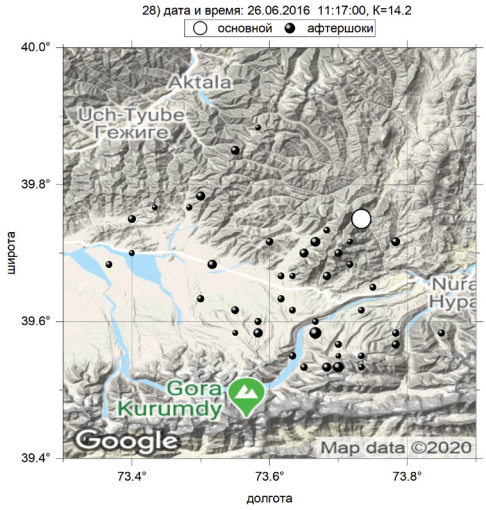

Figure 2 – Aftershocks of a strong earthquake on June 26, 2016, K = 14.2 [4]

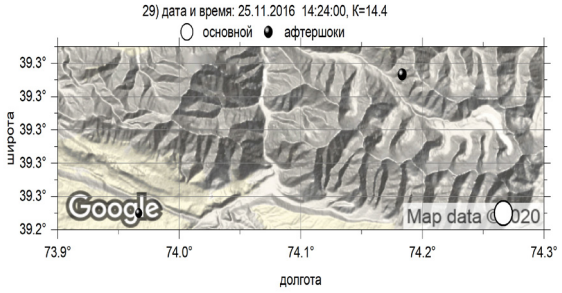

Figure 3 – Aftershocks of a strong earthquake on November 25, 2016, K = 14.4 [4]

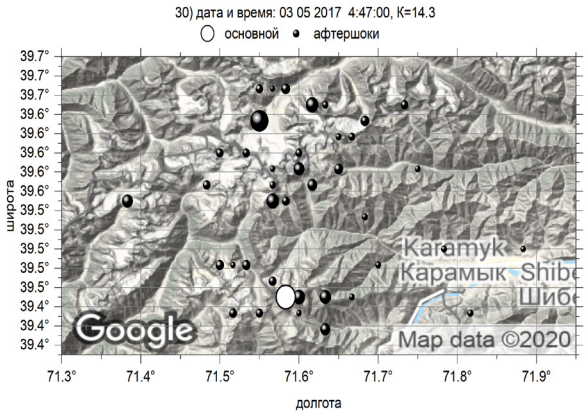

Figure 4 – Aftershocks of a strong earthquake on May 03, 2017, K = 14.3 [4]

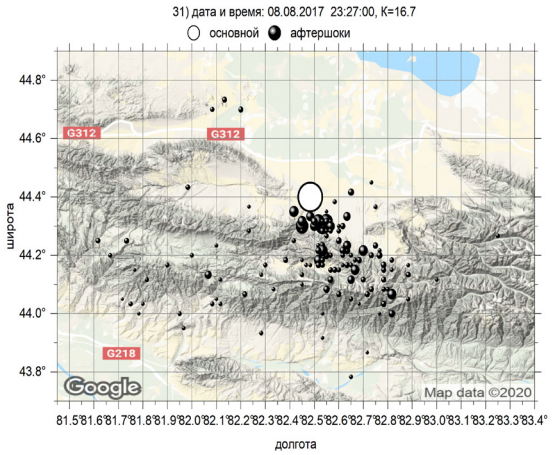

Figure 5 – Aftershocks of a strong earthquake on 08.08.2017, K=16.7 [4]

Conclusion

The following conclusion can be drawn as conclusions. During the period of intensification of seismicity in the Southeastern Kazakhstan research region for 2016-2023, maps-diagrams of the spatial and temporal distribution of aftershocks after strong earthquakes (K≥14) were obtained. The time dependence of the main aftershocks and their aftershocks in the time interval 2016-2023, which occurred on the territory of 39-46 °N, 70-85°E, showed graphs of curves that obey the law of attenuation of Omori aftershocks. The obtained research results made it possible to better understand the physico-mechanical conditions of the occurrence and attenuation of aftershocks after strong earthquakes and showed the need for timely study of aftershocks after strong earthquakes in connection with recent strong earthquakes in different parts of the globe.

The work was performed in the laboratory of Physics of geodynamic and seismic processes within the framework of the "Assessment of seismic hazard of territories of regions and cities of Kazakhstan on a modern scientific and methodological basis", program code F.0980. The source of funding is the Ministry of Education and Science of the Republic of Kazakhstan.

References

1. Aftershock//[Electronic resource]: access mode: https://bigenc.ru/c/aftershok-b80b0f

2. Omori's Law //[Electronic resource]: access mode: https://bigenc.ru/c/zakon-omori-3d1500

3. Aftershocks were recorded in Morocco after a devastating earthquake//[Electronic resource]: access mode: https://news.ru/africa/v-marokko-zafiksirovali-aftershoki-posle-razrushitelnogo-zemletryaseniya/?utm_source=yxnews&utm_medium=desktop

4. Earthquake Catalog / Seismic Experimental and Methodological Expedition (SOME) Ministry of Emergency Situations of the Republic of Kazakhstan [Electronic resource]: access mode: http://some .kz/index.php?p=card&outlang=1& oid =9.

5. Kurskeev A.K., Timush A.V. Conceptual foundations of earthquake prediction theory. SS. 169-178.

6. Baranov S.V., Shebalin P.N. Global statistics of aftershocks of strong earthquakes: independence of times and magnitudes. // Volcanology and Seismology, 2019 No. 2. pp. 67-76.

7. Kurskeev A.K. Gravitational interaction of the planets of the Solar system and seismicity of the Earth. "Evero." Almaty. Kazakhstan. p.547.

8. Kurskeev A.K., Kurskeeva L.A. Geodynamics and interaction of natural processes// Reports of the National Academy of Sciences of the Republic of Kazakhstan.- SS.52-60.

9. Litovchenko I.N., Amirov N.B. "On 3-D visualization of thermodynamic and rheological parameters in earthquake foci of the Earth"// International Scientific Conference "Innovative technologies in solving urgent problems of seismology, hydrogeology and engineering geology" Uzbekistan, Tashkent, IS.- 4s.

10. Litovchenko I.N. On some physical parameters of earthquake foci // Structure, material composition, properties, modern geodynamics and seismicity of platform territories and adjacent regions: Materials of the XXII All-Russian Scientific and Practical Shchukin Conference with international participation. Voronezh, September 22-25, 2020, CC. 208-212.

11. Lyutikova V.S., Litovchenko I.N., Amirov N.B. Activation of seismicity as an indicator of the formation of focal zones of strong earthquakes in the Earth's crust of the northern Tien Shan// International scientific and practical journal. XVI Global Science and Innovation 2022: Central Asia. Nur Sultan. Kazakhstan.Pp.3-7.

12. Lyutikova V.S. Physico-mathematical parameters in the occurrence of earthquake swarms in the conditions of seismicity of the Northern Tien Shan //materials of the international competition of the Commonwealth of Independent States "The best young scientist – 2022". pp.59-62.

ҒТАМР 29.05.15 https://doi.org/10.26577/JPEOS.2023.v25.i3-4.i3

С.А. Жаугашева, К.А. Нұрлан*

Әл-Фараби атындағы ҚазҰУ, Қазақстан, Алматы қ.
*e-mail: kmlnurlan@gmail.com

КВАНТТЫҚ НҮКТЕНІҢ ЭНЕРГЕТИКАЛЫҚ СПЕКТРІН ОСЦИЛЛЯТОРДА ӨРНЕКТЕУ ӘДІСІМЕН АНЫҚТАУ

Жұмыста сыртқы магнит өрісінде орналасқан екі электронды кванттық жүйенің энергетикалық спектрі осциллятордa өрнектеу әдісімен анықталады. Энергетикалық спектрі параболалық конфайнмент потенциалы үшін ангармониялық түзетуді ескере отырып есептелінді. Осы жағдайлар үшін энергетикалық спектрдің ауытқуына талдау жасалды. Күшті магнит өрістерінде екі электронды жүйе үшін қарпу потенциалының параболалық сипаты туралы гипотеза өте орынды екендігі анықталады. Мұндай жүйенің қарапайым өкілі болып табылатын екі электронды кванттық нүктелердің қасиеттерін бақылау және басқару мүмкіндігі оларды болашақ компьютерлер үшін жаңа элементтер базасы ретінде пайдалануға мүмкіндік береді. Шағын бөлшекті электронды жүйелер теориялық және эксперименттік тұрғыдан үлкен қызығушылық тудырады. Бүгінде электрондық құрылғыларға арналған жартылай өткізгіш наноқұрылымдардың алуан түрлілігіне қарамастан, жақсартылған сипаттамалары бар материалды іздеу процесі жалғасуда. Өнеркәсіпте наноматериалдарды пайдалану қарқыны тез өсуде, бұл жаңа нысандарды құру үшін синтез әдістерін әзірлеуді ынталандырады. Жаңа кванттық-өлшемді құрылымдарды құру жүріп жатқан кванттық механикалық процестердің ішкі құрылымын нақты түсінуді талап етеді. Жұмыс барысында кванттық нүктенің энергетикалық спектрі параболалық конфайнмент потенциалы үшін ангармониялық түзетуді ескере отырып есептелді. Ол үшін энергия спектрінің тербелістеріне талдау жасалды. Сыртқы магнит өрісіндегі екі электронды кванттық нүктенің энергетикалық спектріне зерттеу кванттық нүктенің сипаттамаларын басқаруға мүмкіндік береді.

Түйін сөздер: кванттық нүкте, кванттық жүйе, энергетикалық спектр, осциллятордa өрнектеу әдісі.

S.A. Zhaugasheva, K.A. Nurlan*

Al-Farabi Kazakh National University, Kazakhstan, Almaty
*e-mail: kmlnurlan@gmail.com

Determination of the energy spectrum of a quantum dot by the method of oscillatory representation

In this paper, the energy spectrum of two-electron quantum systems located in an external magnetic field is determined by the method of expression on an oscillator. The energy spectrum was calculated taking into account the anharmonic correction for the parabolic confinement potential. For these conditions, an analysis of fluctuations in the energy spectrum was carried out. In strong magnetic fields, it turns out that the hypothesis of the parabolic nature of the retention potential for two electronic systems is quite plausible. The ability to control and control the properties of two-electron quantum dots, which are a common representative of such a system, allows them to be used as a new element base for future computers. Electronic systems with microparticles are of great interest both theoretically and experimentally. Today, despite the wide variety of semiconductor nanostructures for electronic devices, the process of searching for a material with improved characteristics continues. The pace of use of nanomaterials in industry is growing rapidly, which stimulates the development of synthesis methods to create new objects. The creation of new quantum-dimensional structures requires a clear understanding of the internal structure of the quantum-mechanical processes taking place. In the course of the work, the energy spectrum of the quantum dot was calculated taking into account the anharmonic correction for the parabolic confinement potential. To do this, an analysis of fluctuations in the energy spectrum was carried out. The study of the energy spectrum of two electronic quantum dots in an external magnetic field allows you to control the characteristics of a quantum dot.

Key words: quantum system, quantum dot, energy spectrum, method of oscillator representation

С.А. Жаугашева, К.А. Нұрлан*
Казахский национальный университет имени аль-Фараби, Казахстан, г. Алматы
*e-mail: kmlnurlan@gmail.com

Определение энергетического спектра квантовой точки методом осцилляторного представления

В работе энергетический спектр двухэлектронных квантовых систем, расположенных во внешнем магнитном поле, определяется методом выражения на осцилляторе. Энергетический спектр рассчитывался с учетом ангармонической коррекции для параболического конфайнмент-потенциала. Для этих условий был проведен анализ колебаний энергетического спектра. В сильных магнитных полях выясняется, что гипотеза о параболическом характере потенциала удержания для двух электронных систем вполне правдоподобна. Возможность контролировать и управлять свойствами двухэлектронных квантовых точек, которые являются обычным представителем такой системы, позволяет использовать их в качестве новой элементной базы для будущих компьютеров. Электронные системы с микрочастицами представляют большой интерес как в теоретическом, так и в экспериментальном плане. Сегодня, несмотря на большое разнообразие полупроводниковых наноструктур для электронных устройств, процесс поиска материала с улучшенными характеристиками продолжается. Темпы использования наноматериалов в промышленности быстро растут, что стимулирует разработку методов синтеза для создания новых объектов. Создание новых квантово-размерных структур требует четкого понимания внутренней структуры происходящих квантово-механических процессов. В ходе работы энергетический спектр квантовой точки рассчитывался с учетом ангармонической коррекции для параболического конфайнмент-потенциала. Для этого был проведен анализ колебаний энергетического спектра. Исследование энергетического спектра двух электронных квантовых точек во внешнем магнитном поле позволяет контролировать характеристики квантовой точки.

Ключевые слова. Квантовая система, квантовая точка, энергетический спектр, метод выражения на осцилляторе.

Кіріспе

Өздігінен ұйымдастырылған кванттық нүктелері (КН) бар гетероқұрылымдар оптоэлектроникада, атап айтқанда талшықты-оптикалық байланыс желілері үшін жоғары тиімді инжекциялық лазерлер жасаудағы перспективаларының арқасында зерттеушілердің қызығушылығын арттырды. Екіншіден, интенсивті электромагнитті өрістің әр түрлі нанокұрылымдармен өзара әсерлесуі де қарқынды зерттелуде. Электромагнитті өрістің нанокұрылымдармен өзара әсерлесуіне деген қызығушылықтың артуы нанокұрылымдардың көптеген түрлерінің қолданысқы енуіне байланысты, және осы бағытта көптеген эксперименттік және теориялық жұмыстардың пайда болуына алып келді[1]. Сол нанокұрылымдарды қалыптастыру және олардың өзара әрекеттесуін түсіндіру қазіргі заманауи теориялық зерттеулердің негізгі мәселесі болып табылады. Біріншіден, электрондар арасында тебіліс күші әрекет етеді, бірақ қазіргі технологиядағы прогресс жартылай өткізгіш нанокұрылымдарды – кванттық нүктелерді (шұңқырларды) құруға мүмкіндік береді, онда электрондардың ақырлы саны атомдық өлшемдердің реті бойынша шектеулі көлемде "құлыпталады". Екінші жағынан, кванттық нүктелердің қасиеттерін бақылау және басқару мүмкіндігі оларды болашақ компьютерлер үшін жаңа элементтер базасы ретінде пайдалануға мүмкіндік береді.

Практикалық қолдану тұрғысынан кванттық нүктелерге кең перспективалар ашылады. Идеал кванттық нүктелер жүйесінің энергетикалық спектрі 5 функциялардың жиынтығы болып табылады, сондықтан мұндай жүйелерді қолдану оптикалық құрылғыларды құрудың сапалы жаңа деңгейіне, мысалы, тар сызығы бар және температураға сезімталдығы төмен жартылай өткізгіш лазерлерге қол жеткізуге мүмкіндік береді [2]. Жалғыз кванттық нүктенің энергетикалық спектрі атомдық деңгейлерге жақын, бұл кванттық нүктелер негізінде бір электронды транзисторлар мен жад элементтерін құруға мүмкіндік береді.

Жұмыстың мақсаты – сыртқы магнит өрісіндегі екі электрондық кванттық нүктенің энергетикалық спектрін анықтау. Жұмыс кванттық өріс теориясының идеялары мен әдістеріне негізделген осцилляторда өрнектеу әдісінде орындалған.

Зерттеу материалдары мен тәсілдер

Жұмыста потенциалы $V_c(r)$ болатын екі электронды жүйенің энергетикалық спектрін анықтау үшін осциллятора өрнектеу әдісі қолданылады [4]. $z = 0$ жағдайын қарастырайық, яғни кванттық нүктенің моделі бола алатын екі өлшемді жүйені қарастырайық. Екі электронды жүйенің салыстырмалы қозғалысының гамильтонианы:

$$H = -\frac{\hbar^2}{2}\cdot\left[\frac{\partial^2}{\partial\rho^2}+\frac{1}{\rho}\frac{\partial}{\partial\rho}-\frac{m^2}{\rho^2}\right]+ \\ +\frac{\hbar^2}{2}\cdot\Omega^2\rho^2+\frac{k\sqrt{\hbar\omega_0}}{\rho}-\hbar^2\sqrt{\hbar}W\rho^3 \\ +\hbar^3G\rho^4-\frac{\hbar\omega_0}{8}+\frac{1}{2}m\hbar\omega_c \tag{1}$$

мұндағы $m = 0, \pm1, \ldots.$ – магниттік кванттық сан, және

$$\omega_r^2 = \frac{\lambda^2\omega_0^2}{12} \quad , \quad W = \frac{\lambda^3}{48}\omega_0^2\sqrt{\omega_0} \\ \Omega = \sqrt{\omega_r^2+\frac{\omega_c^2}{4}} \quad , \quad G = \frac{\lambda^2\omega_0^2}{160} \quad , \quad k = \frac{\ell_0}{a^*} \quad . \tag{2}$$

(1) гамильтонианы үшін Шрендингер теңдеуі:

$$\left[\frac{1}{2}P_\rho^2+\frac{\hbar^2}{2}\Omega^2\rho^2+\frac{k\sqrt{\hbar\omega_0}}{\rho}-\hbar^2\sqrt{\hbar}W\rho^3+\hbar^3G\rho^4\right]\Psi_m = U_m\Psi_m \tag{3}$$

мұндағы U_m – энергетикалық параметр:

$$U_m = E_m+\frac{\hbar\omega_0}{8}-\frac{m}{2}\hbar\omega_c \tag{4}$$

Ең алдымен тек параболалық потенциалды қарастырамыз, яғни $W = 0$ және $G = 0$. Бұл жағдайда энергетикалық спектр үшін келесі өрнекті аламыз:

$$E_m = \hbar\omega_0\left\{-\frac{1}{8}+t\frac{m}{2}+x^2(1+|m|)\sqrt{\frac{\sigma^2}{2}\left(\frac{1}{6}+\sigma^2\right)+\frac{t^2}{4}}\right. \\ \left.+\frac{3kx}{2}\left[\frac{\sigma^2}{2}\cdot\left(\frac{1}{6}+\sigma^2\right)+\frac{t^2}{4}\right]^{\frac{1}{4}}\frac{\Gamma\left(|m|+\frac{1}{2}\right)}{\Gamma(1+|m|)}+\frac{t}{4}[1-(-1)^m]\frac{m^*}{m_\ell}g^*\right\} \tag{5}$$

x параметрі

$$x^4+x^3\cdot\frac{k}{\left[\frac{\sigma^2}{2}\cdot\left(\frac{1}{6}+c^2\right)+\frac{t^2}{4}\right]^{\frac{1}{4}}}\cdot\frac{\Gamma\left(|m|+\frac{1}{2}\right)}{\Gamma(2+|m|)}-1=0 \tag{6}$$

өрнегінен анықталады.

Спиндік гамильтонианның меншікті мәндері стандартты түрде анықталады:

$$E_{spin} = \hbar\omega_0 g^*[1-(-1)^m]\frac{t}{4}\cdot\frac{m^*}{m_\ell} \tag{7}$$

мұндағы

$$\omega_c = eB/cm^* \equiv B/m^*$$

Спиндік өзара әсерлесудің энергетикалық спектрі Паули принципіне сай анықталған: егер толық толқындық функцияның кеңістіктік

бөлігі $r \longrightarrow -r$ инверсиясына қатысты симметриялы (антисимметриялы) болса, онда сәйкес спиндік күй синглет болуы тиіс (триплет). Мұндағы $t = \omega_c/\omega_0$ – магниттік өрістің салыстырмалы кернеуі, ал g^* эффективті Ланде факторы болып табылады. (5) өрнегіне екі электронның магнит өрісіндегі өзара әсерлесуімен байланысты Зееман эффектінің үлесі кіріктірілген. (5) және (6) өрнектері кванттық нүктенің негізгі күйлерін кванттық нүктенің $k = \ell_0/a^*$ өлшемі және магнит өрісінің t салыстырмалы кернеуінің функциясы ретінде анықтауға мүмкіндік береді.

Зерттеу нәтижелері мен талқылау

(3) гамильтонианының энергетикалық спектрін анықтауға көшейік. Бұл жағдайда айнымалылар ауыстыру келесідей:

$$\rho = q^{2\alpha}$$
$$\Psi_m = q^{2\alpha|m|} \cdot \Phi_m(q) \tag{8}$$

мұндағы α параметрі толқындық функцияның үлкен қашықтықтардағы күйімен байланысқан. Потенциалдың құрылымында ангармоникалық мүшелердің болуына байланысты α параметрін анықтауда [5] жұмысының нәтижелеріне сүйенеміз. ρ шамасының үлкен мәндерінде толқындық функцияның асимптотикасы $\sim G\rho^4$ ангармоникалық мүшесімен анықталады, сонымен қатар $\alpha = 1/3$. G және W шамаларының аз мәндерінде, толқындық функция гаусстік толқындық функцияға жақын болғандықтан [6], $\alpha = 1/2$. Бұл шек параболалық конфайнмент потенциалына сәйкес келеді. Осылайшы, нөлдік жуықтауда негізгі күй энергиясын минимизациялаудағы вариациялық параметр ретінде қарастырылып отырған α параметрі

$$1/3 \leq \alpha \leq 1/2$$

интервалында өзгере алады.

1-суретте α параметрінің $t = \omega_c/\omega_0$ магнит өрісінің кернеуіне тәуелділігі $m = 0 - 1, -2, -3, \ldots$ күйлерінде кескінделген. Талдаудың қорытындысынан байқалатындай, m магниттік кванттық санының аз абсолюттік мәніндегі күйі үшін $\alpha < 1/2$. Магнит өрісі шамасының өсуімен α параметрі гаусстік толқындық функцияға сәйкес келетін $\alpha = 1/2$ шегіне асимптотикалық ұмтылады. Осцилляторда өрнектеу әдісіне α параметрінің енгізілуі Дайсон феномені мәселесін сәтті айналып өтуге мүмкіндік береді [7].

(3) өрнегін түрлендіре отырып модификацияланған Шредингер теңдеуін аламыз:

$$\left\{-\frac{\hbar^2}{2}\left[\frac{\partial^2}{\partial q^2} + \frac{d-1}{q}\frac{\partial}{\partial q}\right] + 4k\sqrt{\hbar\omega_0}\alpha^2 q^{2(\alpha-1)} + 2\alpha^2\hbar^2\Omega^2 q^{2(4\alpha-1)} - 4\hbar^2\sqrt{\hbar}\alpha^2 W q^{2(5\alpha-1)} + 4\hbar^3\alpha^2 G q^{2(6\alpha-1)} - 4\alpha^2 U_m q^{2(2\alpha-1)}\right\}\Phi_m(q^2) = 0 \tag{9}$$

мұндағы $d = 2 + 4\,\alpha|m|$. Нөлдік жуықтаудағы негізгі күй энергиясы:

$$\varepsilon_0(U_m) = \frac{d\omega\hbar}{4} - \frac{4\alpha^2 U_m}{(\omega\hbar)^{(2\alpha-1)}} \cdot \frac{\Gamma\left(\frac{d}{2} + 2\alpha - 1\right)}{\Gamma\left(\frac{d}{2}\right)} + \frac{4k\sqrt{\hbar\omega_0}\alpha^2}{(\omega\hbar)^{(\alpha-1)}} \cdot \frac{\Gamma\left(\frac{d}{2} + \alpha - 1\right)}{\Gamma\left(\frac{d}{2}\right)} - \frac{4\hbar^2\sqrt{\hbar}\alpha^2 W}{(\omega\hbar)^{(5\alpha-1)}} \cdot \frac{\Gamma\left(\frac{d}{2} + 5\alpha - 1\right)}{\Gamma\left(\frac{d}{2}\right)} + \frac{2\alpha^2\hbar^2\Omega^2}{(\omega\hbar)^{(4\alpha-1)}} \cdot \frac{\Gamma\left(\frac{d}{2} + 4\alpha - 1\right)}{\Gamma\left(\frac{d}{2}\right)} + \frac{4\hbar^3\alpha^2 G}{(\omega\hbar)^{(6\alpha-1)}} \cdot \frac{\Gamma\left(\frac{d}{2} + 6\alpha - 1\right)}{\Gamma\left(\frac{d}{2}\right)} \tag{10}$$

ал өзара әсерлесу гамильтонианы үшін:

$$H_I = \int_0^{\infty} d\tau \int \left(\frac{d\eta}{\sqrt{\pi}}\right)^d e^{-\eta^2(1+\tau)} : e_2^{-2i\sqrt{x\hbar\omega}(q\eta)} : \times \left[\frac{4k\sqrt{\hbar\omega_0}\alpha^2}{(\omega\hbar)^{(\alpha-1)}} \cdot \frac{\tau^{-\alpha}}{\Gamma(1-\alpha)} - \frac{4\hbar^2\sqrt{\hbar}\alpha^2 W}{(\omega\hbar)^{(5\alpha-1)}} \cdot \frac{\tau^{-5\alpha}}{\Gamma(1-5\alpha)} - \frac{4\alpha^2 U_m}{(\omega\hbar)^{(2\alpha-1)}} \cdot \frac{\tau^{-2\alpha}}{\Gamma(1-2\alpha)} + \frac{2\alpha^2\hbar^2\Omega^2}{(\omega\hbar)^{(4\alpha-1)}} \cdot \frac{\tau^{-4\alpha}}{\Gamma(1-4\alpha)} + \frac{4\hbar^3\alpha^2 G}{(\omega\hbar)^{(6\alpha-1)}} \cdot \frac{\tau^{-6\alpha}}{\Gamma(1-6\alpha)}\right] \quad (11)$$

$$\frac{\partial\varepsilon_0(U_m)}{\partial\omega} = 0 \quad (12)$$

өрнегінен ω параметрін U_m энергиясының функциясы ретінде анықтаймыз, сонымен қатар потенциалдың басқа да параметрлері анықталады.

(12), (10) ескере отырып және (2) мәнін қолданып, энергетикалық спектр үшін қажетті түрлендірулерден кейін:

$$\frac{E_m}{\hbar\omega_0} = min_\alpha \left\{ -\frac{1}{8} + \frac{m}{2}\cdot t + \frac{t}{4}\frac{m^*}{m_\ell}[1-(-1)^m]g^* + \frac{z^2}{4\alpha}\cdot\frac{\sqrt{\Gamma(2+2\alpha|m|)\Gamma(4+2\alpha|m|)}}{\Gamma(2\alpha+2\alpha|m|)} \cdot\sqrt{\frac{2}{3}+t^2} + \frac{3k\sqrt{\alpha}}{2}\cdot z\cdot\frac{\Gamma(\alpha+2\alpha|m|)}{\Gamma(2\alpha+2\alpha|m|)}\cdot\left[\frac{\Gamma(4\alpha+2\alpha|m|)}{\Gamma(2+2\alpha|m|)}\cdot\left(\frac{2}{3}+t^2\right)\right]^{\frac{1}{4}} + \frac{3}{96z^3\alpha^{\frac{3}{2}}}\cdot\frac{\Gamma(5\alpha+2\alpha|m|)}{\Gamma(2+2\alpha|m|)}\cdot\left[\frac{\Gamma(2+2\alpha|m|)}{\Gamma(4\alpha+2\alpha|m|)}\cdot\left(\frac{2}{3}+t^2\right)^{-1}\right]^{\frac{3}{4}} - \frac{4}{160z^4\alpha^2} \cdot\frac{\Gamma(6\alpha+2\alpha|m|)}{\Gamma(2+2\alpha|m|)}\cdot\frac{\Gamma(2+2\alpha|m|)}{\Gamma(4\alpha+2\alpha|m|)}\cdot\left(\frac{2}{3}+t^2\right)^{-1}\right\} \quad (13)$$

z параметрі келесі өрнектен анықталады:

$$z^4 + 4k\alpha^{3/2}z^3\cdot\frac{\Gamma(\alpha+2\alpha|m|)}{\Gamma(2+2\alpha|m|)}\cdot\left[\frac{\Gamma(2+2\alpha|m|)}{\Gamma(4\alpha+2\alpha|m|)}\cdot\left(\frac{2}{3}+t^2\right)^{-1}\right]^{\frac{1}{4}} - 1 + \frac{3}{4z\sqrt{\alpha}} \cdot\frac{\Gamma(5\alpha+2\alpha|m|)}{\Gamma(2+2\alpha|m|)}\cdot\left[\frac{\Gamma(2+2\alpha|m|)}{\Gamma(4\alpha+2\alpha|m|)}\cdot\left(\frac{2}{3}+t^2\right)^{-1}\right]^{\frac{5}{4}} - \frac{4}{z^2 10\alpha} \cdot\frac{\Gamma(6\alpha+2\alpha|m|)}{\Gamma(2+2\alpha|m|)}\cdot\left[\frac{\Gamma(2+2\alpha|m|)}{\Gamma(4\alpha+2\alpha|m|)}\cdot\left(\frac{2}{3}+t^2\right)^{-1}\right]^{\frac{3}{2}} = 0 \quad (14)$$

(13) энергетикалық спектрі (5) қарпу потенциалының параболалық сипатына негізделген энергетикалық спектрден өзгешелігі айқын. 2-суреттен энергетикалық спектрдің кванттық нүктенің $k = \ell_0/a^*$ өлшемінен және магнит өрісінің $t = \omega_c/\omega_0$ салыстырмалы кернеуінен тәуелділігі параболалық және квази-параболалық потенциалдар үшін ұқсас екендігі көрінеді. Дегенмен, әлсіз магнит өрісінде синглет-триплеттік ауысулар квази-параболалық потенциал үшін магнит өрісінің біршама жоғары мәндерінде жүреді (2a және 2b суреттер). Біз әлсіз магнит өрісінде қарпу потенциалы параболалық конфайнмент потенциалынан өзгешеленеді деп күтудеміз. Дәл сол сәтте күшті магнит өрістерінде $\omega_c \gg \omega_0$, яғни $t \longrightarrow \infty$ шегінде (13) және (12) талдауынан квази-параболалық құрылыммен байланысқан (5) потенциалының

үлесі әлсіз екендігі байқалады. Осылайша, күшті магнит өрістерінде екі электронды жүйе үшін қарпу потенциалының параболалық сипаты туралы гипотеза өте орынды. Жүргізілген есептеулерде біз *GaAs* үшін келесі щамаларды қолдандық: $m^* = 0.067m_e$ және $g^* = -0.44$.

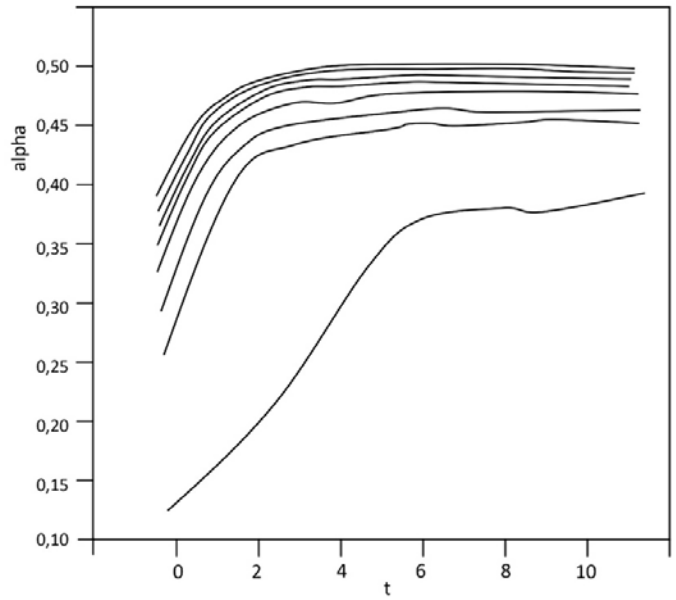

1-сурет. Магниттік кванттық санның әр түрлі мәндері үшін α параметрінің сыртқы магнит өрісінің $t = \omega_c/\omega_0$ салыстырмалы кернеуінен тәуелділігі. Төменгі деңгей $m = -1$, келесі деңгей $m = -2$ және т.б.

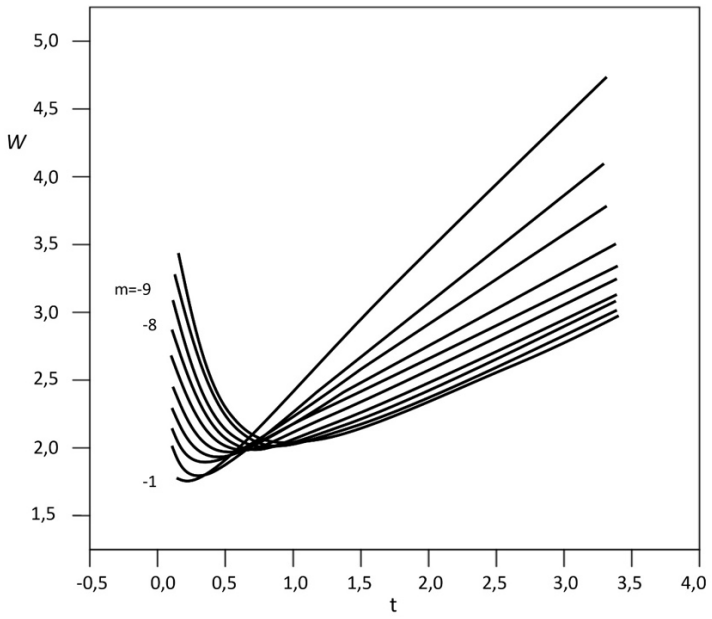

2а-сурет. Параболалық потенциал үшін $t = \omega_c/\omega_0$ сыртқы магнит өрісінің салыстырмалы кернеуіне байланысты Зееман әсерін ескере отырып, салыстырмалы қозғалыс гамильтонианының $W = E/\hbar\omega_0$ энергетикалық спектрлері.

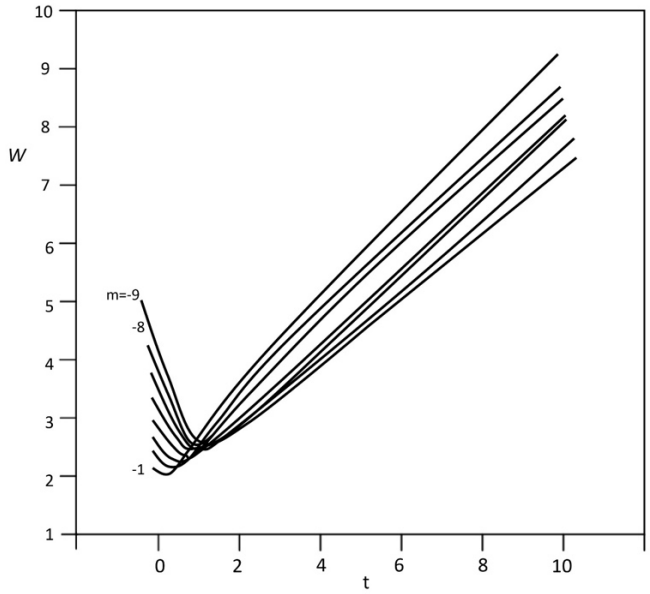

2b-сурет. Квази-параболалық потенциал үшін $t = \omega_c/\omega_0$ сыртқы магнит өрісінің салыстырмалы кернеуіне негізделген Зееман әсерін ескере отырып, салыстырмалы қозғалыс гамильтонианының $W = E/\hbar\omega_0$ энергетикалық спектрлері.

Қорытынды

Нанометрлік өлшемдегі жүйелер соңғы жылдары физикада жаңа зерттеу аймағының пайда болуына алып келді. Аз бөлшекті электрондық жүйелер теориялық түрғыдан да, эксперименталды түрғыдан да үлкен қызығушылық тудырды. Электронды құрылғылар үшін көптеген компонеттердің пайда болуына себепші болған жартылай өткізгіштік наноқұрылымдардың әр түрлілігіне қарамастан, сипаттамалары жақсартылған материалды іздеу процесі әлі де жалғасуда. Өнеркәсіпте наноматериалдарды пайдалану қарқыны тез өсуде, бұл өз кезегінде жаңа объектілерді құру үшін синтездеу әдістерінің дамуын ынталандырады. Жаңа кванттық өлшемді құрылымдарды құру жүріп жатқан кванттық механикалық процестердің ішкі құрылымын нақты түсінуді талап етеді. Жұмыс барысында кванттық нүктенің энергетикалық спектрі параболалық конфайнмент потенциалы үшін ангармониялық түзетуді ескере отырып, есептелінді. Осы жағдайлар үшін энергетикалық спектрдің ауытқуына талдау жасалды. Зерттеу барысында есептелінген сыртқы магнит өрісіндегі екі электронды КН энергетикалық спектрі кванттық нүктенің сипаттамаларын басқаруға мүмкіндік береді.

Әдебиеттер

1. Федорович С.В., Проценко И.Е. Квантовая электроника, 46, 45 (2016) [Quantum Electron., 46, 45 (2016)].
2. Саранцева Т.С., Силаев А.А., Веденскии Н.А., Фролов М.И., Манаков Н.Л. Квантовая электроника, 46, 366 (2016) [Quantum Electron., 46, 366 (2016)].
3. Reimann S. M., Manninen M. Electronic structure of quantum dots //Reviews of Mod- ern Physics. – 2002. – Vol. 74. – No. 4. – P. 1283.
4. Levchuk E. A., Makarenko L. F. On controlling the electronic states of shallow donors using a finite-size metal gate //Semiconductors. – 2016. – Vol. 50. – No. 1. – P. 89-96.
5. Dineykhan M., Efimov G.V., Ganbold G. and Nedelko S.N. “Oscillator representation in quantum physics”. //Lecture Notes in Physics-Springer-Verlag. -Berlin. -1995.-m 26.
6. M. Kammermeier, A. Seith, P. Wenk and J. Schliemann, Persistent spin textures and currents in wurtzite nanowire-based quantum structures // arXiv:2001.06571v2 8 May 2020 Icond-mat.mes-hall] (2020).
7. Mazur, A.M. Shirokov, A.I. Mazur, J.P. Vary, Description of resonant states in the shell model // arXiv:1512.03983 [nucl-th] p. 1-11 (2015).

References

1. Федорович С.В., Проценко И.Е. Квантовая электроника, 46, 45 (2016) [Quantum Electron., 46, 45 (2016)].
2. Саранцева Т.С., Силаев А.А., Веденскии Н.А., Фролов М.И., Манаков Н.Л. Квантовая электроника, 46, 366 (2016) [Quantum Electron., 46, 366 (2016)].
3. Reimann S. M., Manninen M. Electronic structure of quantum dots //Reviews of Mod- ern Physics. – 2002. – Vol. 74. – No. 4. – P. 1283.
4. Levchuk E. A., Makarenko L. F. On controlling the electronic states of shallow donors using a finite-size metal gate //Semiconductors. – 2016. – Vol. 50. – No. 1. – P. 89-96.
5. Dineykhan M., Efimov G.V., Ganbold G. and Nedelko S.N. “Oscillator representation in quantum physics”. //Lecture Notes in Physics-Springer-Verlag. -Berlin. -1995.-m 26.
6. M. Kammermeier, A. Seith, P. Wenk and J. Schliemann, Persistent spin textures and currents in wurtzite nanowire-based quantum structures // arXiv:2001.06571v2 8 May 2020 Icond-mat.mes-hall] (2020).
7. Mazur, A.M. Shirokov, A.I. Mazur, J.P. Vary, Description of resonant states in the shell model // arXiv:1512.03983 [nucl-th] p. 1-11 (2015).

МРНТИ 31.15.28 https://doi.org/10.26577/JPEOS.2023.v25.i3-4.i4

Ж.Б. Омарова[1*], Д.Е. Ережеп[1], С.Р. Жантуаров[2], Н.С. Токмолдин[3]

[1]Satbayev University, Казахстан, г. Алматы
[2] Satbayev University, Физико-технический институт, Казахстан, г. Алматы,
[3]Потсдамский университет, Германия, г. Потсдам
*e-mail: omarovazhansaya7@gmail.com

ИССЛЕДОВАНИЕ СТАБИЛЬНОСТИ ФУНКЦИОНАЛЬНОГО СЛОЯ В ПЕРОВСКИТНОМ СОЛНЕЧНОМ ЭЛЕМЕНТЕ

Одним из видов зеленых возобновляемых источников энергии является солнечная энергетика, которая считается экологически чистой. Солнечная энергетика представляет собой обширную область со многими направлениями, среди которых перовскитная фотовольтаика считается одной из наиболее перспективных направлений. Несмотря на то, что эффективность преобразования солнечной энергии уже достигла более 25%, имеются ряд препятствий в использованиях перовскитных солнечных элементов, одним из которых является низкая устойчивость к внешним факторам деградации. Целью данной работы было исследование деградации поверхности тонкой пленки перовскита $CH_3NH_3PbI_{3-x}Cl_x$ под действием внешних воздействий, таких как атмосферной влага и свет. Полное понимание влияния внешних факторов при изготовлении каждого функционального слоя считается наиболее важным для обеспечения стабильности перовскитного солнечного элемента.

Метод. Для исследования поверхности $CH_3NH_3PbI_{3-x}Cl_x$ использовали сканирующий электронный микроскоп Quanta 200i 3D, FTIR-спектроскопию типа ФСМ 2203, спектроскопия комбинационного рассеяния с использованием спектрометра Solver Spectrum 600/600 и оптическую абсорбцию QEX-10. С помощью спектроскопии возможно было наблюдать деградацию и сопутствующую эволюцию молекулярной структуры внутри слоя перовскита.

Результаты. В исследовании было показано, что деградация функционального слоя перовскита протекает по-разному в зависимости от действующего фактора, присутствующего в окружающей атмосфере и при процессе деградации кристаллической структуры перовскита образуются новые химические связи. После воздействия атмосферы и света ухудшаются качественные характеристики оптических параметров фотопреобразователя, что приводит к разрушению функционального слоя перовскита за счет гидратационной деградации и механизма депротонирования. Механизм деградации может быть инициирован разрывом йодидных связей. Выявлены сильные изменения интенсивности поглощения характеристических частот, соответствующих функциональным группам NH и CH на частотах 3132 1/см и 3179 1/см.

Обсуждение. В этой работе представлен подход к изучению структурной стабильности отдельного функционального слоя перовскита с целью разработки альтернативных концепций изготовления стабильных и устойчивых перовскитных солнечных элементов.

Ключевые слова: Солнечный элемент, перовскит, функциональный слой, деградация, стабильность.

Z. Omarova[1*], D. Yerezhep[1], S. Zhantuarov[2], N. Tokmoldin[3]

[1]Satbayev University, Kazakhstan, Almaty
[2]Satbayev University, Institute of Physics and Technology, Kazakhstan, Almaty
[3]Universitut Potsdam, Germany, Potsdam
*e-mail: omarovazhansaya7@gmail.com

Stability study of the functional layer in a perovskite solar cell

One of the types of green renewable energy sources is solar energy, which is considered environmentally friendly. Solar energy is a vast field with many directions, among which perovskite photovoltaics is considered one of the most promising areas. Despite the fact that the efficiency of solar energy conversion has already reached more than 25%, there are a number of obstacles in the use of perovskite

solar cells, one of which is low resistance to external degradation factors. The purpose of this work was to study the degradation of the surface of a thin film of perovskite $CH_3NH_3PbI_{3-x}Cl_x$ under the influence of external influences, such as atmospheric moisture and light. A complete understanding of the influence of external factors in the manufacture of each functional layer is considered the most important to ensure the stability of a perovskite solar cell.

To study the surface of $CH_3NH_3PbI_{3-x}Cl_x$, a Quanta 200 3d scanning electron microscope, FTIR spectroscopy of the FSM 2203 type, raman spectroscopy using a Solver Spectrum 600/600 spectrometer and QEX-10 optical absorption were used. With the help of spectroscopy, it was possible to observe the degradation and concomitant evolution of the molecular structure inside the perovskite layer. The study showed that the degradation of the functional layer of perovskite proceeds differently depending on the active factor present in the surrounding atmosphere and during the degradation of the crystal structure of perovskite, new chemical bonds are formed. After exposure to the atmosphere and light, the qualitative characteristics of the optical parameters of the photoconverter deteriorate, which leads to the destruction of the functional layer of perovskite due to hydration degradation and the deprotonation mechanism. The degradation mechanism can be initiated by the breaking of iodide bonds. Strong changes in the absorption intensity of characteristic frequencies corresponding to the functional groups NH and CH at frequencies 3132 1/cm and 3179 1/cm were revealed.

Discussion. This paper presents an approach to the study of the structural stability of a separate functional layer of perovskite in order to develop alternative concepts for the manufacture of stable and stable perovskite solar cells.

Key words: solar cell, perovskite, functional layer, degradation, stability.

Ж.Б. Омарова[1*], Д. Ережеп[1], С. Жантуаров[2], Н. Токмолдин[3]

[1]Satbayev University, Қазақстан, Алматы қ.

[2]Satbayev University, Физика-техникалық институт, Қазақстан, Алматы қ.

[3]Потсдам университеті, Германия, Потсдам қ.

*e-mail: omarovazhansaya7@gmail.com

Перовскитті күн элементіндегі функционалдық қабаттың тұрақтылығын зерттеу

Жасыл жаңартылатын энергия көзінің бір түрі экологиялық таза болып саналатын күн энергетикасы болып табылады. Күн энергетикасы – көптеген бағыттары бар кең аймақ, олардың ішінде перовскитті фотовольтаика ең перспективалы бағыттардың бірі болып саналады. Күн энергиясының түрлендіру тиімділігі қазірдің өзінде 25% -дан астамға жеткеніне қарамастан, перовскитті күн элементтерін пайдалануда бірқатар кедергілер бар, олардың бірі сыртқы деградация факторларына төмен төзімділік болып табылады. Жұмыстың мақсаты – атмосфералық ылғал мен жарық сияқты сыртқы әсерлердің әсерінен перовскит $CH_3NH_3PbI_{3-x}Cl_x$ жұқа үлдірінің бетінің деградациясын зерттеу. Перовскитті күн элементінің тұрақтылығын қамтамасыз ету үшін әрбір функционалды қабатты дайындау кезінде сыртқы факторлардың әсерін мұқият түсіну маңызды.

$CH_3NH_3PbI_{3-x}Cl_x$ бетін зерттеу үшін Quanta 200i 3D сканерлеуші-электронды микроскоп, ФСМ 2203 типті FTIR спектроскопиясы, Solver Spectrum 600/600 спектрометрін қолданатын Раман спектроскопиясы және QEX-10 оптикалық абсорбциясы қолданылды. Спектроскопияның көмегімен перовскит қабатының ішінде молекулалық құрылымның деградациясын және қатар жүретін эволюциясын байқауға болады.

Зерттеу көрсеткендей, перовскиттің функционалды қабатының ыдырауы қоршаған атмосферада болатын белсенді факторға байланысты және перовскит кристалдық құрылымының ыдырау процесінде жаңа химиялық байланыстар пайда болады. Атмосфера және жарық әсерінен кейін фототүрлендіргіштердің оптикалық параметрлерінің сапалық сипаттамалары нашарлайды, бұл гидратацияның деградациясы мен протонация механизмінің әсерінен перовскиттің функционалдық қабатының бұзылуына әкеледі. Деградация механизмі йодидтік байланыстарды үзу арқылы басталуы мүмкін. 3132 1/см және 3179 1/см жиілікте NH және CH функционалдық топтарына сәйкес келетін сипаттамалық жиіліктердің сіңіру қарқындылығында күшті өзгерістер анықталды. Бұл жұмыс тұрақты және серпімді перовскит күн элементтерін жасау үшін балама тұжырымдамаларды әзірлеу мақсатында бір функционалды перовскит қабатының құрылымдық тұрақтылығын зерттеу тәсілін ұсынады.

Түйін сөздер: күн элементі, перовскит, функционалды қабат, деградация, тұрақтылық.

Введение

Для улутшения экологической обстоновке в мире, активно исследуются альтернативные методы получения энергии [1–3]. В течение последних десятилетий, перовскитные солнечные элементы (PSC) заметно улучшили свою эффективность за счет научных исследований, в которых производительность тонкопленочного элемента была достигнута больше 25% [4–6]. Однако, коммерциализация и более широкое использование PSC на промышленном рынке по-прежнему затруднительны из-за проблем с сохранением стабильности отдельных функциональных слоев [7,8]. На стабильную работу PSC влияют различные факторы, связанные с деградацией, которые подразделяются на внутренние и внешние. Так, миграция перовскитных ионов, влияющая на прочность связей между катионами и анионами, относится к внутренним факторам деградации, что приводит к термической нестабильности [9]. Поддержание кристаллической структуры и стехиометрического соотношения компонентов PSC происходит за счет подавления миграции ионов, в связи с этим удается сохранить свойства PSC [9]. Внешние же факторы включают воздействие окружающей среды, в том числе влияние влажности [10], кислорода [11], температуры [12] и интенсивного ультрафиолетового излучения [13]. Интенсивная деградация под воздействием окружающей среды приводит к снижению прочности водородной связи $CH_3NH_3^+$, при котором разрушается структура PSC [14]. Перед деградацией структуры PSC наблюдается сильное искажение межатомного расстояния за счет адсорбции молекул воды [15]. Для повышения долговечности и коммерциализуемости необходимы исследования механизмов деградации и стабильности PSC.

Наше исследование сосредоточено в основном на применении FTIR спектроскопии для мониторинга деградации и сопутствующей эволюции молекулярной структуры поверхности в активном функциональном слое ($CH_3NH_3PbI_xCl_x$). Несмотря на высокую чувствительность, неинвазивность и относительную простоту, применение FTIR спектроскопии для изучения деградации перовскитных солнечных элементов весьма ограничено. В данной работе исследуется эволюция химической структуры поверхности отдельного активного слоя под влиянием окружающей атмосферы в диапазоне колебательных характеристик 370-7800 1/см. Дополнительное подтверждение деградации структуры поверхности активного функционального слоя проводились с помощью сканирующей электронной микроскопии и системы измерения квантовой эффективности, а также рамановской спектроскопии. На основе FTIR спектроскопии мы стремимся определить конкретные пути и скорости деградации поверхности тонкой пленки активного функционального слоя. По результатам исследования этот подход может применяться и к другим функциональным слоям и фотоэлектрическим системам. Есть надежда, что представленные результаты помогут еще больше повысить производительность и стабильность материалов и устройств в атмосферных условиях на пути к созданию стабильных и устойчивых перовскитных фотоэлектрических элементов.

Методология

2.1 Материалы

N, N-диметилформамид ($HCON(CH_3)_2$, 99,8%, номер CAS: 68-12-2, Sigma-Aldrich, Великобритания), йодид метиламмония (CH_6IN, >99,5%, номер CAS: 14965-49-2, Люминесцентная технология, Тайвань), хлорид свинца(II) ($PbCl_2$, 99,999%, номер CAS: 7758-95-4, Люминесцентная технология, Тайвань), легированный фтором оксид олова (FTO) (размеры 50*50 мм, толщина 2,2 мм, удельное сопротивление 7 Ом/кв, Solaronix SA, Швейцария), легированный кремний N-типа (диаметр 200±0,5 мм, толщина 200±20 мкм, удельное сопротивление 1,8–13 Ом·см, Atecom Technology, Тайвань), дистиллированная вода, ацетон, этанол, специальный чистящий концентрат от Hellma (Hellmanex III, Германия), газообразный азот, безворсовые салфетки Kimtech Kimwipes science, стеклянный флакон 10 мл. Для приготовления готового раствора использовались реагенты без какой-либо дополнительной очистки.

2.2 Характеристика устройства

Характеристики микроструктуры изучали с помощью сканирующей электронной микроскопии (Quanta 200i 3D, компания FEI, Хиллсборо, штат Орегон, США). Измерение оптических характеристик проводилось на приборе QEX-10 (PV Measurements, Inc., USA). Рамановские спектры регистрировались на спектрометре Solver Spectrum 600/600 в режиме отражения на 180°. В качестве источника возбуждения использовался He-Ne лазер с длиной волны $\lambda = 633$ нм. Оптические спектры исследуемых веществ в инфра-

красном спектральном диапазоне регистрируются при помощи FTIR-спектрометра типа ФСМ 2203 фирмы «ИНФРАСПЕК» производства РФ. Оптический спектральный диапазон измерения составляет 370-7800 1/см с максимальным спектральным разрешением 0,125 1/см. При этом отношение сигнал/шум составляет более чем 60000 у.е.

2.3 Приготовление $CH3NH_3PbI_{3-x}Cl_x$

Тонкая пленка перовскита изготавливалась в открытом воздухе при относительной влажности 40%±2% на очищенных подложках в виде кремния и стекла. Кремниевые подложки очищали ацетоном, этанолом и течение 1 мин соответственно, а затем сушили в сушильном шкафе. Для CH3NH3PbI3-xClx образцы готовили с использованием 3:1 (м/м) CH3NH3I:PbCl2, и реакция происходила при комнатной температуре при перемешивании до растворения всех твердых веществ. Для лучшего растворения твёрдых частиц проводили нагревание флакона при 600 С. Образцы были приготовлены методом центрифугирования в объеме 50 мкл перовскита при 1000 об/мин в течение 30 с, затем оставляли на 10 мин на воздухе, а потом отжигали при 100 °С в течение 90 мин, после был отжиг при 120 °С в течение 10 мин на открытом воздухе. Подготовленные образцы оставляли охлаждаться до комнатной температуры в инертной среде. При этом методе отдельные функциональные слои перовскита давали примерную толщину 200 нм.

Результаты и обсуждения

3.1 Морфология поверхности

На рисунке 1 изображена микрофотография деградированных тонких пленок чистого металламония йодида и хлорида свинца осажденных на подложку из кристаллического кремния.

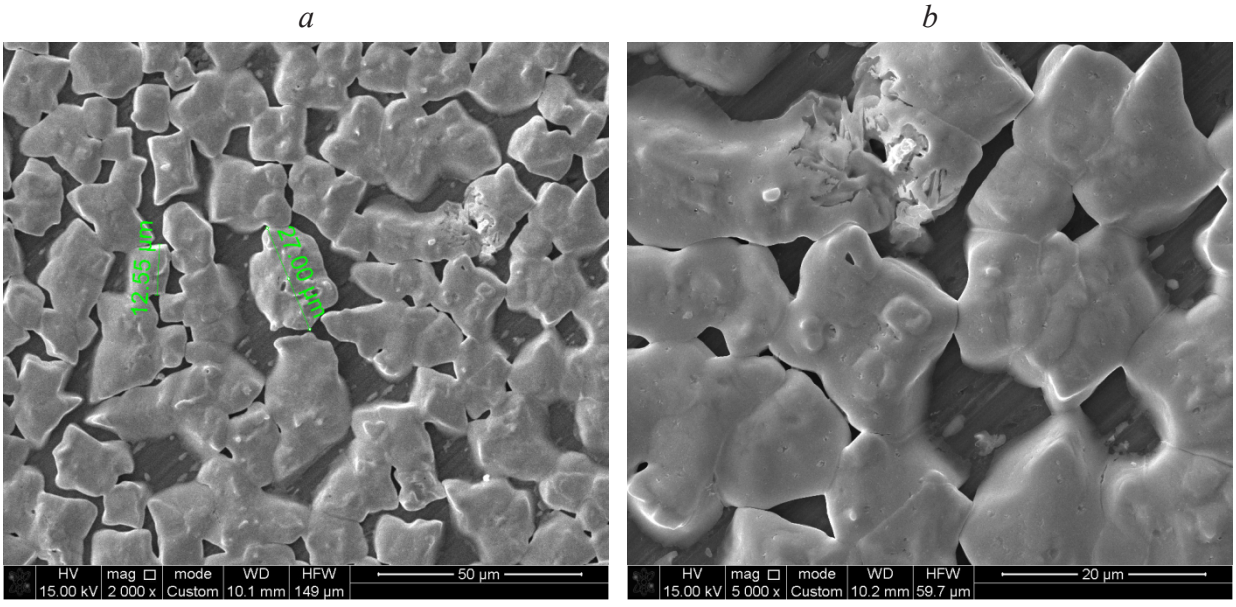

(a) увеличение 2000x, (b) увеличение 5000x

Рисунок 1 – Изображение деградирующий перовскитной пленки

Из рисунка 1 видно, что поверхность деградированной пленки имеет разветвлённую структуру. Можем также наблюдать поры или пустот, что имеет важное значение для оптической спектроскопии. На рисунке 1 а,б представлены снимки SEM тонкой пленки перовскита, полученные при увеличении 2000x и 5000x, соотвественно. На рисунке 2 представлено изображение поперечного сечения разрешенной перовскитной пленки, и видно, что толщина пленки составила 3,7 µm.

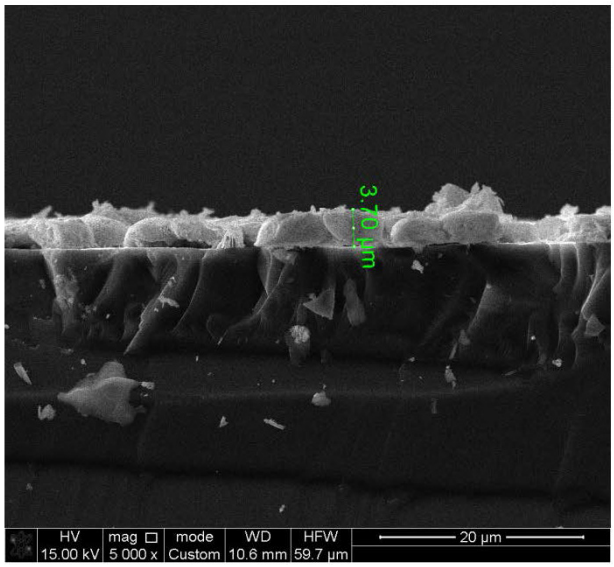

Рисунок 2 – Изображение поперечного сечения деградирующий перовскитной пленки

3.2 Оптическая плотность

Оценка оптических характеристик деградированной поверхности перовскитной пленки проводилась с помощью данных, которые были получены при пропускании широкополосного света через образцы. Процесс ослабления поглощения спектров наблюдается при длительном воздействии внешних факторов, которые вызывают разрушение поверхности образца, что приводит к выделению вещества желтого цвета PbI_2 и к снижению пропускаемости. Измерение пропускания света через пленки образцов осуществлялось в диапазоне от 300 нм до 1100 нм. Полученные результаты деградированной пленки при воздействии различных факторов (света и воздуха в течении 336 часов) показаны на рисунке 3.

При воздействии внешних факторов поглощение снижается в коротковолновом диапазоне 350-400 нм, затем наблюдали небольшой спад оптического поглощения в диапазоне 400-750 нм. Третья часть приходилась на диапазон 800-1100 нм, и в диапазоне 750-800 нм наблюдался интенсивный спад, а далее спектр поглощения стремился к минимуму. Учитывая, что пороговая длина волны эффективного поглощения в видимом диапазоне достигает 850 нм [16], то нет необходимости рассматривать диапазон 850-1100 нм, где поглощение стремиться к минимуму.

Так, при деградации под воздействием солнечного света можем наблюдать интенсивное снижение поглощения фотонов в видимой области 400-750 нм в сравнении с деградацией под воздействием атмосферы, исключая солнечный свет. Таким образом, полученные экспериментальные данные свидетельствуют о влиянии деградации на оптическую плотность пленки перовскита.

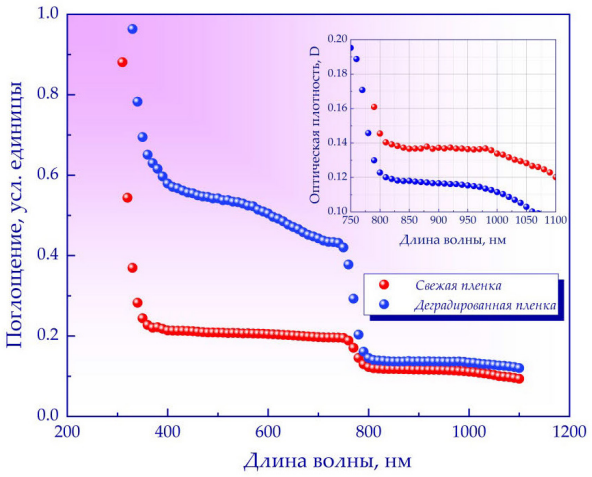

Рисунок 3 – Зависимость изменения поглощения пленок перовскита от различных факторов

3.3 FTIR

Для определения конкретного пути и скорости деградации отдельного перовскитного слоя солнечного элемента, а также характерной энергии активации процессов, лежащих в основе деградации, был сделан спектральный анализ с применением FTIR-спектроскопии. FTIR-спектроскопия дает возможность исследовать эволюцию химической структуры отдельных функциональных слоев и их сочетаний под влиянием окружающей атмосферы и температуры. Несмотря на то, что деградацию, вызванной влиянием атмосферной влаги, можно избежать с помощью метода инкапсуляции, однако существующие на данный момент методы не могут обеспечить полную защиту от процесса гидратации. Поэтому, ИК спектроскопические исследования процесса деградации, вызванного гидратацией, целесообразно для получения стабильных пленок перовскита с прочной кристаллической структурой. Наш спектральный анализ был ограничен средним диапазоном колебательных характеристик 400–4200 1/см. На рисунке 4 представлены колебательные спектры для идентификации эволюции химической структуры при помощи характеристических полос пропускания, зарегистрированных при

высоком отношении сигнал/шум и в диапазоне волновых чисел 400–4200 1/см от монокристалла $CH_3NH_3PbI_{3-x}Cl_x$ толщиной ~ 200 нм до и после деградации образца. Исходя из приведенных литературных данных [17], наблюдается хорошая сходимость колебательных спектров при сравнении с экспериментально получаемыми колебательными спектрами (красная линяя) свежо полученного (нового) образца. В свежо полученной тонкой пленке перовскита наблюдается наиболее интенсивная мода колебаний при частотах равных 3132 1/см и 3179 1/см, которые соответствуют симметричной и ассиметричной валентным модам N-H (связанными с NH_3^+). Необходимо отметить, отсутствие спектра валентных колебаний O–H в области 3400–3700 1/см, который указывает на функциональную гидроксильную группу (гидратов, гидроксида, воды) в исследуемой свежо полученной тонкой пленки перовскита [18].

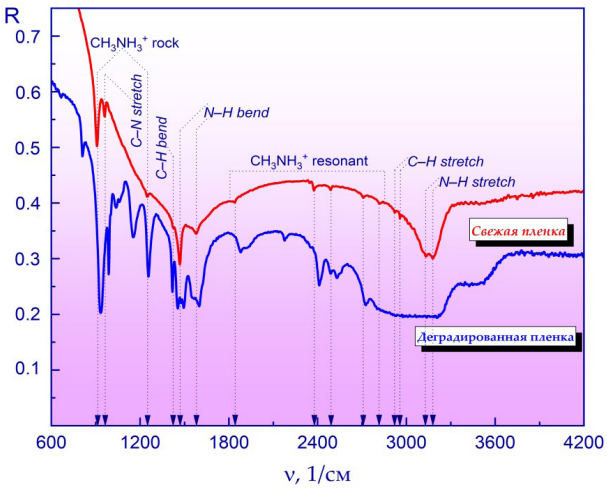

Рисунок 4 – ИК-Фурье-спектры образцов монокристалла $CH_3NH_3PbI_{3-x}Cl_x$, свежо приготовленной (красный) тонкой пленки перовскита и при воздействии атмосферной влаги на перовскит (синий).

Таким образом, для свежо приготовленной тонкой пленки перовскита характерны следующие пики, такие как 910 1/см и 1248 1/см ($CH_3NH_3^+$ rock), 961 1/см (C–N stretch), 1421 1/см (C–H bend), 1468 1/см (N–H bend (symmetric)), 1578 1/см (N–H bend (asymmetric)), 2921 1/см (C–H stretch (symmetric)), 2958 1/см (C–H stretch (asymmetric)).

Тонкая пленка перовскита хранятся при относительной влажности примерно 50% ± 5% без инкапсуляции. Так, при воздействии атмосферной влаги наблюдается расширение полосы NH_3^+, которая сопровождается сдвигом моды растяжения N–H в сторону более высоких частот (синяя линия). Одновременное расширение и смещение колебания N–H на частоте ~ 3200 1/см можно объяснить деградацией поверхности перовскита за счет гидратации. Следующим чувствительным характерным пиком при гидрадации является появление доминирующего пика при частоте 1660 1/см, который также используется для оценки степени деградации [19]. Появление доминирующего пика 1660 1/см возникает из-за изгибной (bending) моды связей N–H и O–H, а пик 1497 1/см возникает из-за растяжения (stretching) связей O-H и C-H [20]. Наблюдаем спектральные сдвиги за счет разрушения кристалической структуры, в районе 900 1/см – 1300 1/см, для трех пиков с частоты 910 1/см и 1248 1/см ($CH_3NH_3^+$ rock), 961 1/см (C–N stretch) на частоту 935 1/см и 1255 1/см, 990 1/см соответственно. Отсюда следует, что гидратация приводит к образованию новых химических связей при деградации кристаллической структуры перовскита за счет механизма депротонирования $CH_3NH_3^+$ [21].

Далее, для исследования влияния воздействия света использовался закрытый герметичный бокс с источником, имитирующим солнечный свет лампой с длиной волны 300-800 нм. Для исследования влияния воздействия света была использована FTIR спектроскопия, так как это хороший инструмент для идентификации гидроксильных групп в образце. Гидроксильная группа играет наиважнейшую роль при фотогальваническом процессе за счет сдерживания инжекции и переноса заряда, а также переноса энергии от кристаллов к колебательным состояниям OH [22]. На рисунке 5 показано сравнение ИК спектров свежо приготовленного (новый) образца с деградированным (decomposed) образцом под воздействием источника света.

При сравнении ИК спектров свежо приготовленного и деградированного образцов, видно, что интенсивность полосы, которая относиться к валентным колебаниям гидроксильных групп, снижается. Это может свидетельствовать о десорбции или диссоциации гидроксильных групп из образца. Соответственно, диссоциация молекул H_2O под воздействием солнечного света может отрицательно сказаться на эффективности и стабильности поглощающего слоя за счет образования дефектов.

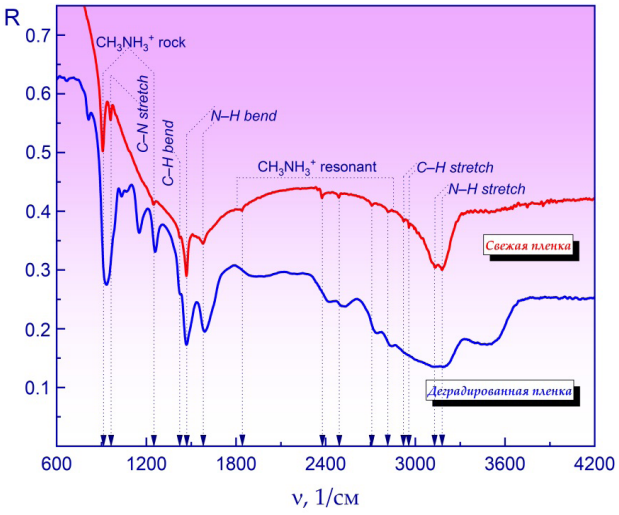

Рисунок 5 – ИК-Фурье-спектры образцов монокристалла $CH_3NH_3PbI_{3-x}Cl_x$, свежо приготовленной (красный) тонкой пленки перовскита и при воздействии источника света на перовскит (синий).

Наблюдается более выраженный пик со смещением 1578 1/см (N–H bend (asymmetric)) до 1590 1/см. Также видим ярко выраженные пики со смещением 936 1/см и 1260 1/см, которые относятся к $CH_3NH_3^+$ rock, что свидетельствует о деградации поверхности тонкой пленки перовскита. Пики колебаний на частотах 810 1/см и 1150 1/см и смещение выше приведенных пиков позволяет предполагать о разрушении связей кристаллической структуры перовскита под влиянием светового излучения. Сохранение эффективности и стабильности перовскитного солнечного элемента можно добиться за счет пассивации ионных дефектов, то есть за счет увеличения времени жизни рекомбинации и снижения плотности ловушек заряда [23].

3.4 Raman Spectroscopy

В данном разделе представлена рамановская спектроскопия, которая хорошо себя зарекомендовала и является прекрасным инструментом для локального анализа органо-неорганических галогенидных слоев перовскита. Для получения рамановских спектров комбинационного рассеяния чистых слоев анализируемого образца использовалась низкая интенсивность возбуждающего He-Ne лазер с длиной волны $\lambda = 633$ нм. Для чистоты получаемого эксперимента были проведены повторные измерения одного и того же образца для наблюдения структурных изменений, которые мы коррелируем с локальной деструкцией перовскитовой пленки, вызванной атмосферными условиями.

На рисунке 6 показан спектр комбинационного рассеяния. Предварительно, мощность лазера была настроена на 10 мкВт для того, что предотвратить непреднамеренное разрушение или чрезмерный нагрев.

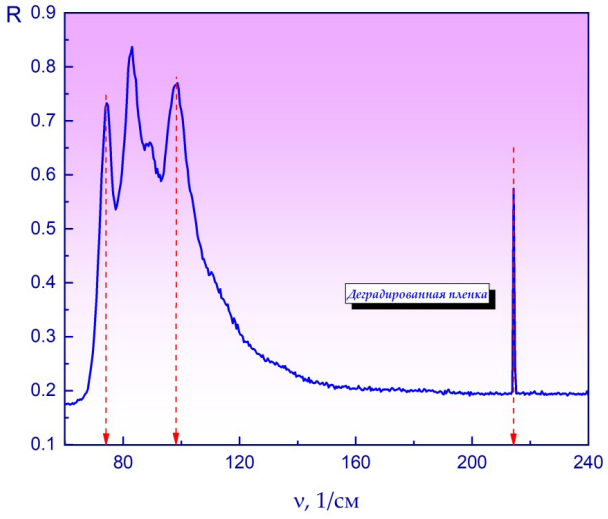

Рисунок 6 – Рамановские спектры деградированных образцов $CH_3NH_3PbI_{3-x}Cl_x$

Наблюдаемые полосы комбинационного рассеяния на частотах 75 1/см, 98 1/см, 215 1/см согласуются со спектрами, описанными для объемных кристаллов PbI_2 в литературе (красные пунктирные линии) [24]. Скорее всего, при сильном освещении лазерным лучом и более высоких температурах деградация значительно ускоряется. Отметим, как доказано в термогравиметрическим анализом работы [25], что температура сама по себе не может быть единственной причиной разложения перовскита до PbI_2. А различие спектральных форм рамановских спектров в работах [26,27] измеренных при возбуждении лазера с длиной волны 532 нм, а нашем случае используется лазера с длиной волны 633 нм. На основании этих результатов мы подтверждаем, что одним из конечных продуктов процесса разложения, индуцированного комбинационным излучением, является PbI_2.

Полученные результаты свидетельствуют о быстрой деградации поверхности тонкой пленки перовскита при воздействии окружающей среды (атмосферной влаги, света). Видно, что различ-

ные виды воздействия окружающей среды, будь это атмосферная влага или свет, ведут к разным путям разложения кристаллической структуры перовскита, то есть приводит к деградации функционального слоя.

Выводы

Таким образом, был исследован функциональный слой тонкой пленки перовскита $CH_3NH_3PbI_{3-x}Cl_x$ путем объединения исследований морфологии поверхности, оптической плотности, FTIR и Раман спектров при воздействии различных факторов. Было показано, что под воздействием света и влажности зафиксированы существенные изменения в ИК-спектрах перовскитового материала относительно характеристических полос поглощения образцов. Обнаружено, что механизм деградации функционального слоя перовскита протекает разнообразно в зависимости от воздействия определенного фактора, который может находится в окружающей атмосфере. При деградации кристалической структуры перовскита обзазуются новые химические связи при процессе гидратации за счет механизма депротонирования. Следовательно, механизм деградации, вызванный как светом, так и влагой, может быть инициирован разрывом йодидных связей. Мы подтвердили деградацию перовскита, сделав снимки с помощью сканирующего электронного микроскопа до и после деградации. Необходима дальнейшая работа, чтобы понять взаимосвязь внешних факторов, как влага, кислород и освещение, участвующие в диссоциации йода и свинца, а также добавить электрическую нагрузку на активную перовскитовую ячейку под действием света с повышенной и пониженной температурой. Однако исследование стабильности полученных пленок приближает нас к тому, чтобы сделать перовскиты конкурентоспособным игроком в тонкопленочной фотоэлектрической промышленности.

Благодарности

Исследование выполнено по гранту AP19174728 при финансовой поддержке Министерство науки и высшего образования Республики Казахстан.

Литература

1. Bulat L.P., Novotel'nova A.V., Tukmakova A.S., Yerezhep D.E., Osvenskii V.B., Sorokin A.I., Pshenai-Severin D.A., Ashmontas S. Temperature fields control in the process of spark plasma sintering of thermoelectrics // Tech. Phys.– 2017.– Vol. 62, № 4.

2. Bulat L.P., Novotelnova A. V., Tukmakova A.S., Yerezhep D.E., Osvenskii V.B., Sorokin A.I., Panchenko V.P., Bochkov L. V., Ašmontas S. Simulation of SPS Process for Fabrication of Thermoelectric Materials with Predicted Properties // J. Electron. Mater.– 2018.– Vol. 47, № 2.– P. 1589–1594.

3. Amin M., Shah H.H., Fareed A.G., Khan W.U., Chung E., Zia A., Rahman Farooqi Z.U., Lee C. Hydrogen production through renewable and non-renewable energy processes and their impact on climate change // Int. J. Hydrogen Energy.– 2022.– Vol. 47, № 77.– P. 33112–33134.

4. Gong O.Y., Seo M.K., Choi J.H., Kim S.-Y., Kim D.H., Cho I.S., Park N.-G., Han G.S., Jung H.S. High-performing laminated perovskite solar cells by surface engineering of perovskite films // Appl. Surf. Sci.– 2022.– Vol. 591.– P. 153148.

5. Omarova Z., Yerezhep D., Aldiyarov A., Golikov O., Tokmoldin N. PERFORMANCE SIMULATION OF ECO-FRIENDLY SOLAR CELLS BASED ON CH3NH3SnI3 // Eurasian Phys. Tech. J.– 2022.– Vol. 19, № 2 (40).– P. 58–64.

6. Omarova Z., Yerezhep D., Aldiyarov A., Tokmoldin N. In Silico Investigation of the Impact of Hole-Transport Layers on the Performance of CH3NH3SnI3 Perovskite Photovoltaic Cells // Crystals.– 2022.– Vol. 12, № 5.– P. 699.

7. Wang H.-Q., Wang S., Chen L., Yin Z., Mei S., Zhong Y., Yao Y., Li N., Wang J., Song W. Understanding degradation mechanisms of perovskite solar cells due to electrochemical metallization effect // Sol. Energy Mater. Sol. Cells.– 2021.– Vol. 230.– P. 111278.

8. Yerezhep D., Omarova Z., Aldiyarov A., Shinbayeva A., Tokmoldin N. IR Spectroscopic Degradation Study of Thin Organometal Halide Perovskite Films // Molecules.– 2023.– Vol. 28, № 3.– P. 1288.

9. Li N., Niu X., Li L., Wang H., Huang Z., Zhang Y., Chen Y., Zhang X., Zhu C., Zai H., Bai Y., Ma S., Liu H., Liu X., Guo Z., Liu G., Fan R., Chen H., Wang J., Lun Y., Wang X., Hong J., Xie H., Jakob D.S., Xu X.G., Chen Q., Zhou H. Liquid medium annealing for fabricating durable perovskite solar cells with improved reproducibility // Science (80-.).– 2021.– Vol. 373, № 6554.– P. 561–567.

10. Meng X., Tian X., Zhang S., Zhou J., Zhang Y., Liu Z., Chen W. In Situ Characterization for Understanding the Degradation in Perovskite Solar Cells // Sol. RRL.– 2022.– P. 2200280.

11. Emery Q., Remec M., Paramasivam G., Janke S., Dagar J., Ulbrich C., Schlatmann R., Stannowski B., Unger E., Khenkin M. Encapsulation and Outdoor Testing of Perovskite Solar Cells: Comparing Industrially Relevant Process with a Simplified Lab Procedure // ACS Appl. Mater. Interfaces.– 2022.– Vol. 14, № 4.– P. 5159–5167.

12. Chen B., Song J., Dai X., Liu Y., Rudd P.N., Hong X., Huang J. Synergistic Effect of Elevated Device Temperature and Excess Charge Carriers on the Rapid Light-Induced Degradation of Perovskite Solar Cells // Adv. Mater.– 2019.– Vol. 31, № 35.– P. 1902413.

13. Wu C., Wang K., Feng X., Jiang Y., Yang D., Hou Y., Yan Y., Sanghadasa M., Priya S. Ultrahigh Durability Perovskite Solar Cells // Nano Lett.– 2019.– Vol. 19, № 2.– P. 1251–1259.

14. Bracher C., Freestone B.G., Mohamad D.K., Smith J.A., Lidzey D.G. Degradation of inverted architecture CH 3 NH 3 PbI 3- x Cl x perovskite solar cells due to trapped moisture // Energy Sci. Eng.– 2018.– Vol. 6, № 1.– P. 35–46.

15. Busipalli D.L., Lin K.-Y., Nachimuthu S., Jiang J.-C. Enhanced moisture stability of cesium lead iodide perovskite solar cells – a first-principles molecular dynamics study // Phys. Chem. Chem. Phys.– 2020.– Vol. 22, № 10.– P. 5693–5701.

16. Kuang Y., Ma Y., Zhang D., Wei Q., Wang S., Yang X., Hong X., Liu Y. Enhanced Optical Absorption in Perovskite/Si Tandem Solar Cells with Nanoholes Array // Nanoscale Res. Lett.– 2020.– Vol. 15, № 1.– P. 213.

17. Makableh Y.F., Dalal'ah T.N. Investigation of the effect of the fabrication temperature on the optical, morphological and crystallinity properties of Perovskites composites // Micro and Nanostructures.– 2022.– Vol. 167.– P. 207259.

18. Li Z., Li B., Wu X., Sheppard S.A., Zhang S., Gao D., Long N.J., Zhu Z. Organometallic-functionalized interfaces for highly efficient inverted perovskite solar cells // Science (80-.).– 2022.– Vol. 376, № 6591.– P. 416–420.

19. Zhu Z., Hadjiev V.G., Rong Y., Guo R., Cao B., Tang Z., Qin F., Li Y., Wang Y., Hao F., Venkatesan S., Li W., Baldelli S., Guloy A.M., Fang H., Hu Y., Yao Y., Wang Z., Bao J. Interaction of Organic Cation with Water Molecule in Perovskite MAPbI 3 : From Dynamic Orientational Disorder to Hydrogen Bonding // Chem. Mater.– 2016.– Vol. 28, № 20.– P. 7385–7393.

20. Gan Z., Yu Z., Meng M., Xia W., Zhang X. Hydration of mixed halide perovskites investigated by Fourier transform infrared spectroscopy // APL Mater.– 2019.– Vol. 7, № 3.– P. 031107.

21. Manser J.S., Saidaminov M.I., Christians J.A., Bakr O.M., Kamat P. V. Making and Breaking of Lead Halide Perovskites // Acc. Chem. Res.– 2016.– Vol. 49, № 2.– P. 330–338.

22. Hoch L.B., Szymanski P., Ghuman K.K., He L., Liao K., Qiao Q., Reyes L.M., Zhu Y., El-Sayed M.A., Singh C.V., Ozin G.A. Carrier dynamics and the role of surface defects: Designing a photocatalyst for gas-phase CO 2 reduction // Proc. Natl. Acad. Sci.– 2016.– Vol. 113, № 50.

23. Zheng X., Chen B., Dai J., Fang Y., Bai Y., Lin Y., Wei H., Zeng X.C., Huang J. Defect passivation in hybrid perovskite solar cells using quaternary ammonium halide anions and cations // Nat. Energy.– 2017.– Vol. 2, № 7.– P. 17102.

24. Nakashima S. Raman study of polytypism in vapor-grown PbI2 // Solid State Commun.– 1975.– Vol. 16, № 9.– P. 1059–1062.

25. Baikie T., Fang Y., Kadro J.M., Schreyer M., Wei F., Mhaisalkar S.G., Graetzel M., White T.J. Synthesis and crystal chemistry of the hybrid perovskite (CH3NH3)PbI3 for solid-state sensitised solar cell applications // J. Mater. Chem. A.– 2013.– Vol. 1, № 18.– P. 5628.

26. Quarti C., Grancini G., Mosconi E., Bruno P., Ball J.M., Lee M.M., Snaith H.J., Petrozza A., De Angelis F. The Raman Spectrum of the CH 3 NH 3 PbI 3 Hybrid Perovskite: Interplay of Theory and Experiment // J. Phys. Chem. Lett.– 2014.– Vol. 5, № 2.– P. 279–284.

27. Grancini G., Marras S., Prato M., Giannini C., Quarti C., De Angelis F., De Bastiani M., Eperon G.E., Snaith H.J., Manna L., Petrozza A. The Impact of the Crystallization Processes on the Structural and Optical Properties of Hybrid Perovskite Films for Photovoltaics // J. Phys. Chem. Lett.– 2014.– Vol. 5, № 21.– P. 3836–3842.

МРНТИ 27.39.27 https://doi.org/10.26577/JPEOS.2023.v25.i3-4.i5

В.И. Капытин

ТОО «Институт ионосферы», Казахстан, г. Алматы
e-mail: kapytinvitaliy1991@gmail.com

ФРАКТАЛЬНЫЕ СВОЙСТВА ВАРИАЦИЙ КОМПОНЕНТ ГЕОМАГНИТНОГО ПОЛЯ ЗЕМЛИ В ПЕРИОД ЗЕМЛЕТРЯСЕНИЙ

Анализируются фрактальные свойства горизонтальных составляющих геомагнитного поля северного и восточного направления, вертикальной составляющей и интенсивности геомагнитного поля с разрешением 1 сек, измеренных различными геомагнитными обсерваториями сети INTERMAGNET по всему миру в период крупных землетрясений 2023 года. Анализировались вариации магнитного поля при сейсмических событиях, произошедших в разных регионах с магнитудой, превышающей ~ 6. Методы фрактального анализа применяются для выявления закономерностей и нелинейных взаимосвязей между изменениями компонент геомагнитного поля и проявлениями сейсмической активности. Исследована динамика фрактальной размерности вариаций компонент геомагнитного поля для дней, когда происходило крупное землетрясение. Полученные результаты показывают временное изменение фрактальной размерности компонент геомагнитного поля, выявляя различия в их нерегулярности (сложности). В результате показано показано, что сильные землетрясения сопровождаются повышенными вариациями магнитного поля Земли.

Ключевые слова: фрактальный анализ, фрактальная размерность, самоподобие, временные ряды, геомагнитное поле; землетрясения.

V.I. Kapytin

Institute of Ionosphere LLP, Kazakhstan, Almaty
e-mail: kapytinvitaliy1991@gmail.com

Fractal properties of variations in the components of the earth's geomagnetic field during earthquakes

The fractal properties of the horizontal components of the geomagnetic field in the northern and eastern directions, the vertical component and the intensity of the geomagnetic field with a resolution of 1 sec, measured by various geomagnetic observatories of the INTERMAGNET network around the world during the period of major earthquakes in 2023, are analyzed. Magnetic field variations were analyzed during seismic events that occurred in different regions with a magnitude exceeding ~ 6. Fractal analysis methods are used to identify patterns and nonlinear relationships between changes in geomagnetic field components and manifestations of seismic activity. The dynamics of the fractal dimension of variations in the geomagnetic field components for days when a major earthquake occurred. The results obtained show a temporary change in the fractal dimension of the geomagnetic field components, revealing differences in their irregularity (complexity). The results show that strong earthquakes are accompanied by increased variations in the Earth's magnetic field.

Key words: fractal analysis, fractal dimension, self-similarity, time series, geomagnetic field; earthquakes.

В.И. Капытин

«Ионосфера институты» ЖШС, Қазақстан, Алматы қ.
e-mail: kapytinvitaliy1991@gmail.com

Жер сілкіну кезіндегі жердің геомагнетикалық өрісінің компоненттеріндегі өзгерулердің фракталдық қасиеттері

Геомагниттік өрістің солтүстік және шығыс бағыттағы көлденең құрамдас бөліктерінің фракталдық қасиеттері, вертикальды құрамдас бөлігі және 1 сек рұқсатымен геомагниттік өрістің қарқындылығы кезең ішінде бүкіл әлем бойынша INTERMAGNET желісінің әртүрлі геомагниттік обсерваторияларымен өлшенген. 2023 жылғы ірі жер сілкіністері талданады. Магнитті өрістің ауытқулары магнитудасы ~ 6-дан асатын әртүрлі аймақтарда орын алған сейсмикалық оқиғалар кезінде талданған. Фракталды талдау әдістері геомагниттік өріс компоненттерінің өзгерістері

мен сейсмикалық белсенділіктің көріністері арасындағы заңдылықтарды және сызықтық емес қатынастарды анықтау үшін қолданылады. Ірі жер сілкінісі болған күндердегі геомагниттік өріс компоненттерінің вариациясының фракталдық өлшемінің динамикасы. Алынған нәтижелер геомагниттік өріс компоненттерінің фракталдық өлшемінің уақытша өзгеруін көрсетеді, олардың біркелкі еместігінің (күрделілігі) айырмашылықтарын ашады. Нәтижелер күшті жер сілкіністері Жердің магнит өрісіндегі вариациялардың жоғарылауымен бірге жүретінін көрсетеді.

Түйін сөздер: фракталдық талдау, фракталдық өлшем, өзіндік ұқсастық, уақыттық қатар, геомагниттік өріс, жер сілкіністері.

Введение

Краткосрочное предсказание землетрясений имеет жизненно важное значение для человечества в плане смягчения последствий стихийных бедствий [1]. Современные методы прогнозирования землетрясений и их геомагнитных предвестий представляют собой одну из актуальных задач в области геофизики и сейсмологии. В связи с постоянным ростом геологической активности нашей планеты, эффективные и точные инструменты для выявления предвестий стихийных бедствий становятся более необходимыми. Одним из подходов, привлекающих внимание исследователей, является применение фрактального анализа к геомагнитным данным с целью выявления связи между этими данными и готовящимися землетрясениями. В течение последних нескольких десятилетий явления, предшествующие землетрясениям, широко исследовались с целью прогнозирования землетрясений. Среди многих предвестников мы можем перечислить некоторые убедительные тематические исследования сверхнизкочастотного литосферного излучения при сильных землетрясениях, включая Спитакское землетрясение 1988 года [2,3], землетрясение в Лома-Приета в 1989 году [4] и Гуамское землетрясение в 1993 году [5], а также по ионосферным возмущениям для землетрясения Кобе 1995 г. с использованием субионосферных очень низкочастотных/ низкочастотных волн [6]. Затем накопление большого количества тематических исследований огромных землетрясений, таких как землетрясение Чи-Чи в 1999 году, землетрясение на Суматре в 2004 году, землетрясение в Вэньчуани в 2008 году и землетрясение в Японии в 2011 году, показало, что существуют определенные электромагнитные предвестники землетрясений (например [1, 7-11]).

Результаты и обсуждение

Магнитное поле Земли оказывает влияние на окружающую среду и может подвергаться значительным изменениям в преддверии землетрясений. Особый интерес представляет изучение фрактальных свойств в этих данных магнитного поля в период разрушительных землетрясений. Фрактальный анализ, изучающий самоподобие и масштабные закономерности в данных, может предоставить новые инсайты в процессы, протекающие перед и во время землетрясений. Он нашел широкое применение в различных дисциплинах, в том числе связанных с изучением катастрофических явлений и космической погодой [12-13]. В контексте геомагнитных полей, методы фрактального анализа позволяют выделить характерные закономерности, предшествующие сейсмической активности. Фрактальные свойства компонент магнитного поля Земли отражают структурные и пространственные характеристики этого поля на различных масштабах. Важно отметить, что магнитное поле Земли неоднородно и подвержено воздействию различных внутренних и внешних факторов. Фрактальный анализ позволяет исследовать их сложную структуру и поведение. Магнитное поле Земли обладает многомасштабной структурой, что означает наличие различных уровней организации на различных пространственных масштабах. Фрактальный анализ позволяет выявить и изучить эти масштабные закономерности. Магнитное поле Земли может обладать фрактальной размерностью, отражающей сложность его геометрической структуры. Высокие значения фрактальной размерности могут указывать на более сложные и разветвленные структуры. Фрактальные методы позволяют анализировать корреляции между компонентами магнитного поля в различных точках Земли и в различные моменты времени. Эти корреляции могут быть важными при изучении влияния различных геофизических и космических процессов на магнитное поле. Фрактальный анализ также может применяться для изучения магнитных аномалий, которые представляют собой отклонения магнитного поля от средних значений. Аномалии могут иметь фрактальные характеристики в своей пространственной структуре. Изменения

в магнитном поле Земли также могут быть связаны с воздействием внешних факторов, таких как солнечный ветер. Фрактальный анализ позволяет выявлять фрактальные закономерности в ответе магнитного поля на эти воздействия.

В данной статье путем применения методов фрактального анализа к вариациям компонент магнитного поля Земли изучается возможность выявления потенциальных предвестников землетрясений. Фрактальный анализ – это метод исследования структурных и статистических свойств объектов или процессов с использованием понятий фрактальной геометрии. Фрактальная геометрия занимается описанием и измерением фракталов, которые являются сложными структурами с самоподобием на различных масштабах. Основными аспектами фрактального анализа является фрактальная размерность (D) и самоподобие. Показатель Хёрста (также известный как Hurst exponent) – это численный показатель, используемый для измерения степени самоподобия или долгосрочной зависимости во временных рядах. Обозначается буквой «H» и может принимать значения от 0 до 1. Значение H = 0,5 соответствует случайному блужданию (броуновскому движению), H < 0,5 – отрицательной корреляции, а H > 0,5 – положительной корреляции. Чем ближе H к 1, тем сильнее долгосрочная зависимость. Обобщенный показатель Хёрста широко используется в различных областях, таких как финансы, климатология, биология и анализ временных рядов, для определения характера динамики данных и прогнозирования будущих значений. Он позволяет выявить и оценить степень структурированности или случайности в данных временных рядов. Показатель Хёрста и фрактальная размерность являются концепциями, связанными с анализом самоподобия и фрактальности в данных, но они измеряют разные аспекты этой фрактальной структуры.

Показатель Хёрста измеряет степень долгосрочной зависимости или корреляции во временном ряде. Высокие значения H могут свидетельствовать о устойчивом тренде, тогда как низкие значения H могут указывать на менее предсказуемое и хаотичное поведение. Фрактальная размерность измеряет степень фрактальности или самоподобия в структуре данных. Фрактальная размерность может быть дробной (например, 1,5), что указывает на фрактальную структуру, которая заполняет пространство промежуточным образом между целыми числами (например, одномерная прямая имеет размерность 1, а двумерный квадрат – 2). Высокие значения фрактальной размерности могут указывать на сложные, нерегулярные структуры. Таким образом, хотя оба показателя могут использоваться для оценки структуры данных, они измеряют разные характеристики. Показатель Хёрста фокусируется на временной зависимости, в то время как фрактальная размерность измеряет самоподобие или фрактальность в пространственной структуре данных. В некоторых случаях эти концепции могут быть использованы вместе для более полного анализа.

Для определения показателя Херста H или фрактальной размерности D по анализируемым данным можно применять различные методы [14]. Примерами методов, которые напрямую оценивают D профиля временного ряда, являются алгоритм Каца [15] или метод Хигучи (HG) [16]. Существует большой класс методов, которые фокусируются на долгосрочных корреляциях (и, следовательно, на оценке H). Например, метод Берри, заключающийся в использовании спектрального анализа мощности (PSA) и существование степенного закона поведения со спектральным показателем β позволяют определить фрактальную размерность, используя соотношение

$$H = 2\text{-}DF = (\beta \pm 1)/2, [12].$$

Другие методы, предложенные для оценки H, включают: анализ интервала Херста с перемасштабированием (R/S) [17], анализ с перемасштабированием RRA) [18], флуктуационный анализ без тренда (DFA) [19]. В данном исследовании применен метод Хигучи для оценки фрактальной размерности, спектральная плотность мощности(PSD).

На рисунке 1 представлена изменчивость фрактальной размерности, полученная методом Хигучи, для 6 февраля 2023 г. (Землетрясение в Турции и Сирии) Реализация представлена для компоненты Y магнитного поля земли для разных геомагнитных обсерваторий, находящихся на разном удалении от эпицентра землетрясения. Кривые показывают распределение вклада всех источников возмущений в компонентах магнитного поля. Особый интерес представляет наличие явно выраженной впадины на кривой, соответствующий моменту начала первого мощного толчка – 1:17:35 UT.

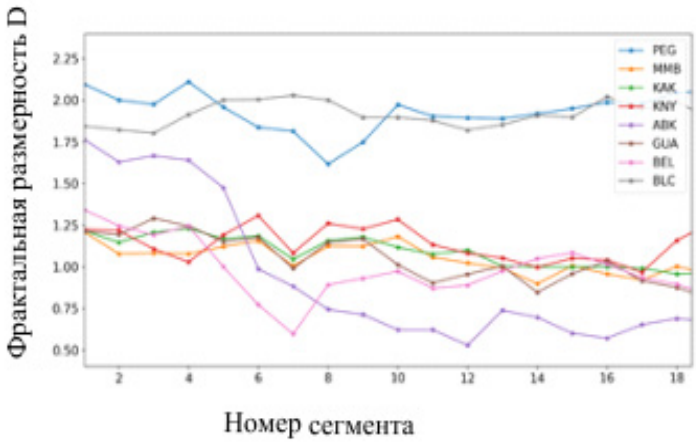

Рисунок 1 – Изменчивость фрактальной размерности, полученная методом Берри, для 6 февраля 2023 г. (Землетрясение в Турции и Сирии)

Для построения этих графиков исходные данные были очищены от выбросов, затем поделены на сегменты длиной 256 с 50% перекрытием, для каждого из сегментов рассчитаны спектральная мощность плотности(PSD), затем наклон β спектра оценивается с помощью линейной аппроксимации спектра, построенного в логарифмическом масштабе. На рисунке 2 представлена изменчивость фрактальной размерности, полученная методом Хигучи, для сегментов длиной 1024. В обоих случаях наблюдается отклик фрактальной размерности в тот же момент времени, когда происходит землетрясение.

В данной реализации приведено изменение фрактальной размерности одного дня 6 февраля 2023г. для 8 геомагнитных обсерваторий сети INTERMAGNET, причем геомагнитная обсерватория Педели(PEG) является ближайшей работающей в тот день обсерваторией. По этой причине на графике изменчивости фрактальной размерности виден отклик, соответствующий моменту начала землетрясения.

Поэтому отклик виден только на графике изменчивости фрактальной размерности только на обсерватории PEG. Остальные графики приведены для сравнения: мы видим схожее поведение изменчивости фрактальной размерности для остальных обсерваторий, что говорит о том, что источником возмущения во всех обсерваториях на тот момент является один источник, а поведение фрактальной размерности PEG вызвано, скорее всего, произошедшим в тот момент землетрясением.

На рисунке 3а представлены графики изменчивости фрактальной размерности для 25 февраля 2023 г. для землетрясения произошедшего на юго-востоке японского острова Хоккайдо. Для исследования выбраны 5 геомагнитный обсерваторий – Мемамбетсу(MMB), Какиока (KAK), Бельск (BEL), Педели(PEG), Абиско(ABK). Как мы видим из рисунка, на графике изменчивости фрактальной размерности для геомагнитной обсерватории MMB (Мемамбетсу), находящейся в 150 км от эпицентра землетрясения наблюдается возрастание показателя спектральной плотности мощности, соответствующий моменту времени 13:28:20, хотя землетрясение произошло 13:27:43. Это свидетельствует о том, что отклик землетрясения в вариациях компонент магнитного поля Земли произошел за время распространения сейсмической волны от эпицентра до геомагнитной обсерватории.

Причем в реализации вариаций компонент магнитного поля Земли наблюдается характерные возмущения, представленные на Рисунке 3б.

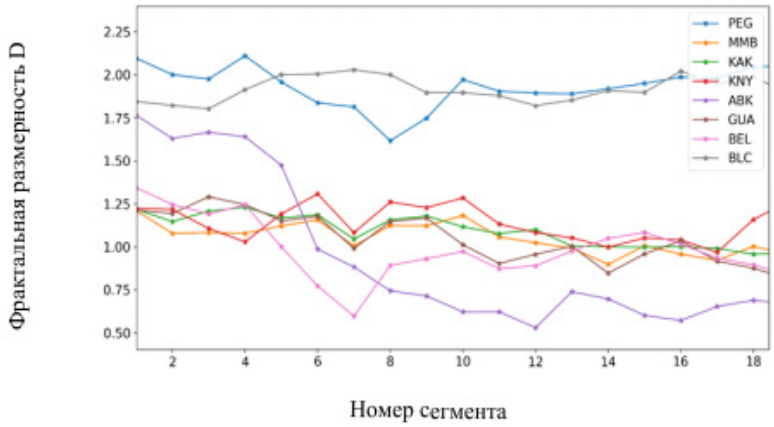

Рисунок 2 – Изменчивость фрактальной размерности, полученная методом Хигучи, для 6 февраля 2023 г. (Землетрясение в Турции и Сирии)

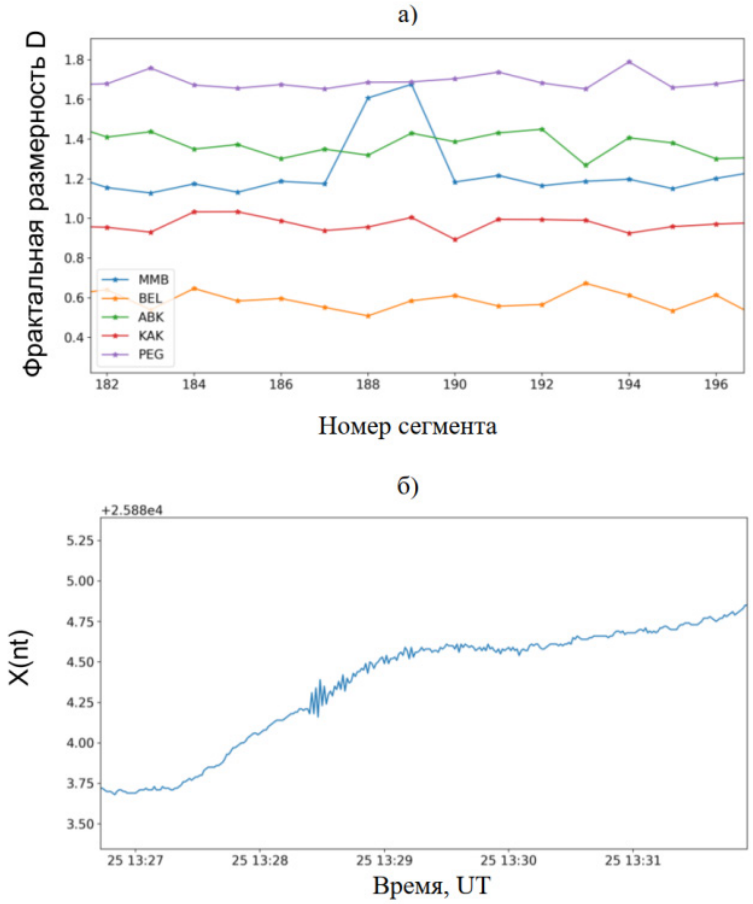

Рисунок 3 – Результат применения фрактального анализа к данным горизонтальной компоненты магнитного поля Земли а) изменение фрактальной размерности в течении одного дня 25 февраля 2023 г., б) график изменения горизонтальной компоненты магнитного поля Земли

Заключение

Анализ временных рядов геомагнитных данных с применением методов фрактального анализа позволил выделить фрактальные закономерности в изменениях компонент геомагнитного поля. Вероятно, в данном случае возмущение магнитного поля может быть обусловлено либо магнитными пульсациями земного происхождения, либо нарушениями в ионосфере Земли в эпицентральной зоне очага землетрясения. Эти нарушения могли вызвать дестабилизацию глобальных токовых систем. В качестве механизма воздействия землетрясения на ионосферу можно рассматривать изменение концентрации электронов под воздействием акустико-гравитационных волн, генерируемых на земной поверхности в период активности геодинамических процессов, как например, непосредственно перед, во время и сразу после землетрясения. Представленные результаты подчеркивают важность дальнейших исследований в этой области, включая расширение объема данных, использование более точных методов анализа и углубленное изучение механизмов взаимодействия между геомагнитными явлениями и сейсмической активностью.

Литература

1. Hayakawa M. Earthquake Prediction with Radio Techniques – John Wiley and Sons: Singapore, 2015. – 294 p.

2. Kopytenko Y.A.; Matiashvily T.G.; Voronov P.M.; Kopytenko E.A.; Molchanov O.A. Detection of ULF emissions connected with the Spitak earthquake and its aftershock activity based on geomagnetic pulsations data at Dusheti and Vardziya observatories // Phys. Earth Planet. Inter. – 1990. –Vol. 77. – P. 85-95.

3. Molchanov O.A.; Kopytenko Y.A.; Voronov P.M.; Kopytenko E.A.; Matiashvily T.G., Fraser-Smith A.C., Bernardi, A. Results of ULF magnetic field measurements near the epicenters of the Spitac (Ms = 6.9) and Loma Prieta (Ms = 7.1) earthquakes: Comparative analysis // Geophys. Res. Lett. – 1992. – Vol. 19. – P. 1495-1498.

4. Fraser-Smith A.C., Bernardi A., McGill P.R., Ladd M.E., Helliwell R.A., Villard O.G. Low-frequency magnetic field measurements near the epicenter of the Ms 7.1 Loma Prieta earthquake // J. Geophys. Res. – 1990. –Vol. 17. – P. 1465-1468.

5. Hayakawa M., Kawate R., Molchanov O.A., Yumoto K. Results of ultra-low-frequency magnetic field measurements during the Guam earthquake of 8 August 1993 // Geophys. Res. Lett. – 1996. –Vol. 23. – P. 241-244.

6. Hayakawa M., Molchanov O.A., Ondoh, T., Kawai E. The precursory signature effect of the Kobe earthquake on VLF subionospheric signals – J. Comm. Res. Lab. – 1996. –Vol. 43. –P. 169–180.

7. Pulinets S.A., Boyarchuk K. Ionospheric Precursors of Earthquakes – Springer: Berlin/Heidelberg, Germany, 2004. – 315 p.

8. Molchanov O.A., Hayakawa M. Seismo Electromagnetics and Related Phenomena: History and Latest Results – TERRAPUB: Tokyo, Japan, 2008. – 189 p.

9. Surkov V., Hayakawa M. Ultra and Extremely Low Frequency Electromagnetic Fields – Springer: Tokyo, Japan, 2014. – 486p.

10. Sorokin V.V., Chmyrev V., Hayakawa M. Electrodynamic Coupling of Lithosphere-Atmosphere-Ionosphere of the Earth. – NOVA Science Pub. Inc.: New York, USA, 2015. – 355p.

11. Ouzounov D., Pulinets S., Hattori K., Taylor P. (Eds.) Pre-Earthquake Processes: A Multidisciplinary Approach to Earthquake Prediction Studies – AGU Geophysical Monograph 234, Wiley: New York, USA., 2018. – 365 p.

12. Mandelbrot B. The Fractal Geometry of Nature. – W.H. Freeman: New York, NY, USA, 1983.

13. Barnsley M.F. Fractals Everywhere, 2nd ed.; Academic Press Professional: Boston, MA, USA, 1993.

14. Klinkenberg B. A review of methods used to determine the fractal dimension of linear // features. Math. Geol. – 1994. – Vol.26, – P.23–46.

15. Katz M.J. Fractals and the analysis of waveforms // Comput. Biol. Med. – 1988. Vol. 18. – P.145-156.

16. Higuchi, T. Approach to an irregular time series on the basis of the fractal theory // Phys. D Nonlinear Phenom. – 1988. –Vol. 31. – P. 277-283.

17. Hurst H.E. Long-term storage capacity of reservoirs //Trans. Am. Soc. Civ. Eng. – 1951. –Vol. 116. – P. 770-799.

18. Peng C.K., Buldyrev S.V., Goldberger A.L., Havlin S., Sciortino F., Simons M., Stanley H.E. Long-range correlations in nucleotide sequences // Nature. – 1992. – Vol. 356. – P.168

19. Peng C.K., Buldyrev S.V., Havlin S., Simons M., Stanley H.E., Goldberger A.L. Mosaic organization of DNA nucleotides // Phys. Rev. E. – 1994. – Vol. 49. – P. 1685.

ҒТАМР 37.29.35 https://doi.org/10.26577/JPEOS.2023.v25.i3-4.i6

А.А. Мерекеев[1,2]*, С.М. Нуракынов[3], Н.К. Сыдык[1], Ә.А. Амангелді[1], Г.М. Искалиева[1], А.А. Калдыбаев[1]

[1]Ионосфера институты, Қазақстан, Алматы қ.
[2]Әл-Фараби атындағы Қазақ ұлттық университеті, Алматы, Казақстан
[3]Satbayev University, Қазақстан, Алматы қ.
*e-mail: merekeev.aibek@gmail.com

БАТЫС ТЯНЬ-ШАНЬ АУМАҒЫНДАҒЫ МҰЗДЫҚТАР АУДАНЫНЫҢ ӨЗГЕРУІН ЖЕРДІ ҚАШЫҚТЫҚТАН ЗОНДТАУДЫ ПАЙДАЛАНА ОТЫРЫП ЗЕРТТЕУ: АРЫС ӨЗЕНІНІҢ БАССЕЙНІ

Бұл жұмыста 1957-2000, 2000-2011 және 2011-2022 жылдар аралығында Батыс Тянь-Шаньдағы Арыс өзені бассейндегі мұздықтардың өзгеруіне зерттеу жүргізілді. Зерттеу Landsat TM/ETM+ және OLI көмегімен алынған деректерді талдау негізінде жасалды. 2000 жылы жалпы ауданы 18,02 км^2 болатын 74 мұздықты зерттеу жасалды. Алайда 2022 жылға қарай мұздықтардың саны 58-ге дейін азайып, жалпы ауданы 11,48 км^2 болды. Бұл 22 жыл ішінде 6,54 км^2, немесе жылына 1,65%-ға қысқаруды білдіреді. Сонымен қатар, мұздықтардың көлеміне, биіктігіне және еңісіне зерттеу жасалды. Нәтижесінде мұздықтардың көлемінің 36,29%-ға азайғаны анықталды. Бұл айтарлықтай төмендеудің негізгі себебі, ең алдымен, температураның жоғарылауының басым тенденциясымен, сондай-ақ Батыс Тянь-Шаньның сыртқы жоталарында шағын мұздықтардың салыстырмалы түрде төмен биіктікте орналасуымен байланысты. Дегенмен, зерттеу нәтижелерде Батыс Тянь-Шаньның солтүстік бөлігіндегі мұздықтармен жабылған аумақтардың басқа аудандармен салыстырғанда төмен екенін көрсетеді. Талдау негізінде Арыс өзені бассейнің аймақтары мұз басуға қолайсыз жағдайда деген қорытындыға келдік. Демек, 1957-2022 жылдар аралығында Батыс Тянь-Шаньның басқа мұздық аймақтарымен салыстырғанда жоғары болды.

Түйін сөздер: Батыс Тянь-Шань, климаттың өзгеруі, мұздықтардың қысқаруы, мұздықтарды картаға түсіру, түгендеу, қашықтықтан зондтау.

A.A. Merekeyev[1,2]*, S.M. Nurakynov[3], N.K. Sydyk[1], Ә.A. Amangeldi[1], G.M. Iskaliyeva[1], A.A. Kaldybayev[1]

[1]Institute of Ionosphere, Kazakhstan, Almaty
[2]Al-Farabi Kazakh National University, Almaty, Kazakhstan
[3]Satbayev University, Kazakhstan, Almaty
* e-mail: merekeev.aibek@gmail.com

Study of glaciers using modern methods of remote sensing of the earth of the western tien shan: arys river basin

A study on changes in glaciers in the Arys River basin in the Western Tien Shan in the periods 1957-2000, 2000-2011 and 2011-2022 was conducted. Our study was based on the analysis of data obtained using Landsat TM/ETM+ and OLI. In 2000, 74 glaciers with a total area of 18.02 km^2 were discovered. However, by 2022, the number of glaciers had decreased to 58, and the total area was 11.48 km^2. This indicates a reduction of 6.54 km^2 or, equivalently, 1.65% per year over 22 years. In addition, we studied the rate of reduction of glaciers, considering their size, height and slope. As a result, there was a significant decrease in the size of glaciers by 36.29%. The main reason for this noticeable decrease is most likely due to the prevailing trend of rising temperatures, as well as the fact that small glaciers are located at relatively low altitudes in the outer ridges of the Western Tien Shan. However, the research results show that the rate of reduction of glacier-covered areas of the northern part of the Western Tien Shan is relatively lower compared to other territories. Based on the analysis, it was concluded that the glacial areas of the Arys River basin are in unfavorable conditions for glaciation. Consequently, in these regions, the rate of glacier reduction is higher than in other glacial regions of the Western Tien Shan in the period from 1957 to 2022.

Key words. Western Tien-Shan, climate change, glacier reduction, glacier mapping, inventory, remote sensing.

А.А. Мерекеев[1,2]*, С.М. Нуракынов[3], Н.К. Сыдык[1],
А.А. Амангелді[1], Г.М. Искалиева[1], А.А. Калдыбаев[1]

[1]Институт ионосферы, Казахстан, г. Алматы
[2]Казахский национальный университет им. аль-Фараби, Алматы, Казахстан
[3]Satbayev University, Казахстан, г. Алматы
* e-mail: merekeev.aibek@gmail.com

Исследование изменения площади ледников с использованием дистанционного зондирования Земли на территории Западного Тянь-Шаня: бассейн реки Арыс

Было проведено исследование изменений ледников в бассейне реки Арыс в Западном Тянь-Шане в периоды 1957-2000, 2000-2011 и 2011-2022 годов. Наше исследование было основано на анализе данных, полученных с помощью Landsat TM/ETM+ и OLI. В 2000 году было обнаружено 74 ледника общей площадью 18,02 км^2. Однако к 2022 году количество ледников сократилось до 58, а общая площадь составила 11,48 км^2. Это говорит о сокращении на 6,54 км^2 или, что эквивалентно, на 1,65% в год за 22 года. Кроме того, мы изучили скорость сокращения ледников с учетом их размеров, высоты и уклона. В результате наблюдалось значительное уменьшение размера ледников на 36,29%. Основная причина этого заметного снижения, скорее всего, связана с преобладающей тенденцией повышения температуры, а также с тем, что небольшие ледники расположены на относительно низких высотах во внешних хребтах Западного Тянь-Шаня. Однако результаты исследований показывают, что темпы сокращения покрытых ледниками районов северной части Западного Тянь-Шаня сравнительно ниже по сравнению с другими территориями. На основе проведенного анализа сделан вывод, что ледниковые районы бассейна реки Арыс находятся в неблагоприятных условиях для оледенения. Следовательно, в этих регионах темпы сокращения ледников выше, чем в других ледниковых районах Западного Тянь-Шаня в период с 1957 по 2022 год.

Ключевые слова: Западный Тянь-Шань, изменение климата, сокращение ледников, картирование ледников, инвентаризация, дистанционное зондирование.

Кіріспе

Орталық Азияның гидрологиялық циклінде мұздықтар маңызды рөл атқарады [1-3]. Тянь-Шань жотасының мұздықтары әлемдегі ең ірі суарылатын алқаптар Қазақстан, Қырғызстан және Өзбекстанның ойпаттарын сумен қамтамасыз етеді [4]. Мұздықтар қыста жиналып және жазда еріген су түрінде шығады [5], құрғақ жылдарда сумен қамтамасыз етеді. Соңғы жылдары мұздықтардың азаюы, жаз мезгілінде өзен ағынының азаюына әкеледі деп күтілуде. Арыс өзенінің бассейні Тянь-Шань Алатауының батыс бөлігінде, Қазақстан а және Өзбекстан, Қырғызстанмен шектеседі (1-сурет, мұнда вегетациялық кезеңінде суару мұздықтардың еруіне байланысты [6]. Арыс, Пскем, Асса, Талас, Шатқал және басқа да өзендерді суару үшін қарқынды пайдаланылады. Мұздықтардың экономикаға маңыздылығына қарамастан, Орталық Азиядағы мұздықтардың нақты жағдайы туралы ақпарат аз. Мұздықтардың алғашқы тугендеу тізімі, «Мұздықтардың каталогы» [7] – 1976 жылы жарияланған және 1957 жылғы аэрофототүсірілімге негізделген. 1990 жылдары КСРО ыдырағаннан кейін тұрақты гляциологиялық өлшемдер тоқтатылды. Осылайша, Тянь-Шань Алатауының батыс бөлігіндегі мұздықтар, оның бассейндердің өзгеруін аз зерттелінген. Бұл мақалада жартылай автоматты әдістерді қолдана отырып, 1957–2000, 2000–2011 және 2011–2022 жылдардағы Арыс өзенінің бассейніндегі мұздықтардың ауданын көрсетілген, жолақ қатынасына негізделген [8].

Осылайша, Тянь-Шань Алатауының батыс бөлігіндегі мұздықтардың, оның ішінде жекелеген бассейндердің беткі қабатының өзгеруі аз зерттелген күйінде қалып отыр.

Бұл жұмыстың мақсаты – ЖҚЗ деректері негізінде Тянь-Шань Алатауының батыс бөлігіндегі Арыс өзені бассейніндегі мұздықтар ауданының өзгеру динамикасын талдау.

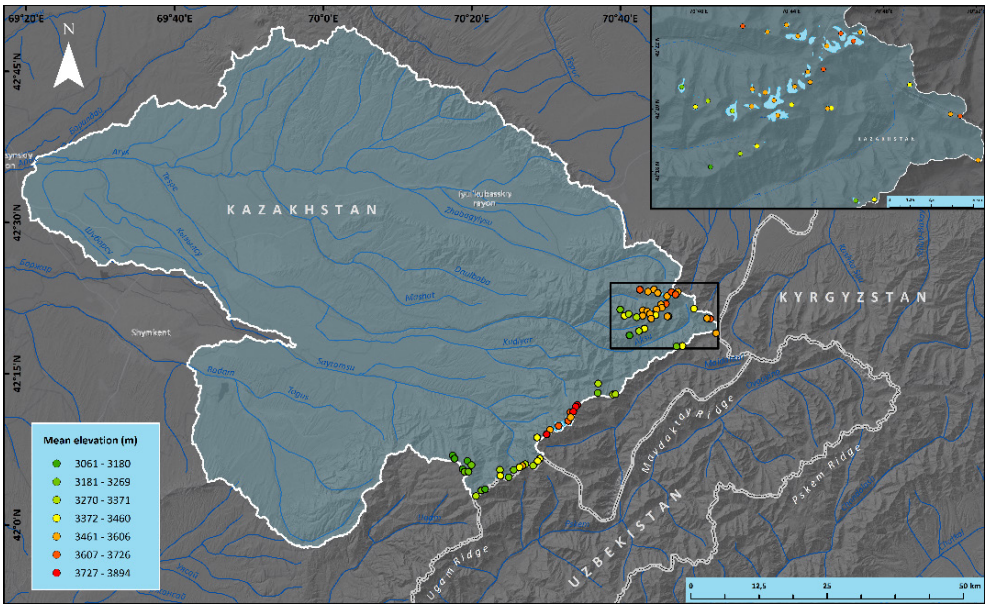

1-сурет – Зерттеу аймағының картасы. Арыс өзенінің бассейні

Зерттеу материалдары мен тәсілдер

Бұл зерттеуде Landsat 5 Thematic Mapper (TM), Landsat 7 Enhanced Thematic Mapper (ETM+), Landsat 8 operational Land Imager (OLI) және Landsat 9 operational Land Imager-2 (OLI-2) сияқты жерсеріктердің оптикалық деректері қолданылды. Мұздықтардың контурын анықтау және анықтау дәлдікті бағалау үшін Google Earth платформасындағы қол жетімді жоғары дәлдіктегі суреттер де пайдаланылды. Барлық суреттер абляция маусымының соңында – 10 тамыз бен 25 қыркүйек аралығында – мұздықтар маусымдық қарсыз және бұлтсыз жағдайда болған кезде алынды, бірақ мұздықтардың кейбір шеттері тау жартастары мен мұздық қабырғаларының көлеңкелерімен жасырылған болды. Барлығы, 2000 және 2011 жылдарға екі Landsat 5 (TM) суреттері, 2011-2012 жылдарға екі Landsat 7 (ETM+) суреттері, 2022 жылға бір Landsat 8 (OLI) суреті және 2022 жылғы бір Landsat 9 (OLI-2) суреті пайдаланылды.

Landsat (L1T деңгейі) георефернтті суреттері АҚШ Геологиялық қызметінің Жерді бақылау және ресурстық ғылым орталығымен (EROS) қамтамасыз етілген және EarthExplorer электрондық ресурсынан жүктелді (http://earthexplorer.usgs.gov/). Суреттердің сапасын жақсарту үшін Pan-sharpening арналарды біріктіру процесі жүргізілді, осылайша, суреттердің дәлдігі 15 м ге дейін жақсартылды (1-кесте).

Мұздықтардың контурын анықтау үшін Google Earth-те қол жетімді ғарыштық суреттер визуалды басқару құралы ретінде қызмет етті. Деректер негізінен Quickbird, Worldview, Pleiades 1A және 1B, сондай-ақ SPOT 6 және SPOT 7 сияқты жоғары дәлдіктегі оптикалық сенсорлардан алынды. Өкінішке орай, олар барлық аймақтарды қамтымайды.

Мұздықтарды инвентаризациялау барысында Alos PALSAR Жер бедерінің сандық үлгісі су алаптары мен топографиялық ақпаратты есептеу үшін пайдаланылды. Сондай-ақ, мұздықтар ауданының өзгеру динамикасын талдау кезінде 1957 жылғы аэрофотосуреттер негізінде жарияланған 1976 жылғы КСРО мұздықтары каталогының (Батыс-Тянь-Шань аумағындағы мұздықтар) 14-томының 1-ші шығарылымы пайдаланылды.

Ғалымдар [8-12] мұздықтардың шекараларын алу үшін әртүрлі әдістерді қолданды, соның ішінде қолмен визуалды интерпретация, арналар қатынасының шекті әдісі, қалыпқа келтірілген қар индексі әдісі және визуалды интерпретациямен біріктірілген жолақ қатынасының шекті әдісі.

1-кесте – Осы зерттеуде пайдаланылған Landsat көріністерінің тізімі

WRS2 Path-Row	Күні	Жерсерік атауы	Кеңістіктік дәлдік (м)	Суреттердің жарамдылығы	Суреттердің жарамдылығы
153-031	23 тамыз 2000	Landsat TM	30/120	Негізгі	
153-031	13 тамыз 2011	Landsat TM	30/120	Негізгі	Маусымдық қар, көлеңкелі аумақтар
	06 қыркүйек 2011	Landsat ETM+	15/30/60	Қосымша ақпарат	
	23 тамыз 2012	Landsat ETM+	15/30/60	Қосымша ақпарат	Жолақтарды толтыру
153-031	04 қыркүйек 2022	Landsat OLI-2	15/30/100	Негізгі	Маусымдық қар
	25 қыркүйек 2021	Landsat OLI	15/30/100	Қосымша ақпарат	

Жоғарыда атап айтылған зерттеулер көрсеткендей, қашықтықтан зондтаудың мультиспектралды суреттеріне негізделген арна қатынасының шекті әдісі визуалды интерпретациямен бірге мұздықтардың шекараларын анықтау кезінде салыстырмалы түрде дәл.

GLIMS семинарындағы бірнеше презентациялар таза немесе аздап ластанған мұзды автоматты түрде алу әдістерін көрсетті.

Әрі қарай әр түрлі әдістерді, соның ішінде Landsat ETM+ (Band 3 / Band 5, Band 4 / Band 5), Landsat OLI (Band 4 / Band 6, Band 5 / Band 6) (2-сурет) арналарының арақатынасын және медианалық сүзгіні және қараңғы нысандарды азайтуды мұқият салыстырды [13,14].

Оның зерттеуіне сәйкес, Landsat ETM+ (TM 3/5) және Landsat OLI (OLI 4/6) арақатынасы сенімді, қарапайым және дәл әдіс болып табылады, ішінара қолмен ажыратудан да жақсы (яғни жалпыланбаған және бүкіл көрініс үшін дәйекті). Бұл әдістің артықшылығы – таза мұзды тіпті жұқа бұлттардың астында және көлеңкелі жерлерде де анықтауға болады.

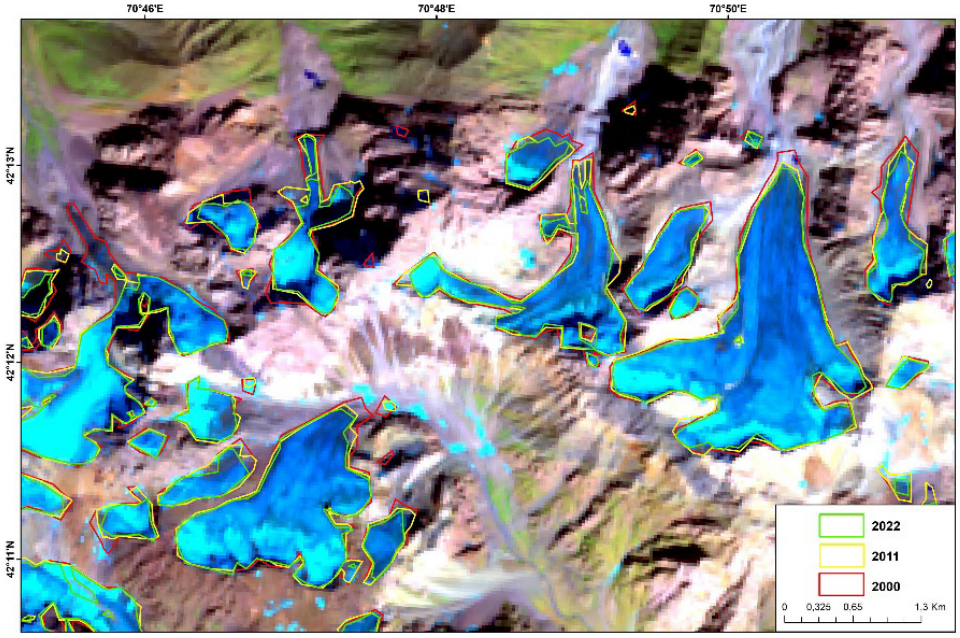

2-сурет – 2000 жылдан 2022 жылға дейін Арыс өзені бассейнінің бөлігіндегі мұздықтардың өзгеруінің мысалы, Landsat 9 OLI-2 (4 қыркүйек 2022)

Жоғарыда аталған зерттеу әдістерін ескере отырып, осы жұмыста Батыс-Тянь-Шань аймағындағы мұздықтардың шекараларын анықтау үшін жолақ қатынасын қолмен түзету әдісі қолданылды. Біріншіден, мұздық аймағының каналдардың жолақ қатынасын қолдану арқылы алынды (Landsat ETM +: Band 3 / Band 5, Landsat OLI: Band 4 / Band 6) және қайта сынақтан кейін шекті мән 1,4 ~ 2,1 диапазонында таңдалынды.

Бұл жұмыста 2000 жылғы мұздықтар тілінің контурын анықтау барысында мұздықтардың шекаралары TM (B6) термалды арнасының көмегімен цифрландырылды және соңғы вектор 1999 жылғы SRTM Жер бедерінің сандық үлгісінен алынған көлеңкелеуге (Hillshade) қойылды. 2011 және 2022 жылдары Жер бедерінің сандық үлгісі қол жетімді болмағандықтан, мұздықтар тілінің контурын цифрландыру үшін сәйкесінше тек ETM+ (B6) және OLI (B10) термалды арнасы пайдаланылды. Соңғы нәтижелер Google Earth қойылды және тағы бір рет талданды.

Көлеңкелі аймақтарды картаға түсіру үшін біз шегі 7400 болатын (қолмен алынған) Band 2 қолдандық. Көлеңкелі аймақтарды картаға түсіру үшін біз Landsat суреттерінің метадеректеріндегідей күн азимутын және басқа параметрлерді пайдаланып есептелген SRTM HillShade қолдандық. Біз көлеңкелі аймақтардағы мұздықтарды Band 2>7400 және hillshade <= 0 (0-ден аз немесе оған тең) қиылысы ретінде алдық.

Зерттеу нәтижелері мен талқылаулар

Мұздықтардың таралу сипаттамалары

2022 жылғы Landsat мәліметтері бойынша Батыс Тянь-Шаньдағы (2-кесте) Арыс өзенінің бассейнінен ауданы 0,005 км^2 асатын жалпы ауданы 15.25 км^2 тең 74 мұздықтар анықталды және картаға түсірілді.

2-кесте – Мұздықтардың саны мен ауданының өзгеруі

Бассейн	1957	2000	2011	2022	1957-2000	1957-2022	2000-2011	2000-2022	2011-2022	Орташа мөлшері 2000/2022
	Аудан км^2 (Саны)				Ауданның азаюы % (% ж-на$^{-1}$)					
1	2	3	4	5	6	7	8	9	10	11
Арыс	34.2 (87)	18.02 (74)	15.25 (74)	11.48 (58)	-47.31 (-1.10)	-66.43 (-1.02)	-15.37 (-1.4)	-36.29 (-1.65)	-24.72 (-2.25)	0.24/0.19
Мұздықтар <0.005 км^2	1.6 (59) <0.1 км^2	0.35 (14)	0.24 (11)	0.17 (9)	78.13 (-1.82)	-89.38 (-1.38)	-31.43 (-2.86)	-51.43 (-2.34)	-29.17 (-2.65)	0.026/0.001

Шағын және орта мұздықтар өте көп, бірақ олардың жалпы ауқымы шектеулі, ал ірілеу және өте ірі мұздықтардың аз болуы мұзды аймақтардың негізгі бөлігін құрайды. Мұздықтың орташа ауданы 0.19 км^2 болды, ал класс мұздығы басым болды. Ауданы 1 км^2 немесе одан да көп екі ірі мұздықтар болды, бірақ олар зерттелетін аймақтағы жалпы мұздану аймағының 36.47% құрады.

Мұз қабатының таралуы ALOS PALSAR DEM көмегімен анықталды және аймақтар арасындағы шамалы айырмашылықтарды көрсетті. Мұздықтардың көпшілігі солтүстікке (солтүстік, солтүстік-батыс және солтүстік-шығыс) (3-сурет) бағытталған және теңіз деңгейінен 3400-3600 м биіктікте орналасқан (4-сурет). Зерттелетін таулы аймақтағы мұздықтардың аспектісі бойынша орналасуы 37.5% (2011-36.4%, 2000-35.8%) солтүстік бөлігіде, 22.1% (2011-21.1%, 2000-21.8%) – солтүстік-шығысқа қарай, 25.7% (2011-26.7%, 2000-25.6%) – солтүстік-батыс бөлігінде. Шығыс бөлігінде 6.9 %, батыста 4.4% – дан астам, оңтүстік-шығыста шамамен 1.9%, ал ең аз таралғаны оңтүстік (0.7%) және оңтүстік-батыс (0.7%-дан астам) бөліктері орналасқан (3-сурет).

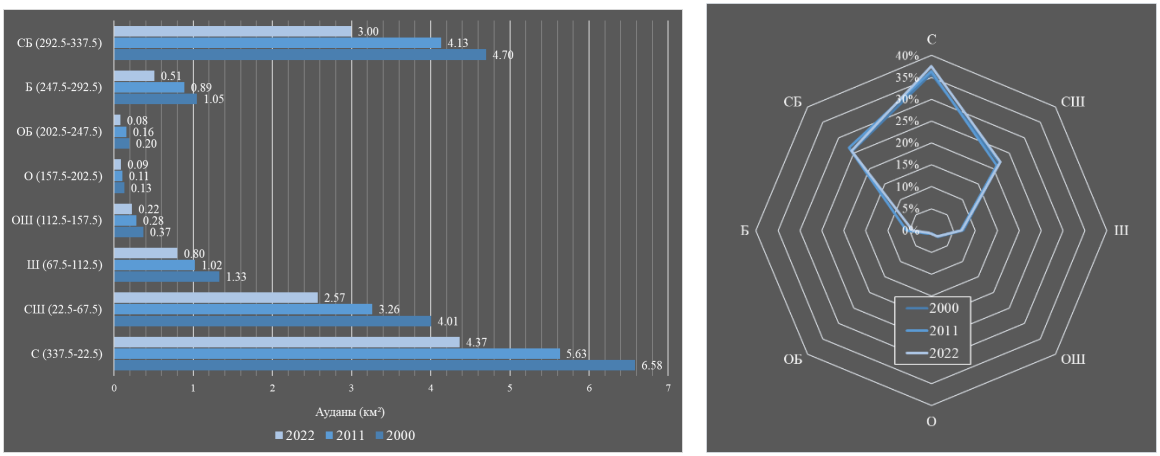

3-сурет – 2000-2022 жж. Арыс өзені бассейніндегі мұздықтар ауданының таралуы және олардың экспозиция бойынша өзгеруі

Мұздықтардың ең үлкен ауданы теңіз деңгейінен 3400-3600 м биіктікте орналасқан. Топографиялық мәліметтерге негізделген ұзақ мерзімді тепе-теңдік сызығының (ELA) қолайлы және кеңінен қолданылатын индикаторы болып табылатын мұздықтардың орташа биіктігі теңіз деңгейінен 3450 м биіктікте орналасқан [15]. Төменгі биіктіктегі мұздықтар негізінен зерттелетін аумақтың солтүстік-батыс бөлігінде, ал ең биік биіктіктегі мұздықтар солтүстік-шығыс бұрышында орналасқан.

Зерттелетін аймақтағы мұздықтардың басым көпшілігі негізінен 3400-3800 м биіктікте шоғырланған (5-сурет). 2022 жылғы мәліметтер бойынша, мұздықтардың 42.85%-ы теңіз деңгейінен 3400-3600 м биіктікте шоғырланған. Сондай-ақ, мұздықтардың 32.82%-ы 3600-3800 м биіктікте, 15.21%-ы 3200-3400 м (4-сурет) биіктікте орналасқан.

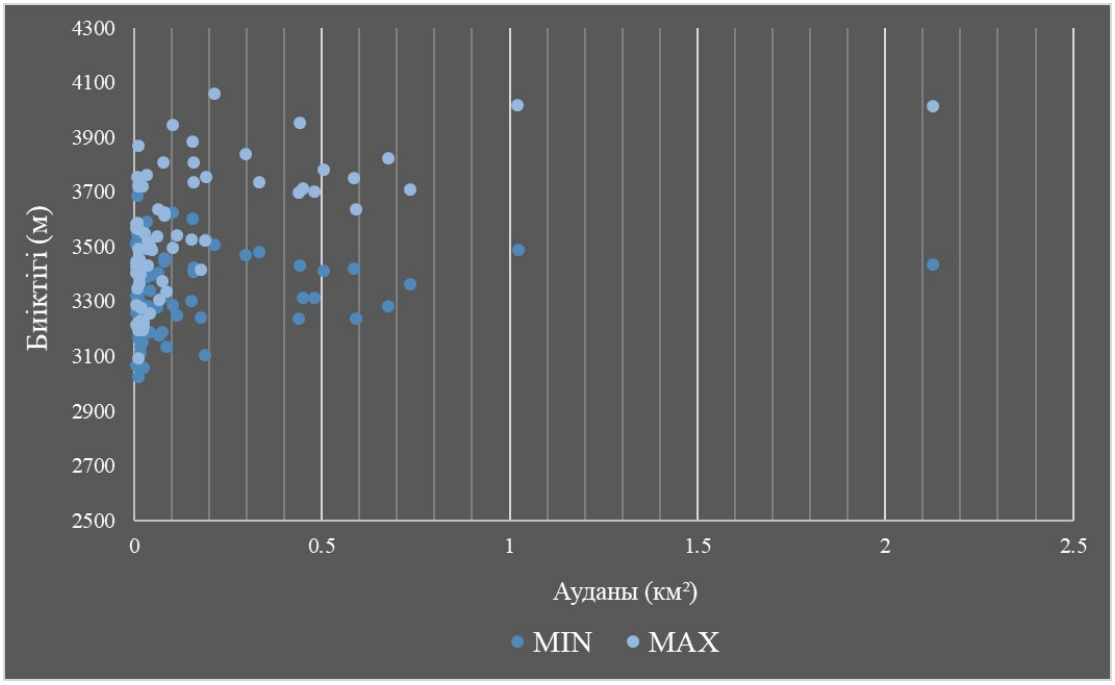

4-сурет – Мұздықтардың зерттеу аймағында максималды және минималды биіктікте орналасуы

Мұздықтар ауданындағы өзгерістер

Біз 2000 жылы 74, 2011 жылы 74 және 2022 жылы 58 мұздықтарды анықтадық, олар сәйкесінше 34,2 м2, 18,02 км^2 және 11,48 км^2 аудандармен мұздықтар каталогына енгізілді. Сонымен қатар, 2000 жылы 0,005 км^2 – 14, 2011 жылы – 11 және 2022 жылы – 9-дан аз мұздықтар анықталды, олардың жалпы ауданы 0,35, 0,24 және 0,17 км^2 (2-кесте).

Осылайша, Зерттеу аумағы бойынша 1957-2000 жылдар аралығындағы ауданның жалпы өзгеруі -47,31% құрады. 2000-2011 жылдардағы өзгеріс -15,37%, ал 2011-2022 жылдар аралығында – -24,72% құрады; бүкіл кезеңде мұзданудың жалпы ауданы 1957 жылы 34,2 км^2 (87 мұздық) 2022 жылы 11,48 км^2 (58 мұздық) дейін, яғни 65 жылда 66.43% – ға азайды.

Біздің зерттеу кезеңінде Каталогталған 30 мұздықтар мен 50 тіркелмеген шағын мұздықтар табылған жоқ. Барлық мұздықтар зерттеу кезеңінде үздіксіз қысқарып отырды.

Біздің нәтижелеріміз 2000-2022 жылдардағы мұздықтар аумағының жоғалуы 36.29% (-1.65% жылдық) құрағанын көрсетеді.

Жоғарыда айтылғандай, орташа ауданы 0.24 км^2 ең үлкен мұздықтар 2000 жылы, ал орташа ауданы 0.19 км^2 болатын ең кішкентай мұздықтар 2022 жылы тіркелді. 2011-2022 жылдар кезеңі ең жоғары төмендеу жылдамдығына ие болды (жылына -2.25%).

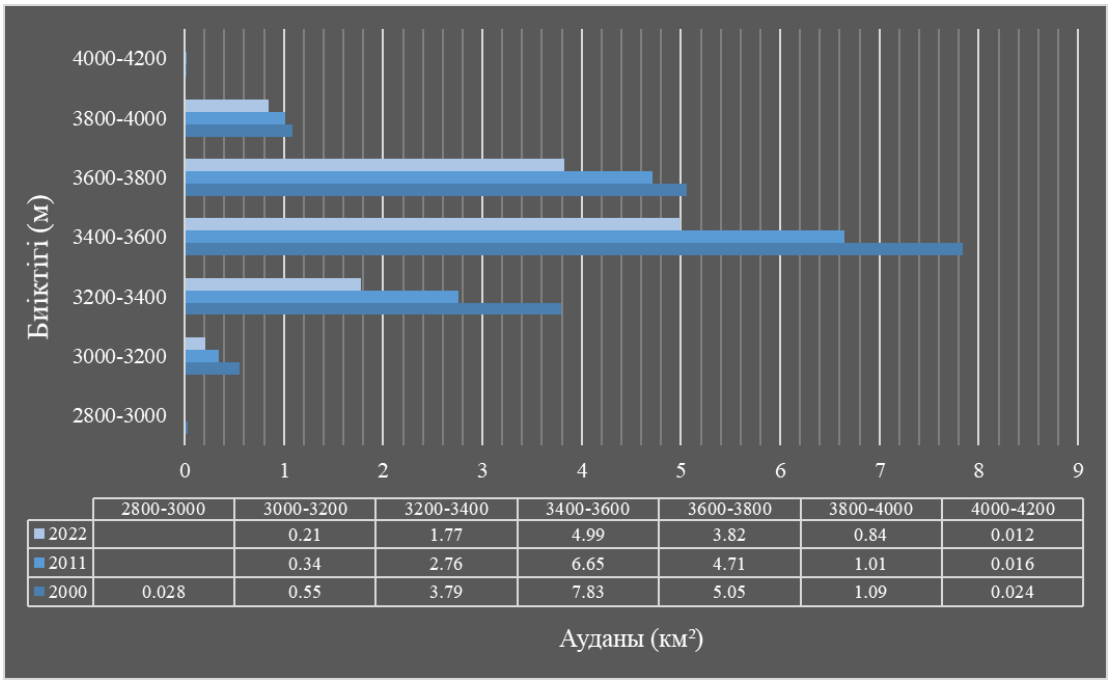

	2800-3000	3000-3200	3200-3400	3400-3600	3600-3800	3800-4000	4000-4200
2022		0.21	1.77	4.99	3.82	0.84	0.012
2011		0.34	2.76	6.65	4.71	1.01	0.016
2000	0.028	0.55	3.79	7.83	5.05	1.09	0.024

5-сурет – Арыс өзені бассейніндегі биіктік интервалына байланысты мұздықтар аудандарының бөлінуі және олардың өзгеруі

Зерттелген мұздықтардың аумағының өзгеруі мұздықтардың азаюының күтілетін және кеңінен жарияланған тенденциясын растады [16-18].

Біздің зерттеуіміздің нәтижелері көрсеткендей, 1957-2000 және 2000-2022 жылдар кезеңінде ауданның қысқаруының жылдық көрсеткіші 1.10-1.65% құрады, бұл көрсеткіш Батыс-Тянь-Шаньның басқа мұзды аймақтарына ұқсас [18, 19].

Қорытынды

Бұл зерттеу қазіргі уақытта бақылау деректерінің жеткілікті жазбалары жоқ Арыс өзенінің бассейндеріндегі мұздықтардың өзгеруін егжей-тегжейлі ұзақ мерзімді қашықтықтан талдаудың ғылыми құндылығын көрсетеді. Біздің зерттеуімізде ғарыштық суреттер (30 м дәлдік) және ALOS PALSAR рельефтің сандық моделі (12,5 м дәлдік) қолданылды. Шекті

қатынас әдісі (TM3/TM5, OLI4/OLI6) және визуалды интерпретация зерттелетін аймақтағы мұз қабатының шекараларын анықтауда жақсы көрсетті. Бассейнде 2000 жылы жалпы ауданы 18,02 км^2 болатын 74 мұздық анықталды, бұл көрсеткіш 2022 жылға қарай 11,48 км^2 дейін азайды, кішірею 6,54 км^2 құрайды (кішірею жылдамдығы жылына 1,65%).

Біздің нәтижелер Тянь-Шаньның кейбір басқа мұзды аймақтарына қарағанда зерттелетін аумақ үшін қысқартудың жоғары қарқынын көрсетеді. Бұл құбылыс біз зерттеп жатқан аймақтың ішкі жоталарға қарағанда Батыс-Тянь-Шаньның климаттық жағдайы қолайсыз шетінде орналасуымен ғана емес, сонымен қатар мұздықтардың кішірек өлшемдерімен бетінде қиыршық тас жамылғысы жоқтығымен да байланысты болуы мүмкін. Суб-бассейндер арасындағы мұздықтардың азаюындағы айырмашылықтарды Өлшем, бағдар және жергілікті климаттық жағдайлардағы айырмашылықтармен түсіндіруге болады. Зерттеу кезеңінде жаңа мұздықтар пайда болған жоқ. Мұздықтар мен климаттың күрделі өзара әрекеттесуін әрі қарай зерттеу қажет екені анық.

Жұмыста жүргізілген зерттеулер Қазақстан Республикасының Ғылым және жоғарғы білім министрлігінің қаржылай қолдауымен № AP14872134 жүзеге асырылды.

Әдебиеттер

1. Armstrong, R. L.: The glaciers of the Hindu Kush-Himalayan region: a summary of the science regarding glacier melt/retreat in the Himalayan, Hindu Kush, Karakoram, Pamir, and Tien Shan mountain ranges. ICIMOD: 20, (2010).
2. Sorg, A., Bolch, T., Stoffel, M., Solomina, O., Beniston, M.: Climate change impacts on glaciers and runoff in Tien Shan (Central Asia). Nat. Clim. Chang, vol. 2, 725–731 (2012).
3. Kaldybayev, A., Chen, Y., Vilesov, E.: Glacier change in the Karatal river basin, Zhetysu (Dzhungar) Alatau, Kazakhstan. Annals of Glaciology, 57(71), 11-19 (2016),
4. Farinotti, D., Longuevergne, L., Moholdt, G., Duethmann, D., Mölg, T., Bolch, T., Vorogushyn, S., Güntner, A.: Substantial glacier mass loss in the Tien Shan over the past 50 years. Nat. Geosci, vol. 8, 716–722 (2015).
5. Narama, C., Kääb, A., Duishonakunov, M., Abdrakhmatov, K.: Spatial variability of recent glacier area changes in the Tien Shan Mountains, Central Asia, using Corona (~1970), Landsat (~2000), and ALOS (~2007) satellite data. Glob. Planet. Chang., vol. 71, 42–54 (2010).
6. Vilesov Ye. N., Severskiy I. V.: Degradatsiya oledeneniya Dzhungarskogo (Zhetysu) Alatau vo vtoroy polovine KHKH v. Lod i sneg. 53(2), 12-20 (2013) (In Russian).
7. Katalog lednikov SSSR. V. 13. Vyp. 2. CH. 6. Basseyny rek Biyen, Aksu, Lepsy. L.: Gidrometeoizdat, 84 (1970) (In Russian).
8. Robson B. A. et al. Decadal scale changes in glacier area in the Hohe Tauern national park (Austria) determined by object-based image analysis //Remote Sensing. – 2016. – V. 8. – №. 1: 67.
9. Racoviteanu A., Williams M. W. Decision tree and texture analysis for mapping debris-covered glaciers in the Kangchenjunga area, Eastern Himalaya //Remote sensing. – 2012. – V. 4. – №. 10: 3078-3109.
10. Rastner P. The local glaciers and ice caps on Greenland: their mapping, separation from the ice sheet and their climate sensitivity: dis. – University of Zurich, 2014: 190.
11. Bolch T (2007) Climate change and glacier retreat in northern Tien Shan (Kazahkstan/Kyrgyzstan) using remote-sensing data. Global Planet. Change, 56(1–2): 1–12 (doi: 10.1016/j.gloplacha.2006.07.009)
12. Paul F, Ka¨a¨b A, Maisch M, Kellenberger T and Haeberli W (2004) Rapid disintegration of Alpine glaciers observed with satellite data. Geophys. Res. Lett., 31(21), L21402. – P. 4. (doi: 10.1029/2004GL020816) data: distribution of debris cover and mapping challenges. Earth System Science Data, 10(4): 1807-1827.
13. Paul, F.; Barrand, N.E.; Baumann, S.; Berthier, E.; Bolch, T.; Casey, K.; Frey, H.; Joshi, S.P.; Konovalov, V.; Le Bris, R.; et al. On theaccuracy of glacier outlines derived from remote-sensing data. Ann. Glaciol. 2013, 54, 171–182.
14. Paul, F.; Kääb, A. Perspectives on the production of a glacier inventory from multispectral satellite data in Arctic Canada: Cumberland Peninsula, Baffin Island. Ann. Glaciol. 2005, 42, 59–66.
15. Braithwaite, R. J., & Raper, S. C. B. (2009). Estimating equilibrium-line altitude (ELA) from glacier inventory data. Annals of Glaciology, 50(53): 127-132.
16. Sorg, A., Bolch, T., Stoffel, M., Solomina, O., & Beniston, M. (2012). Climate change impacts on glaciers and runoff in Tien Shan (Central Asia). Nature Climate Change, 2(10): 725-731.
17. Unger-Shayesteh, K., Vorogushyn, S., Farinotti, D., Gafurov, A., Duethmann, D., Mandychev, A., & Merz, B.: What do we know about past changes in the water cycle of Central Asian headwaters? A review. *Global and Planetary Change* 110 (2013): 4-25.
18. He, Y., Yang, T. B., Ji, Q., Chen, J., Zhao, G., & Shao, W. W. (2015). Glacier variation in response to climate change in Chinese Tianshan Mountains from 1989 to 2012. Journal of Mountain science, 12(5): 1189-1202.
19. Severskiy, I., Vilesov, E., Armstrong, R., Kokarev, A., Kogutenko, L., Usmanova, Z., ... & Raup, B. (2016). Changes in glaciation of the Balkhash–Alakol basin, central Asia, over recent decades. Annals of Glaciology, 57(71): 382-394.

МАЗМҰНЫ – CONTENTS – СОДЕРЖАНИЕ